CHEMICAL CONTRIBUTIONS TO DISPERSION - THEIR

ANALYTICAL IMPACT IN FLOW INJECTION

SAMPLE PROCESSING SYSTEMS

BY

CHIH-DUEN CHAO PAINTON

Bachelor of Science

Providence College

Taiwan, Republic of China

1971

Submitted to the Faculty of the Graduate College
of the Oklahoma State University
in partial fulfillment of the requirements
for the Degree of
DOCTOR OF PHILOSOPHY
December, 1982

CHEMICAL CONTRIBUTIONS TO DISPERSION - THEIR

ANALYTICAL IMPACT IN FLOW INJECTION

SAMPLE PROCESSING SYSTEMS

Thesis Approved:

Horacio A Mottola
Thesis Adviser

M G Rockley

H. Olin Spivey

J Chandler

Harry L. Gearhart II

Norman N Durham
Dean of the Graduate College

ACKNOWLEDGMENTS

TABLE OF CONTENTS

LIST OF TABLES

LIST OF FIGURES

xi

LIST OF FREQUENTLY USED SYMBOLS

a   tube radius (cm)

C   concentration (M)

C_o original concentration of a sample solution (M)

Cm   mean concentration (M)

Cmax   concentration corresponding to the peak maximum (M)

C^* normalized concentration, $C^* = C/C_o$ (dimensionless)

D   molecular diffusion coefficient (cm^2/sec)

D   practical dispersion number, **D** $= C_o/Cmax$ (dimensionless)

D_{eff} effective diffusion coefficient (cm^2/sec)

D'   apparent diffusion coefficient (cm^2/sec)

F   volumetric flow rate (mL/min)

f   correction factor for the time scale of a concentration-time curve (dimensionless)

H   height equivalent to a theoretical plate (cm)

Hmax   signal height measured at the peak maximum (cm)

H_o signal height obtained with an undispersed sample (cm)

k   rate coefficient for pseudo-first order conditions (sec^{-1})

L   length of reactor tube (cm)

M   mass of injected sample plug (g)

N   number of mixing tanks (dimensionless)

Re   Reynolds number (dimensionless)

R_i rate of sample injection (mL/sec)

r   radial distance from the tube axis (cm)

t	time (sec)
t_A	time for the first appearance of signal (sec)
Δt_B	time taken for the appearance of the entire concentration-time curve, this symbol is equivalent to t_{bas} (sec)
t_m	mean residence time (sec)
Umax	maximum velocity occurs in the center axis of the tube (cm/sec)
u	linear velocity of the flow (cm/sec)
$\bar{u}$	mean velocity of the flow in axial direction (cm/sec)
V	volume of the reactor vessel (mL)
Vm	volume of a mixing chamber (mL)
V_s	volume of each liquid segment (for segmented flow); or volume of an injected sample (for unsegmented flow) (mL)
X	reduced distance, $X = (xD)/(a)^2 Umax$ (dimensionless)
x	axial distance (cm)
η	dynamic viscosity (poise)
Ω	notation for longitudinal dimension in numerical method
μ	mean of a distribution
ν	kinematic viscosity, $\nu = (\eta/\rho)$ (cm^2/sec)
ρ	density (g/mL)
γ	liquid surface tension (dyne/cm)
γ'	tortuosity factor (dimensionless)
θ	normalized time, $\theta = (t/tm)$ (dimensionless)
σ^2	variance (dimensionless)
$(\sigma_i)^2$	variance predicted by the ideal model (dimensionless)
$(\sigma_r)^2$	peak spreading caused by radial mixing (dimensionless)
$(\sigma_{r,x})^2$	peak spreading, $(\sigma_r)^2$, expressed in length unit (cm^2)
$(\sigma_t)^2$	variance in time unit (min^2)

τ reduced time, $\tau = (tD)/a^2$ (dimensionless)

τ_m reduced mean residence time, $\tau_m = (t_m)D/a^2$ (dimension)

CHAPTER I

INTRODUCTION

Purpose and General Outline of

the Present Study

Flow injection analysis is a new concept of continuous flow analy-
sis for discrete samples, which is based on the injection of a sample
into a continuously moving, nonsegmented carrier stream. The injected
sample is physically dispersed and may chemically interact with the car-
rier stream as it travels downstream. The resulting concentration pro-
file, which carries the desired analytical information, is monitored at
a suitable detector. Reproducibility of the readout, as well as the
sensitivity and the determination rate are dictated by the controlled
dispersion of the injected sample plug.

Experimental approaches used for studying the dispersion theory of
flow injection analysis, in the past, have mostly involved injections of
a color dye into a noncolor carrier where no chemical reaction(s) is
considered. For most flow injection systems in practice, however, a
chemical reaction(s) is essential for the determination. The above stud-
ies, therefore, are unrealistic and do not provide enough information
for the users who try to optimize a given flow injection system.

The present study was intended to modify previous dispersion stud-
ies and extend the usefulness of these studies so that they may be a-
dopted for use in flow injection systems where chemical kinetics also

contributes to the overall dispersion.

Previous dispersion studies for flow injection analysis were based on the existing dispersion treatments in areas such as the physiological circulation research, chemical reactor engineering, and column chromatography, these are discussed in Chapter II. The dispersion theories developed for the counterpart of the flow injection analysis, the segmented continuous flow analysis, are briefly discussed in Chapter III. Finally, the dispersion treatments developed for flow injection analysis are discussed extensively also in Chapter III where the justification for the present study is presented.

The modification of the previous dispersion treatments for flow injection analysis was performed by including a kinetic term into the dispersion equation where only physical dispersion was accounted for. Calculations of dispersion were conducted by using numerical methods, and were restricted to sample injection into a stream, away from the detector, with laminar flow through a narrow, straight, open cylindrical tube (Chapters V and VI). The chemical kinetics involved were assumed to be overall pseudo-first order. To verify the validity of the theoretical calculations, some necessary experimental work was performed and the experimental methods and procedures are presented in Chapter IV. Experiment-based comparisons were also made for conditions that could affect the control of the dispersion, such as sample injection methods, reactor geometry, etc. (Chapter VII). The dependence of chemical kinetics on dispersion and the dependence of dispersion on chemical kinetics, as expected, resulting in a wave pattern of rate coefficients along the axial coordinate of the injected sample plug. The significance of this discovery is discussed in Chapter VIII where the con-

clusion for the entire thesis is made.

Introduction to Flow Injection Analysis
and Dispersion

Continuous flow analysis is a general technique that was introduced by Skeggs (1), who published a landmark article in 1957 that described the first segmented automatic analyzer, for carrying out automated chemical reaction assays. For more than 20 years, this technique has provided the bases for analyses of water, soil, plants, biological fluid, food, and pharmaceuticals. AutoAnalyzers, based on Skegg's idea and produced by Technicon (Technicon Instruments Corporation, Tarrytown, N. Y.), are an indispensable part of any clinical laboratory and find an increasing number of applications in all other types of laboratories that deal with vast amount of routine analyses. Millions of test results based on segmented continuous flow analysis testify to the usefulness of the technique.

Continuous flow analysis utilizes a flowing, air-segmented stream of reagents, interspersed by samples. The samples undergo, for instance, mixing, dialyzing, heating, and chemical reactions as they travel along the transporting tube, and are measured in an appropriate monitor unit (Figure 1). In this way, virtually every kind of wet chemical analysis has been successfully automated.

Since Skeggs' work, for almost twenty years, air segmentation had been considered to be a necessity in continuous flow analysis. Attainment of a steady-state signal were essential parts of continuous flow analysis. Because of these, the development of flow systems in which no air bubbles were present had been questioned strongly (2).
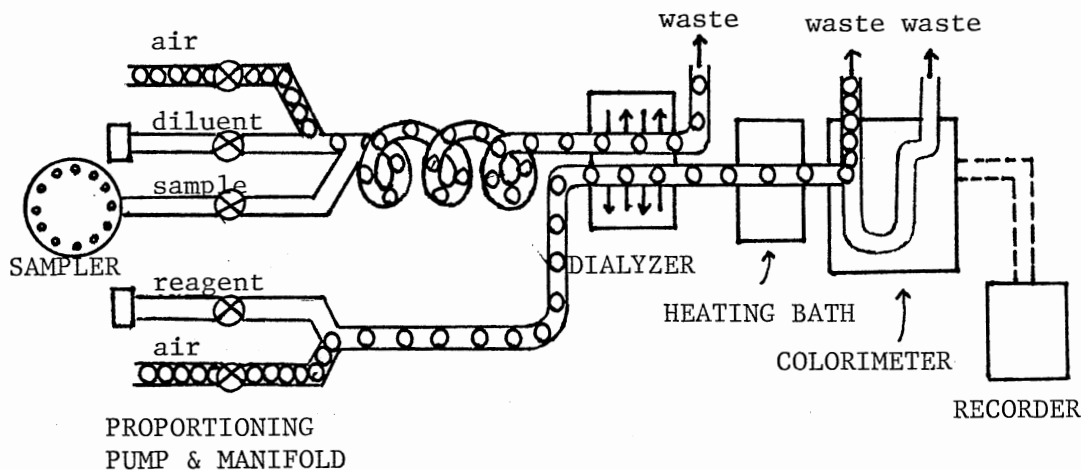
Figure 1. Prototype of a Continuous Flow System - Technicon AutoAnalyzer

The concept of continuous flow analysis without air segmentation received earliest attention in 1970 (3). Over the past six years, classical continuous flow analysis has undergone modifications, primarily by Ruzicka and Hansen (4) in Copenhagen, Denmark. They have shown that analysis without air segmentation is not only possible but also in many instances advantageous and promising. The result of this modification: an unsegmented continuous flow analysis, is known as flow injection analysis (FIA). FIA is based on injection of a sample into a continuously moving, nonsegmented carrier stream, either propelled by a pump or simply by gravitational flow. The carrier stream might constitute a reagent. The injected sample thereby forms a well defined zone which is then transported by the carrier stream toward a detector (Figure 2). During this transport the sample solution is mixed with the carrier stream, and may react with its component(s) to form a species which can be monitored in a flow-through dectector; the output being a peak which yields the analytical result. Controlled dispersion, a re-

producible timing and a reproducible sample injection technique gener-
ate precise signals such that a steady-state signal is no longer neces-
sary, sampling frequency is substantially increased and sample and rea-
gent consumptions are reduced.
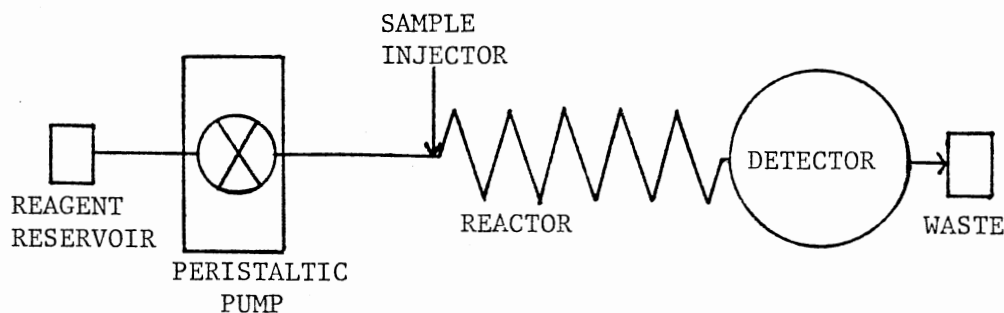
Figure 2. General Scheme of a Prototype Flow Injection
System

The advantages of FIA have been demonstrated in an ever increasing
number of applications in variety of fields, such as industrial,
clinical, chemical, academic, pharmaceutical, agricultural, and environ-
mental. Many different analytical instruments and techniques are used.
FIA's adaptability to the requirements of many analytical procedures
makes it a very powerful tool for analytical determinations. In addi-
tion, the versatility and simplicity of FIA systems will possible
lead to a significant change of attitude towards automation in the
analytical laboratory where the use of an automated system is still
viewed as justifiable only when heavy loads of routine analysis have to
be run daily. Yet, it is worthwhile to analyze even small numbers of
samples with a simple system which can be started and closed down in a

few minutes, and which can be easily reprogrammed from one type of measurement to another.

One of the less understood, yet very important aspects of continuous flow analysis is the dispersion process which takes place during the transport of the sample from the injection port towards the detector. Within the past twenty-five years, several thousand papers have been devoted to AutoAnalyzer technique and applications but only a small fraction of these has dealt with the theoretical aspects of the segmented flowing mass transfer phenomena. The same situation is found true in the area of unsegmented continuous flow analysis. Research into basic aspects of this analytical approach has been rather limited.

The conceptual frame of the dispersion theory, discussed by some authors in the area of FIA, is based on the dispersion models provided by chemical reactor engineers and the indicator dilution theory provided by physiologists. Peak broadening studies in column chromatography resemble FIA dispersion theory. The tanks-in-series model adopted by some FIA workers is intimately related to the plate model in chromatography, but peak spreading in FIA arises mainly from diffusion phenomena, while in chromatography it also arises from partition and random-walk due to packing. The dispersion theories developed in these fields, however, constitute the historical perspective on the dispersion study of FIA.

CHAPTER II

HISTORICAL PERSPECTIVE ON DISPERSION

Dispersion Theories in Physiology

Indicator Dilution Technique

It has been known for about one hundred and fifty years that it is possible to determine the time of transport of blood from one part of the cardiovascular system to another, by injecting an easily detected and non-toxic substance into the cardiovascular bed at one point and determining its time of appearance at another point (7). About eighty-five years ago, Stewart (8) introduced the indicator dilution technique to estimate the quantity of blood put out by the heart and lungs from the dilution of a known amount of injected substance by the blood which passes through the heart during a known period of time. Hamilton and his colleagues developed and extended the indicator dilution technique for the measurements of cardiac output (7), mean transit time, and the volume of a vascular bed (9). It is of interest that measurement of the mean transit time has also been applied in hydraulic engineering for the measurement of water in conduits of power plants (10).

The indicator dilution technique, as used widely for circulation studies in animals and plants, consists of injecting a suspension containing dye(s) or radioactive component(s) into the flow, and monitoring their appearance as a function of time at a point downstream. The form

of the resulting indicator-time curve depends on the manner by which the indicator is transported between the injection and observation points.

Figure 3 presents the first published indicator-dilution curves by Hamilton et al. (7). The elaborate method they used for simultaneously determining the pulmonary circulation time and the cardiac output in men was to inject an indicator into a vein and collect a small volume of blood sample from the radial artery at discrete time intervals. The concentration of the indicator in plasma of the collected samples was determined colorimetrically using standards made by diluting the indicators with known quantities of blood from the experimental subject. The pulmonary circulation time was calculated from the concentration versus time curve. To calculate cardiac output they pooled all the separately collected fractions of plasma samples containing the indicator and including the portion that contains recirculated indicator. In this way, they obtained an average indicator concentration. From the calculated volume of blood in which the indicator was diluted and from the collection time, the flow rate was determined. By using the same method, the flow of blood under the influence of a drug, such as morphine, can also be calculated.

Concentration-Time Curve

In 1954, Meier and Zierler (11) performed an experiment by injecting an indicator at a selected site of a vascular bed and measuring continuously the indicator concentration at another site as a function of time. The indicator was injected almost instantaneously or continuously at a constant rate. In the instantaneous injection method, the concentration at the measuring site rises to a maximum and then de-
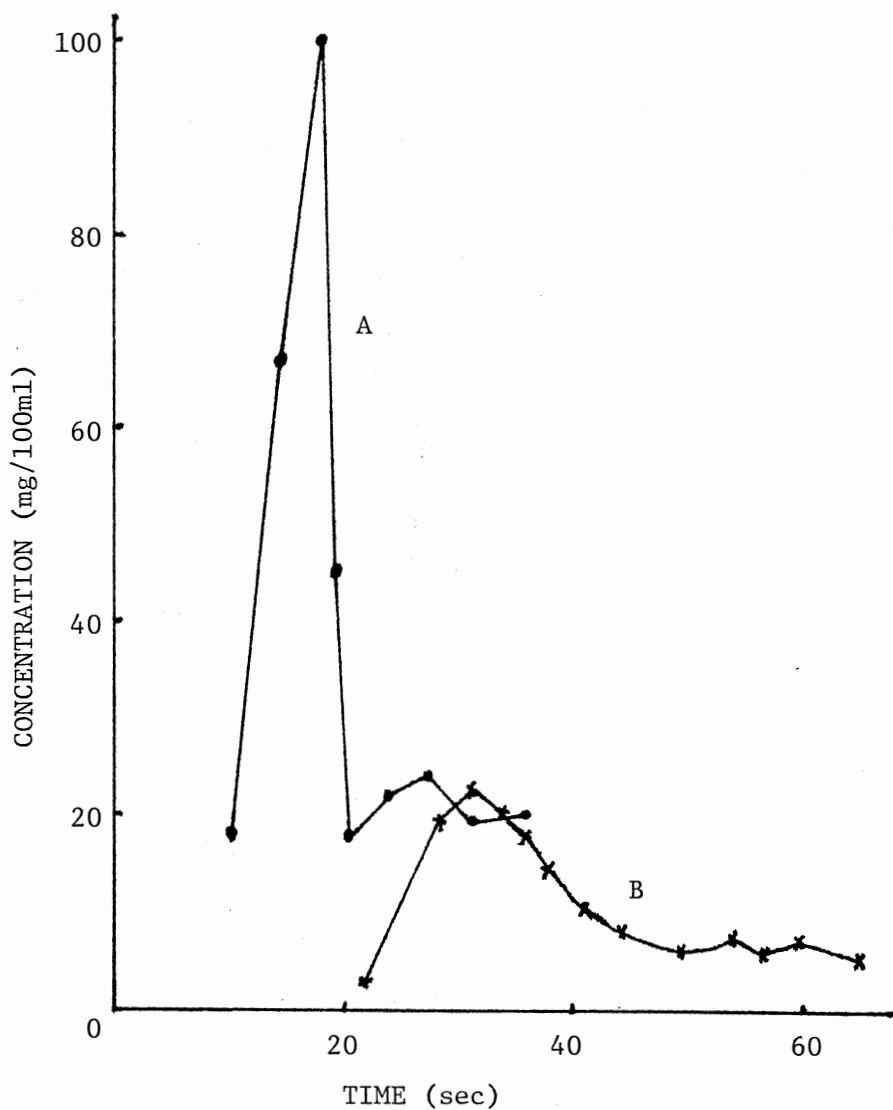
A: Subject Weighed 75 kg, Pulse 124, 700 mg In-
   dicator Injected.

B: Subject Weighed 85 kg, Pulse 72, 300 mg In-
   dicator Injected.

   Indicator: Phenol-Tetraiod-Phthalein Sodium

   Injection Site: Jugular

Figure 3.   Curve of Concentration of Injected Substance
            in Blood Plasma from the Radial Artery of
            a Man (Adapted from Reference 7)

creases to zero. In the continuous injection method, the concentration of indicator monitored at the measuring site rises asymptotically to a constant level. Hamilton and Remington (12) pointed out that the curve resulting from constant injection is simply the integral of that resulting from single injection. Hamilton et al. (9) proposed a formula to describe the descending portion of the curve obtained by adopting the instantaneous injection method, i.e. the wash out of the injected sample:

$$C = C_0\{\exp(-Ft/\alpha V)\} \tag{1}$$

where C is concentration of the indicator, C_0 is the original concentration of the injected indicator, F is the volumetric flow rate, t is time, α is an experimentally determined factor to correct for the fact that mixing is not really instantaneous, and V is the volume of the flow system. The shape of a concentration-time curve reflects the profile of transit times.

Transit Time

The transit time is the time taken for molecules of the indicator fluid to traverse the system. Different molecules will probably travel at different velocities through different pathways. This will be in part due to variation in length and cross-sectional area of the various fluid elements traversed. Even in a uniform diameter tubing, the variation in transit time can be caused by variations in velocity of flow over the cross-section of the vessel. Therefore, the mean transit time, $\bar{t}$, is defined as:

$$\bar{t} = (t_1C_1 + t_2C_2 + \cdots + t_nC_n)/(C_1 + C_2 + \cdots + C_n) \qquad (2)$$

where C's are concentration readings at corresponding times, t's.
Hamilton et al. (9) claimed that the mean transit time can be calculated
directly from the ratio of vessel volume and the volumetric flow rate,
i.e. $\bar{t}$ = V/F, which has been mathematically proved by Meier and Zierler
(11). Its validity, however, was questioned by Lane and Sirs (13) who
indicated that this relationship is true only for the bolus injection system
with turbulent flow. The same argument appeared when Spalding (14)
claimed that $\bar{t}$ is independent of the dispersion process in the system
Gonzalez-Fernandez (15) pointed out that Spalding's claim is not cor-
rect for other methods of injection. Bate et al. (16) experimentally
proved Gonzalez-Fernandez's observation. The equations provided by Lane
and Sirs seem to be more useful for their applicability for many experi-
mental conditions. The equations are:

    i. for a system with transverse mixing:

$$\bar{t} = t_0/\{1 - [(t_e - t_0)/2t]\} \qquad (3)$$

where t_0 is the time taken for the first molecule(s) to arrive at the
detector after travelling through a tubing of length L and radius a,
i.e.

$$t_0 = a(\pi^2)L/2F \qquad (4)$$

and t_e is the time taken for the passage of the entire injected indica-
tor;

    ii. for a laminar flow system with no transverse mixing:

$$\bar{t} = \int_0^\infty C dt \Big/ \int_0^\infty C t^{-1} dt \qquad (5)$$

These equations are useful in mathematical models used for simulating concentration-time curves.

Mathematical Models Which Simulate the Concentration-Time Curve

A number of mathematical models for simulating concentration-time curve have been proposed. Although some models may seem unclear in terms of their physical significance, others do appear to be useful. The most representative ones are discussed below.

In 1953, Rossi, Powers, and Dwok (17) carried out an indicator experiment with a straight tube. The indicator used was Na^{24} and a Geiger counter was used as the detector. Assuming that the volume of the injected indicator is small in relation to the volume of the flow system, then

$$F = \pi(a)^4 P/8\eta L \qquad (6)$$

where a is the tubing radius, P is the pressure drop along the length of the tubing, η is the viscosity of the injected sample, and L is the length of the tubing.

The introduction of the indicator alters the flow in the tubing, therefore the mean concentration, C_m, at the detector at time

$$t \leqslant t_o \qquad C_m = 0 \qquad (7)$$

$$t_o \leqslant t \leqslant t_o + t_i \qquad C_m = (C_o R_i/F)\{(1 - t_o)/t\} \qquad (8)$$

$$t_o + t_i \leqslant t \leqslant \infty \qquad C_m = (C_o R_i t_i t_o/F)\{1/t(t - t_i)\} \qquad (9)$$

where t_i is the total injection time, and R_i is the rate of injection.

A review and analysis of the various mathematical models for circulatory indicator-dilution curves was provided by Harris and Newman[18] in 1970. They classified all the available models into two major categories according to the theoretical mechanism of each model, i.e.:

    i. compartmental model, and

    ii. distributive model.

The compartmental model (multi-compartment) assumes that mixing in the system is concentrated at certain regions between the injection and measuring sites [19 - 21]. The change of concentration with time in each sequential compartment is:

$$\frac{dC_1}{d\omega} = \frac{R_i}{V_1} - \frac{F}{V_1}(C_1) \tag{10}$$

$$\frac{dC_i}{d\omega} = \frac{F}{V_i}(C_i - C_{i-1}) \qquad i = 1, 2, \cdots, n \tag{11}$$

where ω, the time, is defined as

$$\omega = t - (V_d/F) \tag{12}$$

C_i is the concentration in the ith compartment, V_i is the volume of the ith compartment, and V_d is the volume of the compartment where no mixing occurs. The mean transit time can be expressed as:

$$\bar{t} = (V_1/F) + (V_2/F) + (V_3/F) + t_a \tag{13}$$

where t_a is the appearance time, under the assumption that the injection approximates an ideal impulse. This model has been of value as an aid

for the computation of the area and the first moment of the output signal (18). However, the lack of precision in the experimental interpretation of the parameters has limited its use.

The distributive model, on the other hand, does not have such limitation. This model assumes a mixing process that is uniformly distributed between the injection and detection sites. Table I provides a brief discussion of this model.

Taylor (22) has provided a model useful for describing a laminar dispersion in cylindrical pipes. It is similar to the distributive model with an additional diffusion term in the radial direction.

Taylor's Solution for Dispersion of Soluble
Matter in Solvent Flowing Through a Tube

For solute laminar flow in a cylindrical tube of radius a, the flow velocity at a radial distance r from the center of the tube is given by the Poiseuille-Hagen (29) relation,

$$u = U_{max} \{1 - (r^2/a^2)\} \tag{18}$$

where U_{max} is the maximum velocity which occurs at the center axis of the tube. When the effect of velocity profile is combined with the effect of diffusion, the following partial differential equation results (6):

$$\frac{dC}{dt} = D(\frac{d^2C}{dr^2} + \frac{1}{r}\frac{dC}{dr} + \frac{d^2C}{dx^2}) - 2\bar{u}(1 - \frac{r^2}{a^2})\frac{dC}{dx} \tag{19}$$

where $\bar{u}$ is the mean velocity of flow in the axial direction (cm/sec).

Taylor (22) presented a solution of Equation 19 for two extreme flow conditions:

TABLE I

DISTRIBUTIVE MODELS FOR THE CIRCULATORY
INDICATOR-DILUTION CURVE

Formula	Comment(s)	References
$$\frac{dC}{dt} + \frac{u}{L}\frac{dC}{dx'} = \frac{D}{L^2}\frac{d^2C}{dx'^2} \quad (14)$$ $$x' = \frac{x}{L}$$	Diffusion and convection were both considered.	22 23
$$\frac{dC}{dt} + u\frac{dC}{dx} = D\frac{d^2C}{dx^2} + \frac{R_i}{V} \quad (15)$$ V — volume of the system between the injection and detection points (ml)	More general than Eq.14 A source term representing the rate of injection is included.	24
$$\frac{dC}{dt} + \frac{F}{A'}\frac{dC}{dx} = 0 \quad (16)$$ A' — cross-sectional area of the flowing tube. (cm^2)	Dispersion is not accounted for as a part of the flow. Dispersion was considered to be accomplished only by flowing through a number of vessels of various lengths. No mixing parameter is shown. It can be used as a comparison for concentration curves for diffusible and non-diffusible samples.	25
$$\frac{dC}{dt} = D\frac{d^2C}{dx^2} - \frac{FL}{\lambda V}\frac{dC}{dx} \quad (17)$$ λ — partition coefficient between extra- and intravascular spaces.	This model has the mathematical form of the time-dependent Fick's diffusion equation to which a convection term was added. It is just a diffusional interpretation of Eq. 14	26

i. The changes in concentration due to convective transport along the tube take place in a time which is so short that the effect of molecular diffusion may be neglected. In such a case dispersion is determined by convective transport alone.

For a solution of constant concentration which enters a tube filled with solvent at time $t \geqslant 0$ (constant flow injection): at $t = 0$,

$$\begin{cases} C = C_o \text{ for } x = 0; \\ \\ C = 0 \text{ for } x > 0 \end{cases} \tag{20}$$

and at $t > 0$,

$$\begin{cases} C_m = C_o \text{ for } x = 0; \\ \\ C_m = C_o\{1 - [x/(U_{max})t]\} \text{ for } 0 < x < (U_{max})t; \\ \\ C_m = 0 \text{ for } x > (U_{max})t \end{cases} \tag{21}$$

For solute initially confined to a length X (bolus injection) so that at $t = 0$

$$\begin{cases} C = 0 \text{ for } x = 0; \\ \\ C = C_o \text{ for } 0 < x < X; \\ \\ C = 0 \text{ for } x < X \end{cases} \tag{22}$$

the distribution can be obtained by superimposing two examples of the constant flow injection, namely

$$\begin{cases} C = C_o \text{ for } x < X; \\ \\ C = 0 \text{ for } x > X \end{cases} \tag{23}$$

and

$$\begin{cases} C = -C_O \text{ for } x = 0; \\ \\ C = 0 \text{ for } x > 0 \end{cases} \tag{24}$$

The mean concentration in the tube is distributed as: for $t < (X/U_{max})$,

$$\begin{cases} C_m = 0 \text{ for } x < 0; \\ \\ C_m = (C_O)x/(U_{max})t \text{ for } 0 < x < (U_{max})t; \\ \\ C_m = C_O \text{ for } (U_{max})t < x < X; \\ \\ C_m = C_O\{1 - [(x - X)/(U_{max})t]\} \text{ for } X < x < \{X + (U_{max})t\}; \\ \\ C_m = 0 \text{ for } x > \{X + (U_{max})t\} \end{cases} \tag{25}$$

and for $t > X/U_{max}$,

$$\begin{cases} C_m = 0 \text{ for } x < 0; \\ \\ C_m = C_O\{x/(U_{max})t\} \text{ for } 0 < x < X; \\ \\ C_m = C_O\{x/(U_{max})t\} \text{ for } X < x < (U_{max})t; \\ \\ C_m = C_O\{(X + U_{max} - x)/(U_{max})t\} \text{ for } (U_{max})t < x < (U_{max})t + X; \\ \\ C_m = 0 \text{ for } x > X + (U_{max})t \end{cases} \tag{26}$$

ii. The time necessary for appreciable effects to appear, due to convective transport is long compared with the "time of decay" during which radial variation of concentration are reduced to a fraction of their initial value through the action of molecular diffusion. The flow dispersion is dominated by the molecular diffusion. Taylor's (22)

suggestion for achieving this condition is that

$$\frac{a^2}{14.4D} << \frac{L}{Umax} \qquad (27)$$

For constant flow injection

$$C/C_O = \tfrac{1}{2} + \tfrac{1}{2}\{erf(\tfrac{1}{2} x'K^{-\frac{1}{2}} t^{-\frac{1}{2}})\} \text{ for } x' < 0;$$
$$\qquad (28)$$

$$C/C_O = \tfrac{1}{2} - \tfrac{1}{2}\{erf(\tfrac{1}{2} x'K^{-\frac{1}{2}} t^{-\frac{1}{2}})\} \text{ for } x' > 0$$

where

$$erf(Z) = 2\pi^{-\frac{1}{2}} \int_0^Z e^{-z^2}dz \qquad (29)$$

x' is a fixed distance, and K is the effective diffusion coefficient with the expression

$$K = (a)^2(U_{max})^2/192D \qquad (30)$$

For bolus injection, the only solution provided by Taylor is for a special case. When the length of the sample bolus is negligible compared to the length of reactor tubing (x' >> X), it can be looked at as if the sample of mass M is concentrated at a point x = 0 at a time t = 0. The concentration distribution is

$$C = \tfrac{1}{2} M(a)^{-2}(\pi)^{-3}/2(K)^{-\frac{1}{2}}(t)^{-\frac{1}{2}} exp\{-(x')^2/4Kt\} \qquad (31)$$

Other than for the above two extreme conditions where Taylor has provided simple analytical solutions, Equation 19 can only be solved by a numerical method. Bate et al.'s (29) work described in the next

section is a representative one.

Numerical Solution for Indicator Concentration-
Time Curves

Bate et al.'s (29) numerical solution can be described in two parts:

Continuous Injection Approach. Assuming that originally the tube is filled with colored solution of concentration C_0, and that an uncolored fluid is allowed to flow in at time $t > 0$. At the solution interface the colored solution is displaced by uncolored solution. If what is monitored is the cross sectional mean concentration, C_m, at a fixed distance downstream, then the value of C_m/C_0 starts to decrease from 1 to 0 as t becomes larger. Figure 4 presents the concentration profiles of the monitored species under four different experimental conditions.

Curve A is the result for convective transport without diffusion, which is equivalent to Taylor's solution under condition i. Curve D is the result for diffusion dominated flow, which is equivalent to Taylor's solution under condition ii. Curves B and C represent intermediate flow conditions where Taylor's solutions are not applicable.

Note that a parameter, A_x (See the legend in Figure 4), was used for characterizing different flow conditions. A_x is defined as

$$A_x = (a)^2 \bar{u}/Dx \tag{32}$$

This implies that a dispersion curve is the result combining the effects of all four parameters, i. e. the mean flow velocity, $\bar{u}$, the tube radius, a, the tubing length, x, and the diffusion coefficient, D.
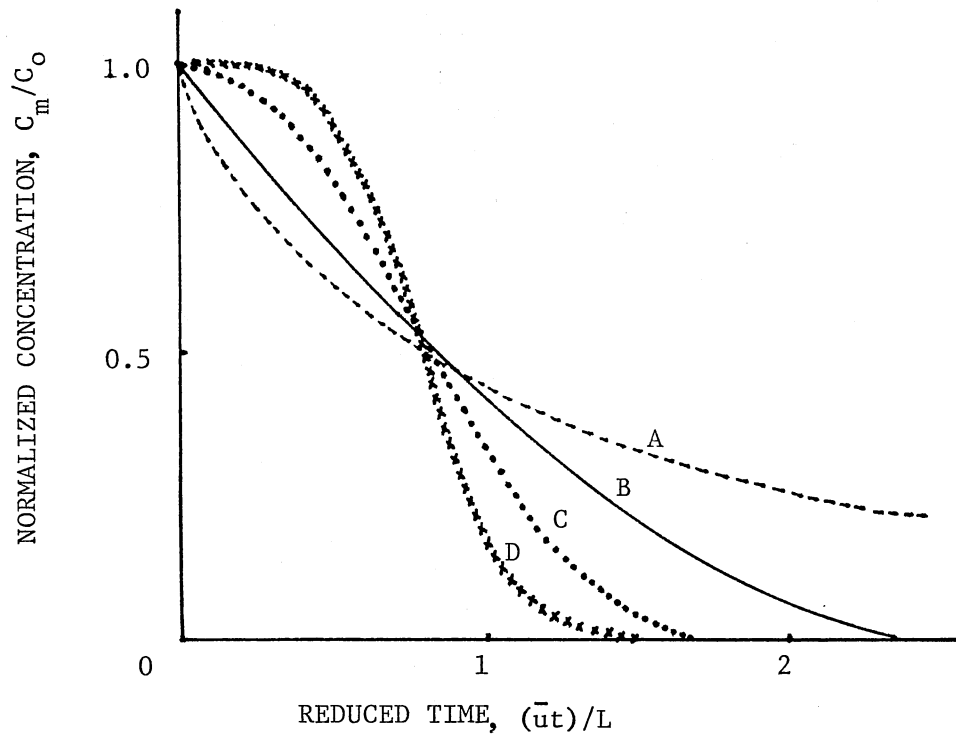
The Magnitude of A_x Value for each Curves is in the
  Following Order: Curve A > Curve B > Curve C >
  Curve D. A_x is Defined as

$$A_x = \bar{u} \cdot a^2/D \cdot x$$

Figure 4. Dispersion Curves of an Injected Sample with a
          Single Interface Boundary (Adapted from
          Reference 16)

Bolus Injection Approach. For injection of a finite amount of in-
dicator which results in two concentration boundaries, the dispersion
can be treated by combining the result for uncolored displaced by
colored solution (monitored at a distance x_1) with the result for
colored displaced by uncolored solution (monitored at a distance x_2)
where $x_1 \neq x_2$. The graphical representation of this approach is shown
in Figure 5.

The following relationships apply:

$$A_x \text{ (trailing edge)} = (x_1/x_2) \cdot A_x \text{ (leading edge)}$$

$$\quad (33)$$

$$T \text{ (trailing edge)} = (x_1/x_2) \cdot T \text{ (leading edge)}$$

where T is defined as

$$T = \bar{u}t/x$$

The concentration of indicator obtained from this approach is

$$C_m/C_o = (C_m/C_o)_{\text{trailing}} - (C_m/C_o)_{\text{leading}} \qquad (34)$$

The concentration-time curves resulting from Equation 34 are presented
in Figure 6. This figure again demonstrates the influence of convection
and diffusion on the shape of the dispersion curves. The symmetry of
the dispersion curve is attributed to the predominant diffusion force.

The numerical method used by Bate et al. was an explicit finite
difference replacement method which was claimed to place an un-
desirable restriction on the time increment and cause excessive com-
putation time (28).
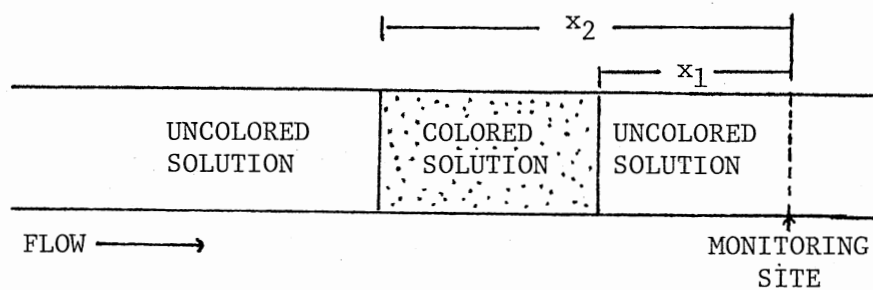
Figure 5. Initial Distribution for Bolus Injection
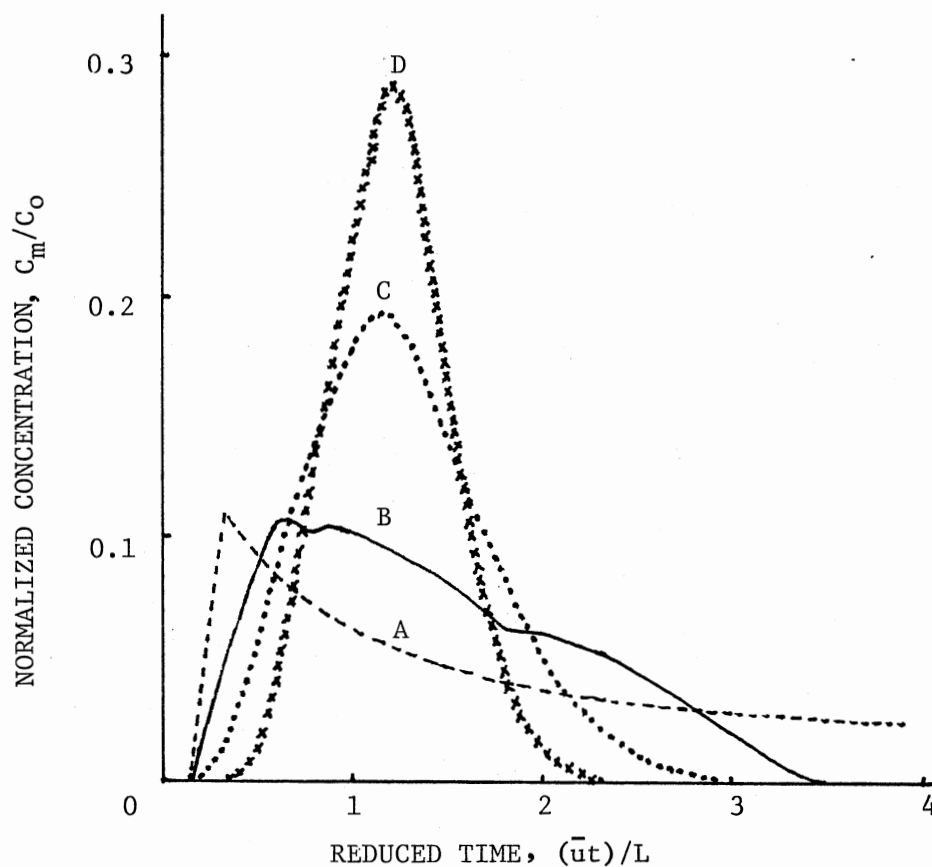
The Magnitude of A_x Value for each Curves is in the
Following Order: Curve A > Curve B > Curve C >
Curve D.

Figure 6. Dispersion Curves of an Injected Sample with
Two Interface Boundaries (Adapted from
Reference 16)

Dispersion Treatments in Chemical

Reactor Engineering

Because the design, analysis, and simulation of chemical reactors are of unique interest to chemical engineers, and because the transport phenomena is one of the most important basic approaches in studying chemical reactor engineering, it is not surprising that there are a substantial number of papers devoted to the study of dispersion authored by chemical engineers. They provide numerous dispersion models in describing the flow pattern in various kind of reactors under many possible flow conditions. Some selected ones which are of particular interest to the present study will be discussed next.

Flow Patterns

In a vessel with a stabilized flow, two idealized flow patterns can be visualized: plug flow and mixed flow (5).

Plug flow, also called piston flow, is the flow where elements of fluid which enter the vessel at the same moment move through it with constant and equal velocity on parallel paths, and leave at the same moment. This is normally assumed when considering flow through heat exchangers, catalytic reactors, packed towers, and chromatographic columns.

Mixed flow, also referred to as perfect mixing or back-mix flow, is the flow where the fluid in the vessel is completely mixed so that its properties are uniform and identical with those of the outgoing stream. The behavior of many vigorously stirred-tank reactors or blenders closely approximates this flow model.

In a plug flow reactor, there is no longitudinal (axial) mixing so there is no dilution. Consequently, this limiting model sets up the

upper limit of the sample throughput rate for a given flow rate. On the other hand, in a perfect mixing reactor any sample or fluid entering the reactor is instantaneously mixed with all of the fluid in the reactor. So for a given volume of reactor and flow rate, this model sets up the lower limit of the sample throughput rate. With the existence of nonuniform velocity, short circuiting, by passing, channeling, stagnant region, and recycling, flow behavior of a majority of the actual reactors deviates from these two limiting models, and the amount of deviation affects the residence time distribution within each reactor.

Residence Time and Its Distribution in a
Chemical Reactor

Residence time is the length of time that an element of fluid stays in a reactor. This parameter becomes very important when dealing with kinetic studies. The discussion that follows is taken from Aris (30).

Consider a cylindrical tube reactor of radius a, the distribution of the linear longitudinal velocity is

$$u(r) = 2\bar{u}\{1 - (r^2/a^2)\} \tag{35}$$

The volumetric flow rate for sample flow through an annulus between the radii r and (r + dr) is $\{u(r)2\pi r dr\}$. Let L be the length of the reactor, then

$$t_m = L/\bar{u}$$

and

$$t(r) = L/\{u(r)\} = t_m/\{2\ 1 - (r^2/a^2)\ \} \tag{36}$$

$$dt = \{r(t_m)dr\}/\{a^2(1 - (r^2/a^2))\} \tag{37}$$

The fraction of the fluid passing through in times between t and t + dt is the same as the fraction of fluid passing through between radii r and r + dr. Therefore the residence time distribution is

$$P(t)dt = 4(r/a^2)\{1 - (r^2/a^2)\}^3 a^2\{1/(t_m)r\}dt \tag{38}$$

The residence time probability density P(t) can be expressed as

$$P(t) = (4/t_m)\{1 - (r^2/a^2)\} \tag{39}$$

The least possible residence time is $\frac{1}{2}(t_m)$. Therefore, the complete specification of the residence distribution is

$$P(t) = 0 \text{ for } 0 \leqslant t < \tfrac{1}{2}(t_m)$$

$$\tag{40}$$

$$P(t) = (t_m)^2/2t^3 \text{ for } t \geqslant \tfrac{1}{2}(t_m)$$

Those elements of the material in the vessel which have been in it for a time t are said to have an "age" t. Danckwerts (31) has defined a series of terms: **I** is the internal age distribution function for a fluid in a vessel, and **E** is the exit age distribution function of fluid leaving a vessel or the residence time distribution of fluid in a vessel. Then **F** and **C** diagrams derived from these age distribution function and described below become two useful distributions.

F-Diagram. Suppose some property of the inflowing fluid undergoes a sudden change, e.g. change in color from white to red. Call **F**(t) the fraction of red material in the outflow at time t. The plot of **F**(t) versus Ft/V is called an **F**-diagram, where V is the volume of the vessel occupied by the fluid and F is the volumetric flow rate. As Figure 7

Ft/V $\longrightarrow$
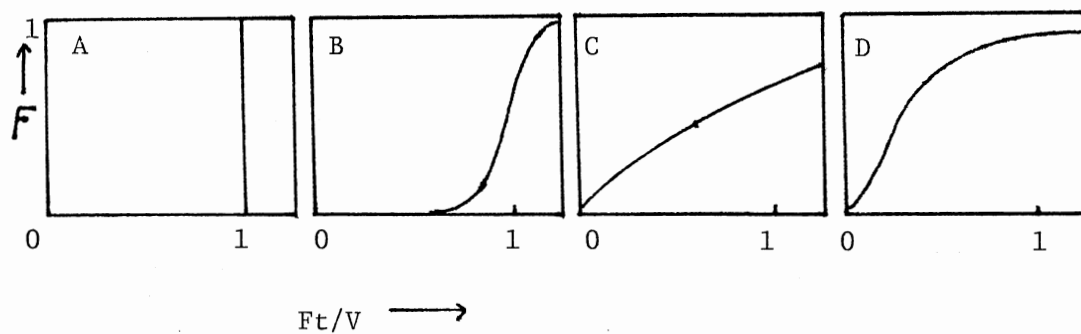
A: Piston Flow.   B: Piston Flow with Some Axial Diffusion.

C: Complete Mixing.   D: Dead Space.

Figure 7.   F-Diagram (Adapted from Reference 31)

Ft/V $\longrightarrow$
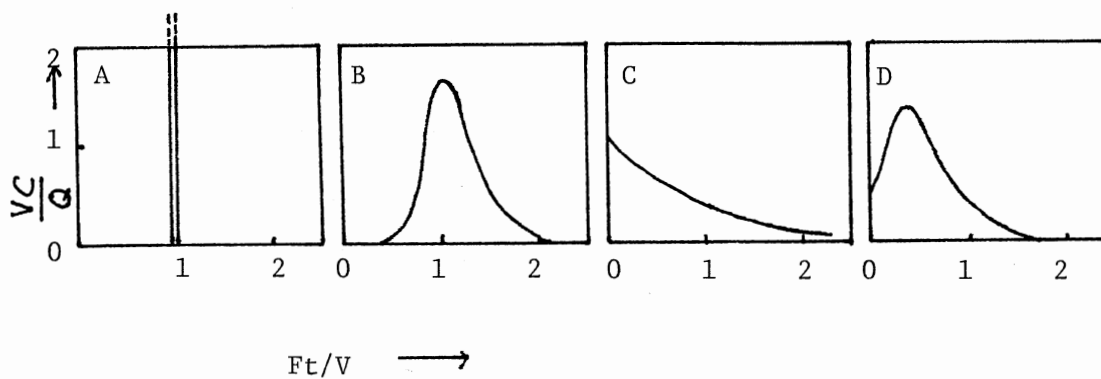
A: Piston Flow.   B: Piston Flow with Some Axial Diffusion.

C: Complete Mixing.   D: Dead Space.

Figure 8.   C-Diagram (Adapted from Reference 31)

shows, the shape of the **F**-diagram depends on the relative times taken by various portions of the fluid to flow through the vessel or, in other words, on the distribution of residence times. The **F**-diagram for complete mixing flow can be represented by a simple equation

$$\mathbf{F}(t) = 1 - \exp(-Ft/V) \tag{41}$$

C-Diagram. Suppose a quantity Q of some substance is injected into the entering stream instantaneously, that is, within a period of time t" where t" << V/F. The resulting concentration as a function of time at the exit is $\mathbf{C}(t)$. $\mathbf{C}(t)$ can be expressed as

$$\mathbf{C}(t) = \frac{Q}{F} \frac{d\{\mathbf{F}(t)\}}{dt} = \frac{Q}{F}\{\mathbf{E}(t)\} \tag{42}$$

where $\mathbf{E}(t)$ is the fraction of the material having ages between t and t + dt at the moment of leaving the system. The **C**-diagram is the plot of $\mathbf{C}(t)(V/Q)$ versus Ft/V as illustrated in Figure 8. Note that

$$\frac{V}{Q} \int_o^\infty \mathbf{C}(t)d(Ft/V) = 1 \tag{43}$$

The relations among the **F, C, I,** and **E** functions in a closed vessel have been provided by Levenspiel (32), i.e.

$$\mathbf{F} = (1 - \mathbf{I}) = \int_o^\theta \mathbf{E}(d\theta) = \int_o^\theta \mathbf{C}(d\theta) \tag{44}$$

$$\mathbf{C} = \mathbf{E} = d\mathbf{F}/d\theta = (-d\mathbf{I}/d\theta) \tag{45}$$

where θ is the normalized time ($\theta = t/t_m$).

The profiles of these age distributions distinctly characterize the flow patterns involved in a reactor, and the characterization of flow patterns can be measured in terms of moments.

Moments

Associated with every age distribution $y = f(x)$ are two sets of parameters called the moments of the distribution which are discussed fully in Levenspiel's (32) book.

The k-th moment about the origin is defined by

$$M_k' = \frac{\int_0^\infty x^k \, f(x) \, dx}{\int_0^\infty f(x) \, dx} \quad \text{for } k = 1, 2, \cdots \tag{46}$$

and the k-th moment about the mean or centroid μ of the distribution is defined by

$$M_k = \frac{\int_0^\infty (x - \mu)^k \, f(x) \, dx}{\int_0^\infty f(x) \, dx} \tag{47}$$

The moments are important parameters that can be extracted from a distribution, thus they can be used to compare distributions without comparing the actual curves themselves. The two moments used most frequently in dispersion studies are:

i. The first moment about the origin, commonly called the mean or centroid of the distribution, is the location parameter of the distribution.

ii. The second moment about the mean, commonly called the variance, measures the spread of the distribution about the mean and is equivalent to the square of the radius of gyration of the distribution. The second moment is used frequently for defining the axial dispersion (32, 33).

The treatments of dispersion in chemical reactor engineering are mostly based on assumptions of a specific flow pattern, and the dis-

person is expressed in terms of age distributions, concentration pro-
files, or peak spreading. Different dispersion models discussed next
have resulted from different treatments.

Dispersion Models for Various Flow Systems

In 1977, Gatsev and Zaitsev (34) adopted a collision theory in
constructing a flow model which describes the dispersion phenomena from
a probability point of view. The model is unique, however, because
its approach involves complex probability theories. Therefore it has
rarely been used in dispersion studies. Physical diffusion theories of
mass transfer and mechanical transport, on the other hand, have been
more commonly adopted by researchers who work on theoretical flow models.
Table II lists such kind of models. Each of the models will be briefly
discussed below.

Velocity Profile Model. It is also called the convective model.
For laminar flow in pipes, the sample solute becomes progressively dis-
persed as the fluid moves down the pipe. The extent of dispersion de-
pends on the flow conditions. The velocity can be used to characterize
three different mechanisms of dispersion.

i. At high velocity, dispersion of the sample solute occurs solely
as a result of convection. Such a flow may be called a segregated flow.
The F-function of the segregated flow resulting from a constant flow in-
jection can be expressed as (33):

$$F = C_m/C_o = \{1 - [x/(U_{max})t]\} = 2 \quad \text{for } \theta \geqslant 0.5$$

$$F = 0 \quad \text{for } \theta < 0.5$$

(48)

TABLE II

CHARACTERIZING MODELS FOR FLOW SYSTEMS

Model	Description	Reference(s)
Velocity profile model	For a reactor whose velocity profile is rather simple and is describable by a mathematical expression.	33
Dispersion model	Draws analogy between mixing and diffusion and is a superimposition of diffusion and plug flow.	32, 33
Tanks-in-series model	Consists of a series of equal sized perfectly mixing compartments.	32, 33
Mixed model	Combines mixing, short circuiting, and plug flow in various arrangements.	32, 33

ii. At moderate velocity, dispersion of the sample solute occurs as a result of convection and molecular diffusion. However, the effect of velocity still dominates over the effect of molecular diffusion in the longitudinal direction. That is

$$Umax(1 - r^2/a^2)dC/dx \gg D(d^2C/dx^2)$$

Therefore the dispersion equation (Equation 19) is reduced to

$$\frac{dC}{dt} = D \left(\frac{d^2C}{dr^2} + \frac{1}{r}\frac{dC}{dr}\right) - Umax \left(1 - \frac{r^2}{a^2}\right) \frac{dC}{dx} \tag{49}$$

which can be solved either numerically or analytically.

Gill (35) formulated the equation as a series expansion then solved it with a differential approach. He obtained an expression for the mean concentration,

$$Cm = \frac{1}{2}\left\{erfc \, \frac{X}{2\sqrt{(\kappa\tau)}} + exp\frac{X+(\frac{1}{2}\tau)}{2\kappa}erfc \, \frac{X+\tau}{\sqrt{(\kappa\tau)}}\right\} \tag{50}$$

where

$$\kappa = D/a^2(U_{max})^2\{D + [a^2(U_{max})^2/192D]\} \tag{51}$$

$$\tau = Dt/a^2 \tag{52}$$

$$X = Dx/a^2(U_{max}) \tag{53}$$

Earlier Taylor provided a solution in terms of the normalized concentration C^* ($C^* = C/C_o$), i.e.

$$C^* = \frac{1}{2 \, (a^2\bar{u}\pi\theta/48DL)} \, exp\left\{- \frac{[(x/L) - \theta]^2}{(a^2\bar{u}/DL)\theta/12}\right\} \tag{54}$$

under the strict condition, $4L/a \gg a\bar{u}/D \gg (48)^{0.5}$. Ananthakrishnan et
al. (36), however, pointed out that Taylor's solution is only applicable
in the region of $a\bar{u}/D > 50$ and the criterion, $4L/a \gg a\bar{u}/D$, does not in
fact put an upper limit on the value of $a\bar{u}/D$ as it seemed to. Subse-
quently, Aris (37, 38) showed that the restrictions imposed on some of
the parameters for Taylor's solution can be removed by describing the
dispersion in terms of its moments. In addition, Aris showed that the
axial effect is additive and the effective axial dispersion coefficient,
K, is equal to the sum of the molecular diffusivity and the dispersion
coefficient due to the velocity effect. That is

$$K = D + (a^2\bar{u}^2/48D) \tag{55}$$

or

$$K/D = 1 + (N_{pe})^2/48 \tag{56}$$

where N_{pe} is the Peclet number and is defined as

$$N_{pe} = a(U_{max})/D \tag{57}$$

Wissler (39) stated that the Taylor-Aris solution is valid only when
$ka^2/(3.8)^2D < 1$ where k is the chemical rate coefficient, for a
flow system involving a first order chemical reaction.

iii. At low velocity, convective dispersion which results from the
velocity profile is much smaller than the molecular diffusion, and dis-
persion of the sample solution is then controlled by molecular diffusion
alone. Equation 19 then is further reduced to

$$D\left(\frac{d^2C}{dx^2}\right) = \frac{dC}{dt} \tag{58}$$

which is Fick's second law and applies to diffusion in a circular pipe.

Analytical solutions of Equation 58 for flow systems under different injection techniques were provided by Taylor (22) in his physiological circulation research, and have been discussed previously (pp.17 - 18). The approximate condition for these solutions to be applicable in chemical reactor engineering has been estimated by Ananthakrishnan et al. (36) as

$$N_{pe} (Dt/a^2)^{\frac{1}{2}} < 0.07$$

Apart from the velocity profile model, the dispersion model discussed below describes the dispersion in terms of peak variances.

Dispersion Model. The parameter which can correctly characterize the role played by dispersion is a dimensionless term, $D/\bar{u}L$, called the reactor dispersion number (32). It is the reciprocal of the N_{pe} and varies from zero for plug flow to infinity for complete mix flow. The relationship between $D/\bar{u}L$ and the variance of theoretical C-curve depends on the end conditions of the reactor vessels, and is described as follows:

i. For a closed vessel which has no dispersion at either the entrance or exit outlet of the vessel:

$$\sigma^2 = (\sigma_t)^2/(t_m)^2 = (2D/\bar{u}L) - 2(D/\bar{u}L)^2\{1 - \exp(-\bar{u}L/D)\} \tag{59}$$

ii. For an open vessel which has no discontinuity of dispersion at any point in the vessel:

$$\sigma^2 = (\sigma_t)^2/(t_m)^2 = (2D/\bar{u}L) + 8(D/\bar{u}L)^2 \tag{60}$$

iii. For an open-closed vessel which is the intermediate case of the above two types of vessel:

$$\sigma^2 = (\sigma_t)^2/(t_m)^2 = 2(D/\bar{u}L) + 3(D/\bar{u}L)^2 \tag{61}$$

An alternate approach to the dispersion model for dealing with small deviation from the plug flow is the tanks-in-series model.

Tanks-in-Series Model. This model assumed that the actual reactor is represented by a series of j equally sized backmix flow vessels. In this case, the C-curve can be expressed as

$$c^* = C/C_o = \{(j)^j(\theta)^{j-1}/(j-1)!\}\cdot\exp(-j\theta) \tag{62}$$

where the variance σ^2 equals $(1/j)$.

Mixed Model. The reactors of this type consist of interconnected flow regions with various types of flow such as plug flow, complete mix flow, dispersed plug flow, and dead space. Industrial stirred-tank reactors and fluidized-bed reactors are the examples which are rarely found to be used in flow injection systems. Therefore the discussion of these will not be carried any further.

The models that have been discussed above do not include any factor from chemical reactions that may occur in a chemical reactor. Should a chemical reaction occur in the reactor, the concentration profile is expected to be affected by the reaction.

Chemical Reaction and Dispersion

Assuming a chemical reaction,

A → B

whose rate is given by a n-th order kinetics,

$$-(dC/dt) = k(C)^n \tag{63}$$

Danckwerts (31) provided an expression for describing the concentration-time relationship for systems with the reactant, A, flows through a tubular reactor. Assuming that the chemical reaction occurs simultaneously with the longitudinal diffusion and convection, then the expression is

$$u(dC/dt) - D(d^2C/dx^2) + k(C)^n = 0 \tag{64}$$

with the boundary conditions:

$$u(C_o) = u(C) - D(dC/dx) \quad \text{at } x = 0 \tag{65}$$

$$uf(C_o) = u(C) - D(dC/dx) \quad \text{at } x = L \tag{66}$$

where f is the unreacted fraction of the reactant during its passage through the reactor tube. Thus fC_o is the concentration of the exit stream, and at the exit where x equals L

$$dC/dx = 0 \tag{67}$$

Danckwerts' solution for Equation 64 for a first order reaction is

$$C* = \exp\left(\frac{ux}{2D}\right)\left\{\frac{2(1+b)\exp(ub/2D)(L-x) - 2(1-b)\exp(ub/2D)(x-L)}{(1+b)^2\exp(ubL/2D) - (1-b)^2\exp(-ubL/2D)}\right\} \tag{68}$$

where

$$b = \{1 + (4kD/u^2)\}^{\frac{1}{2}} \tag{69}$$

Wehner and Wilhelm (40) also provided a solution for Equation 64 for a first order reaction, i.e.

$$C^* = \frac{2(1+\alpha)\exp(\alpha uL/2D) \ - \ 2(1-\alpha)\exp(-\alpha uL/2D)}{(1+\alpha)^2\exp(\alpha uL/2D) \ - \ (1-\alpha)^2\exp(-\alpha uL/2D)} \tag{70}$$

where

$$\alpha = \{1 + (4kD/u^2)\}^{\frac{1}{2}} \tag{71}$$

Note that Equation 70 is a special case of Equation 68 for x = 0. Equations 68 - 71 clearly show that chemical reaction in a reactor is dependent on D, a physical dispersion parameter. In addition, any type of gradients, temperature gradient, pH gradient, etc., resulting from the chemical reaction will give point-to-point variations in the value of the reaction velocity constant, so that the chance of a molecule reacting depends on its path through the reactor, as well as its residence time. Furthermore, if the reaction is of an order other than first, the chance of a given molecule reacting depends on the molecules which it encounters in its passage through the reactor. The nature of these encounters is largely determined by diffusional processes caused by point-to-point variations in composition in the fluid, which can not be deduced from the F-function.

It should be mentioned that the solutions stated in Equations 68 - 71 were derived from Equation 64. Equation 64 does not include the contributions of radial diffusion to the dispersion. Consequently, these solutions are for a limiting case where the radial diffusion is assumed negligible. The solutions for a general case where all physical dispersion forces are accounted for excluding the chemical factor will be discussed next.

Solutions to Dispersion Equation and

Their Applicabilities

Recall Equation 19, the dispersion equation for fully developed laminar flow in a cylindrical tube,

$$\frac{dC}{dt} = D(\frac{d^2C}{dr^2} + \frac{1}{r}\frac{dC}{dr} + \frac{d^2C}{dx^2}) - Umax(1 - \frac{r^2}{a^2})\frac{dC}{dx}$$

Taylor (22) first assumed that the molecular diffusion in the axial direction is negligible compared with that in the radial direction, i.e., the d^2C/dx^2 term can be eliminated from the equation. An injected soluble material flowing in streamline motion, under the above condition, will be dispersing symmetrically relative to a frame of reference which moves with the mean speed of flow, $\bar{u}$, and has an apparent diffusion coefficient D' where

$$D' = (a)^2(\bar{u})^2/48D \tag{72}$$

Later he showed that the conditions under which this analysis is valid could be expressed as (41)

$$4(L/a) \gg (a\bar{u}/D) \gg 6.9$$

which is equivalent to a relationship (42)

$$D' \gg D$$

In an extension of Taylor's analysis by the method of moments, also allowing for the effect of axial molecular diffusion as discussed previously in page 32, Aris (37) derived a more general relationship by substituting D' with K, the effective diffusion coefficient defined in

Equation 55.   K corresponds to the rate of growth of the variance which is the direct result of the dispersion. Aris' study lead to a less stringent criterion for the applicability of Taylor's solution, that is

$$15(L/a) >> (a\bar{u}/D)$$

But Philip's (42, 43) study using eigenfunction expansions, changed the criterion to a more moderate one, that is

$$10(L/a) >> (a\bar{u}/D)$$

In 1961 Bournia et al. (44) applied Taylor's analysis to the flow of gases by studying the dispersion of a gaseous sample in another gaseous flowing stream. Since Geankoplis (45, p.263) stated that "when mass is being transferred from one phase to another or through a single phase, the basic mechanisms are the same whether the phase is a gas, liquid, or solid." the dispersion theory derived for liquid phase is expected to be applicable to gas phase as well. Bournia et al.'s experiment involved a gaseous bolus of a finite length, x_s, injected into a flowing stream of another gas under Taylor's conditions. The initial and boundary conditions are:

$$\begin{cases} C_m(x',0) = 0 \quad \text{for } x < -0.5(x_s); \\[2ex] C_m(x',0) = C_o \quad \text{for } -0.5(x_s) < x < 0.5(x_s); \\[2ex] C_m(x',0) = 0 \quad \text{for } x > 0.5(x_s); \\[2ex] C_m(\infty,t) = 0; \end{cases} \tag{73}$$

$$\{d(C_m)/dx'\} = 0 \quad \text{for } x' = 0 \tag{74}$$

$$x' = x - \bar{u}t \tag{75}$$

The gaseous sample is dispersed according to

$$\frac{Cm}{C_o} = Cm* = \tfrac{1}{2}\text{erf}(\frac{\tfrac{1}{2}x_s - x'}{2\sqrt{(Kt)}}) + \tfrac{1}{2}\text{erf}(\frac{\tfrac{1}{2}x_s + x'}{2\sqrt{(Kt)}}) \tag{76}$$

where

$$K = a^2(\bar{u})^2/48D \tag{77}$$

If the monitoring point is fixed at a distance, L, downstream then

$$Cm* = \tfrac{1}{2}\text{erf}(\frac{\tfrac{1}{2}x_s - L + \bar{u}t}{2\sqrt{(Kt)}}) + \tfrac{1}{2}\text{erf}(\frac{\tfrac{1}{2}x_s + L - \bar{u}t}{2\sqrt{(Kt)}}) \tag{78}$$

The maximum mean concentration, C_{pm}, passes the monitoring point at a time t' where t' equals $L/\bar{u}$, thus

$$C_{pm}/C = (C_p)^* = \text{erf}\{(x_s/4)(\bar{u}/KL)^{\tfrac{1}{2}}\} \tag{79}$$

Although an excellent agreement with the Taylor's solution was obtained by Bournia et al., their data, obtained at low velocity, do not agree with Aris' results. Evans and Kenney (46) explained that this is because Bournia et al. considered a stop-start injection method, for the extented source of sample, which creates a greater flow disturbance than anticipated. On the other hand, Ananthakrishnan et al.'s (36) explanation is that the difference in density between the injected and the carrier gases accounts for a large increase in axial dispersion in a vertical tube at low velocities (36).

Bailey and Gogarty (47) found that the experimental dispersion coefficient increases slowly with time. This observation leads to the

need for a solution that provides validity over a wider time range. In order to accomplish this, they have solved Equation 19 by neglecting the axial molecular diffusion term as Taylor did and by use of a numerical implicit finite difference method. They obtained the following result:

$$
\begin{cases}
L' = 0.8\tau \quad \text{for } \tau < 0.01 \\
\\
L' = 0.262(\tau)^{0.541} \quad \text{for } 0.5 < \tau < 6
\end{cases}
\tag{80}
$$

where L' is the distance from the 10% to the 90% signal height on the mean concentration–time curve. Ananthakrishnan et al. (36) pointed out that Bailey and Gogarty's numerical approach essentially accounts for molecular diffusion and convection alternately rather than simultaneously. They also rejected the empirical concentration equation derived from Equation 80 by Bailey and Gogarty, that is:

$$
C = 0.5 \, \text{erfc}\{[X - (\tau/2)]/[(\tau)^{0.541}/6.9]\}
\tag{81}
$$

for lacking justification for yielding an exponent of 0.541 rather than 0.50 of τ. Ananthakrishnan et al.'s investigations covered a much wider range of τ (0.01 – 100) and N_{pe} (1 – 23,000), and resulted in exact numerical solutions to the convective dispersion problem with both axial and radial molecular diffusion accounted for. A summary of their work is presented in Table III.

Based on a numerical computation, Ananthakrishnan et al. have shown that axial molecular diffusion vanishes at high N_{pe} numbers and sufficiently large values of τ. The axial molecular diffusion becomes significant at lower values of the N_{pe}, and the magnitude of N_{pe} at which this occurs depends on the value of τ. Generally when N_{pe} is smaller

TABLE III

A SUMMARIZATION OF ANANTHAKRISHNAN ET AL.'S SOLUTIONS TO THE DISPERSION EQUATION

Np_e	τ	Solutions	Comment(s)
> 500	~ 0.012	$$C_{avg} = C_o\left(\frac{x_L - x_T}{U_{max}\, t}\right), \text{ for } 0 < \frac{x}{\tau} \leq 1 \quad (82)$$ $$C_{avg} = 0 \quad\quad , \text{ for } \frac{x}{\tau} > 1$$ where x_L is the length from the sample bolus leading edge to the detecting point and x_T is the length from the sample bolus trailing edge to the detecting point.	Convective effect is the dominant force (pure convection region).
	$0.5 < \tau < 6.0$	$$C_{avg} = 0.5\, C_o \cdot$$ $$\left\{ erfc\, \frac{\frac{x_T D}{a^2 U_{max}} - \frac{Dt}{2a^2}}{\left(\frac{Dt}{a^2}\right)^{0.541}\frac{1}{\sqrt{48}}} - erfc\, \frac{\frac{x_L D}{a^2 U_{max}} - \frac{Dt}{2a^2}}{\left(\frac{Dt}{a^2}\right)^{0.541}\frac{1}{\sqrt{48}}} \right\}$$ $$(83)$$	Suggested by Bailey and Gogarty from their numerical results.
	$\tau > 0.8$	$$C_{avg} = 0.5\, C_o \cdot$$ $$\left\{ erfc\, \frac{\frac{x_T D}{a^2 U_{max}} - \frac{Dt}{2a^2}}{\left(\frac{Dt}{48 a^2}\right)^{0.5}} - erfc\, \frac{\frac{x_L D}{a^2 U_{max}} - \frac{Dt}{2a^2}}{\left(\frac{Dt}{48 a^2}\right)^{0.5}} \right\}$$ $$(84)$$	Ananthakrishnan et al.'s numerical result which fits better than Equation 83.
~ 100 ~ 50 ~ 25 ~ 10 ~ 5 ~ 1	≥ 0.80 ≥ 1.10 ≥ 1.25 ≥ 1.75 ≥ 4.50 > 20.0	$$C_{avg} = 0.5\, C_o \left\{ erfc\, \frac{x_T - \frac{\tau}{2}}{\left(\frac{\tau}{48} + \frac{4\tau}{Np_e^2}\right)^{\frac{1}{2}}} - erfc\, \frac{x_L - \frac{\tau}{2}}{\left(\frac{\tau}{48} + \frac{4\tau}{Np_e}\right)^{\frac{1}{2}}} \right\}$$ (In reduced parameters) $\quad (85)$	Axial diffusion is the dominant force.
Any Np_e	≥ 1.34	$$\frac{C_{bulk}}{C_o} = 0.5\, erfc\left(\frac{x_L - \frac{\tau}{2}}{\sqrt{K_1}}\right) + \frac{1}{96\sqrt{K_1 \pi}} exp\left[-\frac{\left(x_L - \frac{\tau}{2}\right)^2}{K_1}\right]$$ $$-0.5\, erfc\left(\frac{x_T - \frac{\tau}{2}}{\sqrt{K_1}}\right) - \frac{1}{96\sqrt{K_1 \pi}} exp\left[-\frac{\left(x_T - \frac{\tau}{2}\right)^2}{K_1}\right]$$ where $\quad K_1 = \frac{\tau}{48} + \frac{4\tau}{Np_e}$ (In reduced parameters) $\quad (86)$	Only holds for $\tau \geq 1.34$.

than 100, axial molecular diffusion can not be neglected. Thus Taylor's solution applies only for flow conditions with $N_{pe} \geqslant 100$ and $\tau \geqslant 0.8$. With Aris' modification which takes axial dispersion into account, the applicable region can be extended to lower N_{pe} values.

<div align="center">

Dispersion Theory in Column

Chromatography

</div>

Chromatography, as a method of separation, involves partition and dispersion processes. The center of concern where these processes take place is known as the chromatographic column and the following discussion will be devoted to these processes and to open columns since this approaches the situation in continuous flow analysis. Band broadening in chromatography, however, is also contributed by extra-column components, such as connecting tubes, injection loops, post-column reactors, and detector flow cell. The band broadening attributed to extra-column dispersion has been widely discussed (49 - 52), and part of this discussion will be included in the next chapter.

Column Efficiency and the Golay's Equation

In chromatography, the relative band broadening, represented by the quantity H, is called the height equivalent to a theoretical plate (HETP). This quantity usually represents the column efficiency (53) which is used for evaluating the column performance (54).

Starting from the Taylor-Aris equation discussed previously, Golay (55 - 57) derived an equation for calculating the height equivalent to a theoretical plate for a chromatographic process in an ideal open tube. An ideal open tube, as defined by Halasz (58), is a straight tube with a

constant circular cross-section, a smooth inner wall and smooth inlet and outlet surfaces. By assuming that the diffusion time in the stationary phase is not negligibly small, Golay's equation states that

$$H = \frac{K\ell}{u} + K_m \cdot u + K_s \cdot u \tag{87}$$

where

$$K_\ell = 2\gamma'D \tag{88}$$

$$K_m = \frac{1 + 6k' + 11(k')^2}{(1 + k')^2} \frac{a^2}{24D} \tag{89}$$

$$K_s = \frac{2(k')^3}{3(1 + k')^2} \tag{90}$$

and

$$k' = (V_R)'/(V_A) \tag{91}$$

Here, γ' is the tortuosity factor (approximately 1 for an open column), k' is the capacity factor, $(V_R)'$ represents an adjusted retention volume while V_A represents the reference retention volume, $K\ell$ is the longitudinal diffusion term, K_m is the resistance to mass transfer term in the mobile phase, and K_s measures the diffusion effect of the time-lag between the sample concentration at the mobile-stationary interface and within the stationary phase.

Golay's equation resembles the well-known van Deemter's (147) equation which describes the column efficiency of a packed column in chromatography.

van Deemter's Equation

The most commonly used, simplified form of van Deemter's equation is

$$H = A + \frac{B}{u} + C \cdot u \qquad (92)$$

where the A term represents band broadening due to eddy diffusion from random-walk, the B term describes band broadening due to molecular diffusion along the direction of flow, and the C term is the resistance to mass transfer in and out of the mobile-stationary phases. The A term is absent in Equation 87, as it should be in columns in which there is a single flow path. The B term corresponds closely to the K_ℓ term of Equation 87, while the K_m term of Golay's equation is missing in van Deemter's equation. All four terms (A, B or K_ℓ, C or K_s, and K_m) were accounted for when Rajcsanyis (53) calculated the HETP of a high-speed liquid chromatographic column, that is:

$$H = A + \frac{B}{u} + C \cdot u + K_m \cdot u \qquad (93)$$

Applicability of Golay's Equation

By differentiation of Golay's equation, the velocity at the minimum of the H versus u curve (U_{min}) is

$$U_{min} = \frac{13.86D}{2a} \left\{ \frac{1 + 6k' + 11(k')^2}{[1 + (k')]^2} \right\}^{-\frac{1}{2}} \qquad (94)$$

In routine liquid chromatography, however, $u \gg U_{min}$. Consequently, the first term in the Golay's equation can be neglected. The

Golay's equation was used to obtain the minimum H value (H_0) for reference peak; the minimum H value (H_{min}) for a retarded peak; the maximum number of theoretical plates (N_{max}) and the maximum number of effective plates (n_{max}), by making respective assumptions (58). These assumptions are:

    i. The inner diameter of the tube is less than 0.1 mm;

    ii. The linear velocity is less than 100 cm/sec (or the inner diameter is less than 0.5 mm and the linear velocity is less than 20 cm/sec);

    iii. The roughness of the tubing wall is negligible;

    iv. The coil diameter is greater than 5 cm; (however, the Golay's equation applies the best for staight tubes)

    v. The flow is laminar.

Effect of Wall Roughness

If the roughness of the tubing wall is not negligible, that is, if the smooth inner walls of these capillary tubing were replaced by a roughened surface (such as the modification of walls by "whisker" growth [149]), then the Golay's equation needs to be modified. Hofmann and Halasz pointed out that a small inner diameter and a rough wall destroy the classic laminar flow and enhance radial mass transfer, thus the mass transfer between the mobile and stationary phases is facilitated.

For the roughened surface with an effective area Q times larger than the area of the smooth walls, Golay (57) suggested that the K_s term in Golay's equation is diminished by a factor of Q^2.

Slug Flow in Chromatography

Slug flow in chromatography is a hypothetical analog of bolus flow in segmented flow system. Giddings (60) provided an expression of dispersion for an analogous case in coated tubes. That is,

$$H = \frac{(1 - R)^2 a^2 u}{4D} \tag{95}$$

where R is the retention factor which represents the fraction of total sample within the column that is not contained in the moving liquid phase or segments. Giddings' equation was used by Snyder and Alder (61) for developing their dispersion model in segmented continuous flow system.

CHAPTER III

DISPERSION IN CONTINUOUS FLOW ANALYSIS

Segmented Version

Sample dispersion in segmented continuous flow analysis can be il-
lustrated by the following figure (Figure 9). Due to the longitudinal
dispersion and mixing of analyte molecules along the flowing stream the
output signals lose the discreteness of the input samples.
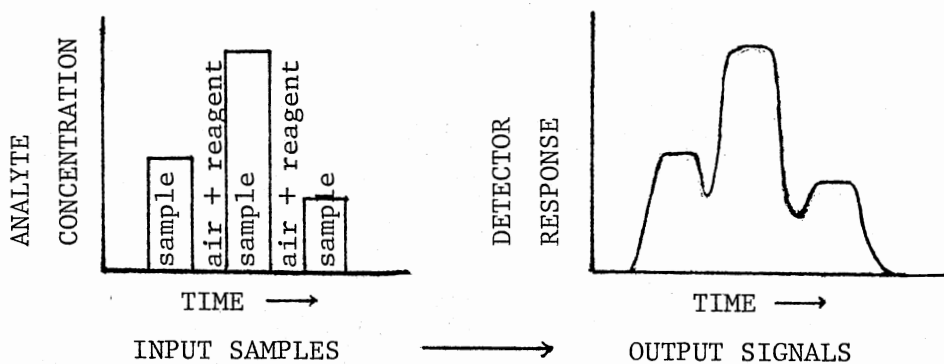
Figure 9. Illustration of Sample Dispersion in Segmented
Continuous Flow Analysis (Adapted from
Reference 62)

Sample dispersion is required for the analytical processing of the
sample. Excessive dispersion, however, causes large sample carry-over.
To avoid sample overlapping resulting in poorly resolved signals,

the intersample wash time can be increased at the expense of reducing
sampling rate. This approach will also further reduce the "plateau"
time on the top of the response signal and eventually results in a sig-
nal maxima that are not at a steady state. Obtaining signals at steady
state is considered essential for maximum precision of the determina-
tion[1], thus it was suggested to avoid the non-steady state output when-
ever possible (62).

Sample dispersion in segmented continuous flow analysis is concep-
tually similar to certain other processes of interest to analytical
chemists, such as the countercurrent distribution and chromatography.
Early attempts at describing dispersion in segmented flow systems were
limited to empirical relationships, and offered very limited insight in-
to the dispersion process (63 - 66).

A set of mathematical models was developed to predict the concen-
tration distribution along a line of sample segments, namely, linear
model and non-linear model (67 - 71). These two models are the funda-
mental basis of the dispersion theory in segmented flow analysis, and
will be described briefly in the following sections.

Linear Model

In an air-segmented flowing stream, assuming that the segment #0
contains originally an undiluted sample of concentration C_0 while the
segment #1 contains C_1 ($C_1 < C_0$), and all following segments contain no
sample.

---

[1]However, in an unsegmented flow injection system highly reproducible
signals (with error less than 1%) can be obtained with precise sample
injection technique and controlled dispersion process.

As sample #1 pushes segment #0 forward as the flow progresses, segment #1 gains concentration by taking up the wall deposit from segment #0. In the mean time, segment #1 loses concentration to segment #2. Because the loss is replaced by a gain of higher concentration, C_1 increases with time. Neglecting the longitudinal diffusion in the tubular layer on the wall and assuming that instantaneous and complete mixing occurs in the liquid segments, the change of C_1 with time can be expressed as

$$C_1 = (1/V_s)(R_\alpha t \cdot C_0 - \int_o^t R_\alpha C_1 dt) \tag{96}$$

where R_α is the rate of the wall deposit influxes and effluxes into and out of each segment (ml/sec) and V_s is the volume of each liquid segment (ml).

A more complex situation prevails in segment #2, because the concentration of its inflowing stream, segment #1, exponentially changes with time instead of being constant. Segment #3 receives an even more complex influx than segment #2, and so on. Thus,

$$C_2 = (1/V_s)(\int_0^t R_\alpha C_1 dt - \int_0^t R_\alpha C_2 dt) \tag{97}$$

$$C_3 = (1/V_s)(\int_0^t R_\alpha C_2 dt - \int_0^t R_\alpha C_3 dt) \tag{98}$$

For segment #(n + 1) the change of concentration with time is

$$C_{n+1} = (1/V_s)(\int_0^t R_\alpha C_n dt - \int_0^t R_\alpha C_{n+1} dt) \tag{99}$$

thus

$$(dC_{n+1}/dt) = (C_n - C_{n+1})(R_\alpha/V_s) \tag{100}$$

By integrating the mass transfer process occurring in each segment over the entire length of the tubing, the resulting concentration in these segments can be described by a Poisson distribution. That is

$$C_{n+1}/C = 1 - e^{-q}\{1 + q + \frac{q^2}{2!} + \frac{q^3}{3!} + \cdots + \frac{q^n}{n!}\} \qquad (101)$$

where q is a constant defined as

$$q = (R_\alpha t/V_s) = (V_f/V_s) \qquad (102)$$

and V_f is the total volume of liquid film deposited from any segment during its passage through a given tube.

The linear model assumed that the rate at which liquid films influx into and efflux out of each segment are constant and independent of concentration. This assumption has limited the use of the linear model. Therefore a more general model, the non-linear model, was developed.

Non-Linear Model

This model generalizes the situation where the rate of the liquid film transferring between liquid segments is not a constant and depends on sample concentration.

In this model R_α is given by:

$$R_\alpha = k_1 + k_2 C \qquad (103)$$

where k_1 and k_2 are constants.

A non-linear model for predicting concentration distribution along a line of segments is then expressed as follows.

$$(R_{n+1}t/L) - (R_n t/L) = d(V_s)_{n+1}/d\ell \qquad (104)$$

where L is the length of the tube and ℓ is the distance that a liquid segment was travelled; Thus

$$C_{n+1}(R_{n+1}t/L) - C_n(R_n t/L) = d\{(V_s)_{n+1}C_{n+1}\}/d\ell \qquad (105)$$

which can only be solved by numerical integration method.

The major shortcoming which is common to both linear and non-linear models is their inability to predicting dispersion as a function of experimental parameters. To compensate this shortcoming Snyder et al. (50, 61, 62, 72) developed two models, based on the above, called the ideal and non-ideal models for use in the design of high-speed continuous flow systems.

Ideal Model

The ideal model was derived from Begg's linear model but ruling out the non-linear dispersion arising from a change in liquid surface tension as the sample concentration varies, since such effects are counter-acted in normal practice by the addition of a surfactant.

Assuming that there is a perfect mixing within each moving liquid segment, from Equation 101 the following equation is obtained:

$$C_k/C_0 = e^{-q}q^k/k! \qquad (106)$$

where

$$q = V_f/V_s = 2\pi a\phi L/\pi a^2 Ls = 2L\phi/aLs \qquad (107)$$

C_k is the concentration of sample in k-th segment, Ls is the length of a liquid segment, and ϕ is the average thickness of the liquid film.

To complete the derivation of the ideal model, the parameter, ϕ, is converted to some measurable parameters. Concus (73) and Levich (74) provided a theoretical value of ϕ for the case of perfectly-wetted (0° contact angle), small diameter tube, that is

$$\phi = 1.34a(u\eta/\gamma)^{2/3} \tag{108}$$

where u is the linear velocity, η is the viscosity, and γ is the surface tension. Substituting Equation 108 into Equation 107 yields:

$$q = 2.68a^2(u\eta/\gamma)^{2/3}\pi L/Vs \tag{109}$$

By comparing the derived value of q with a theoretical value and using the data calculated from Equation 106 the comparison showed consistent agreement, except that all q values were lower by 0.68 unit. Consequently, Equation 108 and Equation 109 are corrected to

$$\phi = 1.0a(u\eta/\gamma)^{2/3} \tag{110}$$

$$q = 2.0\pi a^2 L(u\eta/\gamma)^{2/3}/V_s \tag{111}$$

For a Poisson distribution model, q represents the retardation of the center of the original sample distribution for a single sample segment, thus q equals the variance, σ_i^2, of the resulting dispersed sample concentration distribution, that is

$$q = \sigma_i^2 \tag{112}$$

As the mixing within the liquid segments slows down, the sample displacement, equal to q, is expected to remain constant, but sample

dispersion will increase as does the variance. Hence

$$\sigma^2 > \sigma_i^2$$

where σ^2 is the variance resulting from slow mixing. This leads to a
more generalized treatment of the matter, namely, the non-ideal model.

Non-Ideal Model

In a segmented continuous flow system transport of the analyte sample
in discrete sample zones is commonly referred to as a bolus flow. The
mixing in a bolus flow has an unique pattern. As Figure 10 shows the
injected sample disperses into a characteristic 8-shape pattern. The
sample starts from the center axis and immediately disperses along
the edge of the liquid segment, slowly moving into adjacent regions
of streamlines.
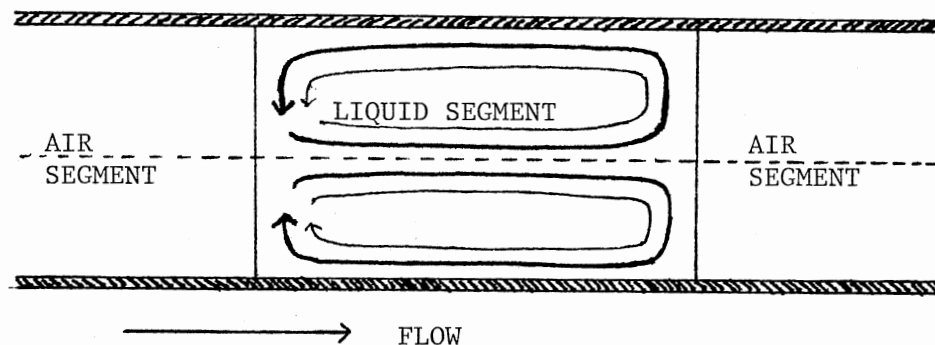
Figure 10. Diagrammatic Representation of the Dispersion
Pattern Within a Moving Liquid Segment for
Bolus Flow (Adapted from Reference 61)

Since bolus circulation prevents mixing across streamlines, longitudinal mixing within the segment is rapid, while radial mass transfer is slow. The latter occurs by a combination of molecular diffusion plus convective mixing. Since longitudinal mixing is fast in bolus flow, it does not alter the part of dispersion that is predicted by the ideal model. On the other hand, the slow radial mixing increases the predicted dispersion value. Let σ_r^2 be the variance caused by slow radial mixing, then the total variance of the system

$$\sigma^2 = (\sigma_i)^2 + (\sigma_r)^2 \tag{113}$$

Recall the equation describing a hypothetical analog of bolus flow, called a slug flow, which was developed in chromatography, i.e. Equation 95

$$H = (\sigma_{r,x})^2/L = (1 - R)^2(a)^2 u/4D$$

where $(\sigma_{r,x})^2$ is the variance expressed in length units and R is the retention factor. Snyder and Adler (61) assumed the validity of this equation for bolus flow under the following conditions:

i. The diffusion coefficient, D, is replaced by an effective diffusion coefficient, D' which includes the additional mass transfer between streamlines as a result of convective mixing.

ii. Only one of the two symmetrical lobes of the bolus flow is compared with slug flow, therefore the effective radius, a', of the hemicircle that comprises the cross-section of a single bolus lobe, is approximately equal to (2/3)a.

Applying these assumptions to Equations 110, 111, and 95, Snyder and Alder obtained

$$\sigma_r^2/q = \pi a^4 u^{5/3} \eta^{2/3}/(4.5 D' V_s \gamma^{2/3}) \qquad (114)$$

Equation 114 can be modified to reflect the dependence of D' on η. That is,

$$D' = D'_{w,25}(\eta/0.0089)^{-1.7} \qquad (115)$$

where $D'_{w,25}$ refers to the value of D' at 25°C with water as the reference, and

$$\sigma_r^2/q = \pi a^4 u^{5/3} \eta^{7/3}/(1.71 \times 10^{-3} D'_{w,25} V_s \gamma^{2/3}) \qquad (116)$$

Combining Equations 112, 113, and 116, the resulting dispersion equation is

$$\sigma^2 = (\frac{\pi a^4 u^{5/3} \eta^{7/3}}{1.71 \times 10^{-3} D'_{w,25} V_s \gamma^{2/3}} + 1)\{2\pi L a^2 (\frac{u\eta}{\gamma})^{2/3} (\frac{1}{V_s}) \qquad (117)$$

the non-ideal model equation allows the prediction of sample dispersion in segmented flow over a broad range of experimental conditions.

Application of Dispersion Models to Extra-Column Band Broadening

Consider the case of a reaction colorimeter used as the detector in high performance liquid chromatography as shown in Figure 11.

Based on Equation 117 Snyder (50) derived an expression of dispersion for this system represented in Equation 118.

$$\sigma_t^{\,2} = \{\frac{272.6a^{2/3}(F + 7.36a^3\varepsilon)^{5/3}\eta^{7/3}}{D'_{w,25}F\gamma^{2/3}} + \frac{1}{\varepsilon}\}\{\frac{2.35(F + 7.36a^3\varepsilon)^{5/3}\eta^{2/3}t}{2.52a^{4/3}F\gamma^{2/3}}\}$$

(118)

where $(\sigma_t)^2$ is the variance measured in time units, ε is the air seg-
mentation frequency per time unit, and F is the flow rate of the liquid
stream (ml/sec).
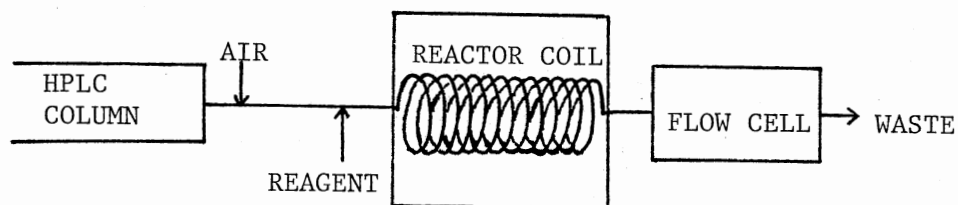
Figure 11.   An Extra-Column Reaction Colorimeter for HPLC
(Adapted from Reference 50)

Equation 118 can be used for optimizing the values for the segmen-
tation frequency and the flow rate so as to yield a desired degree of
dispersion. However, it predicts smaller σ_t than are found in practice.
Because of the need to eliminate bubbles by either electronic (75) or
physical (1) means, the additional mixing in the debubbling device re-
sults in an increase in σ_t. Usually a 10% increase for physical de-
bubbling (76) and a 25% increase for electronic debubbling (77).

Unsegmented Version

As mentioned previously, flow injection analysis (FIA) is a new
concept of continuous flow analysis of discrete samples. Ruzicka and

Hansen (79, p.6) have indicated that "Flow injection analysis is based on the injection of a liquid sample into a mixing, nonsegmented continuously moving carrier stream of a suitable liquid[2]." The injected sample forms a zone, which is then transported toward a detector which continuously records the absorbance, electrode potential, or other physical parameter as it continuously changes as a result of by passage of the sample material through the flow cell. Since the quality of the readout in FIA determines the usefulness of the technique and the quality of the readout depends on the "form" of the travelling sample zone, controlling the dispersion of the sample zone becomes one of the major tasks in FIA.

The theory of dispersion in FIA is not well developed. Although there are a vast number of papers published every year in the area of FIA, most of them deal only with the applications of the technique. Very few discuss the theoretical basis of controlled dispersion. The dispersion models developed in chemical engineering have been frequently adopted for setting up guidelines of controlled dispersion. But the major concern in chemical engineering is the yield, where in FIA, the primary function has been to automate wet chemical methods. The major concern is the quality of the analytical readout, namely method sensitivity, reproducibility, and sample throughput rate.

---

[2]However, Ramasamy, Jabbar, and Mottola (80) have successfully adapted the FIA technique to an all-gas system with detection at a gas-solid interface.

From Turbulence to Laminar Flow – Early

Stage of FIA

Because of differences in physical properties, such as density and viscosity which determine the inertial and viscous forces for a flowing stream, the flowing fluid can exhibit either turbulent or laminar characteristic. Laminar flow fixes the fluid elements in well-defined streamlines. That is, elements at the center axis of the tubing move at twice the average flow velocity while the elements at the walls hold still. On the other hand, when fluid elements are randomly fluctuating in the form of eddies, the flow is said to be a turbulent flow.

Before 1977, Ruzicka and Hansen (4, 81) recognized that turbulence is the key to control of band spreading in a fluid stream. They recommended turbulent flow stream in FIA was essential for avoiding sample carry-over by yielding a flat velocity profile. They opposed the use of laminar flow simply because the parabolic flow profile leads to rapid axial mixing which is seen as peak spreading. They soon abandoned this viewpoint, however, when they found a contradictory result. The fact that dilution decreases with decreasing pumping rate opposes the expectation of using turbulent flow in FIA (82).

The quantity that is frequently used to differentiate the flow as laminar or turbulent, is the Reynolds number. The Reynolds number, Re, is commonly recognized as the ratio of the inertial forces to the viscous forces. For very dilute aqueous solutions, Ruzicka et al. (83) defined the quantity to be:

$$Re = 10.6(F/a) \tag{119}$$

where F is the flow rate (ml/min) and a is the tubing inner radius (mm).

In general when Re is less than 1000 the flow is said laminar. Turbulent flow has Re value greater than 2000, while the intermediate values (1000 - 2000) represent an incipient turbulent flow.

At large Re($>10^4$) the chaotic movement of the elements of the fluid causes the dispersion in all directions to be similar in magnitude, yielding a flat velocity profile and dispersion is minimized. At very small Re ($\simeq 0.1$) the parabolic velocity profile of the laminar flow is averaged by the radial molecular diffusion and dispersion is also prevented. However, Ruzicka et al. recognized that the velocity profile is not the only factor influencing the band spreading. Tube length also has a significant effect on peak spreading. Consequently, they realized that turbulent flow is not a necessary condition for achieving the preservation of discrete sample patterns in an unsegmented flowing stream. As a matter of fact, laminar flow is more preferable not just because it can provide a well-defined sample zone, but because it also provides the advantages of reducing reagent consumption and eliminating the need for high pumping pressure.

Dispersion in FIA

Effective dilution of a sample in FIA is dependent on the dispersion processes occurring as the sample travels between the point of injection and the point of detection. Dispersion is the result of the diffusion and convection in axial and radial directions. The nature and the magnitude of the dispersion depend on physical parameters of the flow, mechanical parameters of the manifold, geometry of the reactor, and chemical factors.

van den Berg et al. (84) stated that:

> . . . axial dispersion should be kept as low as possible, be-
> cause it adversely affects the sample integrity and the
> throughput, it also causes sample dilution and thus decreases
> the sensitivity of the method (p.91).

Ranger (85, p.22A) in a recent review article stated that "it is radial rather than axial dispersion that contributes most significantly to sample dispersion in flow injection analysis systems." They both ruled out the type of flow injection systems in which the axial dispersion is the dominant force of dispersion, particularly in those systems where a stretched-out long sample zone is required, such as in flow injection titrations[3].

For laminar flow in a cylindrical tubing, the axial dispersion results from diffusion and convection. Axial diffusion is a spontaneous molecular movement from higher concentration regions to lower concentration regions. Convection arises from the parabolic movement of the flowing fluid. Thus the magnitude of it is directly proportional to the mean velocity of the fluid, $\bar{u}$. Radial dispersion results from molecular diffusion. For laminar flow with parabolic profile, transport of solute occurs radially from the slower moving regions at the mean velocity of the sample zone, to the faster moving stream at the center axis. A diagrammatical representation of the effects of convection and diffusion on the concentration profile of the injected sample is given in Figure 12.

Radial dispersion dictates the peak height obtained, thus it is intimately related to the analytical sensitivity, while axial dispersion dictates the spreading of the signal and is related to the sample

---

[3]Pardue, H. L. has initiated an argument about the term "FIA titration" whether it is appropriate to be called titration, in discussion at the International Conference on Flow Analysis, Amsterdam, 1979. This term is still open to criticism.

throughput rate.

NO DISPERSION   CONVECTION   CONVECTION AND   DIFFUSION
                 PREDOMINANT   DIFFUSION   PREDOMINANT
                 DISPERSION   DISPERSION   DISPERSION
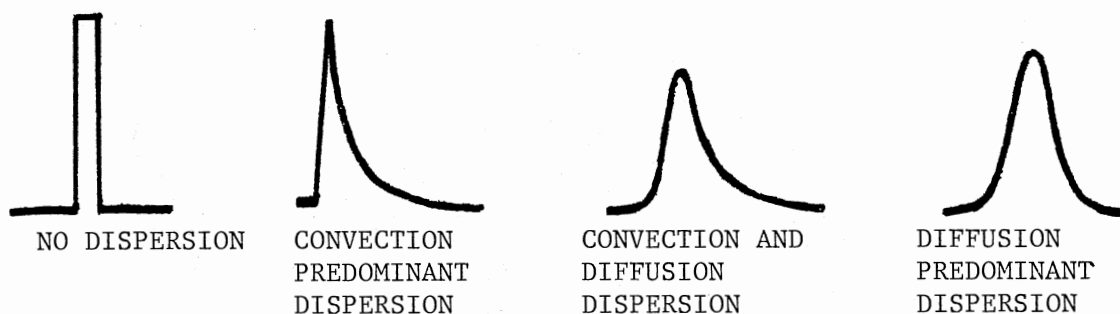
Figure 12.   Signals Obtained for Injected Samples Under Different In-
             fluences of Dispersion Force (Adapted from Reference 86)

The relative importance of axial and radial dispersion processes,
as suggested by Betteridge (86) in his review article, depends on the
flow rate, the radius of the tube, residence time, and the magnitude
of the diffusion coefficient. It should be mentioned here that
Betteridge left out one important factor, that is, the geometric shape
of the reactor tube, as it is commonly known that the radial dispersion
can be facilitated in a curved channel.

Dispersion Patterns

A convenient way of describing the dispersion pattern is to use the
concentration gradients formed when a sample "plug" is flowing in the
carrier stream through a narrow open tube. For all the variations in
flow parameters that one would encounter in FIA experiments, the value
of the concentration gradient varies in a wide range. Ruzicka et al.

(87) divided this range into three regions and called limited, medium, and large dispersion; each corresponds to a value range of the practical dispersion parameter, D ($D = C_0/C_{max}$).

Any dispersion has a negative effect on sampling frequency and sensitivity. The appropriate degree of dispersion in a flow injection analysis system, however, must be a compromise based on consideration of the degree of mixing desired, the sampling interval that can be accepted, the degree of completeness to which the reaction has to proceed, and most critically, the type of analytical readout one uses, i.e. peak height or peak width[4]. Based on this understanding, a general comparison among the limited, medium, and large dispersions is summarized in Table IV.

For applications where limited dispersion is needed, the flow injection system serves merely as a means of precise timing and transport. Compared to the manual batch techniques, the advantage of FIA would be higher sampling rates and better reproducibility.

Systems with medium dispersion are the most interesting from an analytical viewpoint as they can be applied to a large number of analytical procedures. In this type of determination, sufficient amount of mixing can be achieved by using mixing aids such as a mixing coil. Nevertheless, too short a residence time is frequently a problem which does not allow chemical reactions to proceed to the desired degree[7].

---
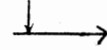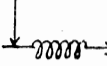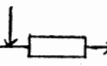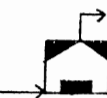
[4] In most FIA methods the analytical readout is based on measurement of the peak height. For FIA titrations, however, the analytical readout is based on measurement of the peak width (88, 89).

[7] Reijn et al.'s (95) single-bead-string reactor provides a sufficient amount of residence time without sacrificing the degree of dispersion.

TABLE IV

A GENERAL COMPARISON FOR THE LIMITED, MEDIUM, AND LARGE DISPERSION

Comparison / Dispersion type	D**	Reactor geometry used	Response signal shape	Tube Radius	Line length	Sample volume	Mixing device	Analytical readout	Applications	References
Limited dispersion	1 - 3			Small <0.5mm in i.d.	Short (L<l_s)	≥ $S_{\frac{1}{2}}$*	Not used (mixing is limited)	Peak height	pH, pCa or conductivity measurement of the original sample solution	90
Medium dispersion	3 -10			Small ~ 0.5-1.0 mm in i.d.	More flexible $D \propto (L)^{\frac{1}{2}}$	Depends on the geometry of the manifold	Depends on the chemistry involved; some degree of mixing is needed	Peak height	Color or complex formation; change of pH; adjustment of ionic strength etc.	90 91 92
Large dispersion	≥ 10			--	--	Depends on the volume of the mixing chamber	Use a mixing chamber	Peak width	Titration; kinetic measurement; multicomponent resolution	90 93 94

[5]This parameter, D, is defined as C_0/C_{max} where C_{max} is the concentration corresponds to the maximum of recorded peak.

[6]This quantity, $S_{\frac{1}{2}}$, is the volume of sample whose resulting D value is exactly 2.

Large dispersion is generally achieved by using a stirred gradient chamber which exhibits exponential dilution behavior over a large order of magnitude. Analytical applications such as a FIA titration were developed by utilizing the concentration gradient in interfacial regions between the sample and the carrier stream solution formed as a result of large dispersion. There are some non-traditional FIA processes derived from the concept of large dispersion. They are being found very useful in dealing with some special FIA problems such as: when samples are too high in concentration but advance dilution is inconvenient; when large dispersion is required but the sample volume used is too large to achieve it. These processes include merging-zone, stream-splitting (or called split sample zone), and zone-sampling processes.

Special Processes for Large Dispersion

Merging-Zone Process. For highly concentrated samples, effective and rapid mixing is desirable but at the same time too extensive dilution is to be avoided in order to maintain a certain sample throughput rate. Merging-zone is the approach developed for this use.

Reis et al. (96, p.309) defined an merging-zone concept as:"It is based on synchronized injection of sample and reagent into inert carrier streams, with further merging and reaction of the injected species." A schematic merging-zone set-up is given in Figure 13.

The merging-zone process has been adopted by many workers (96 - 99). An additional advantage is that the reagent consumption is reduced as it is only consumed when the sample is injected.

Stream-Splitting Process. This process can also be used for ana-
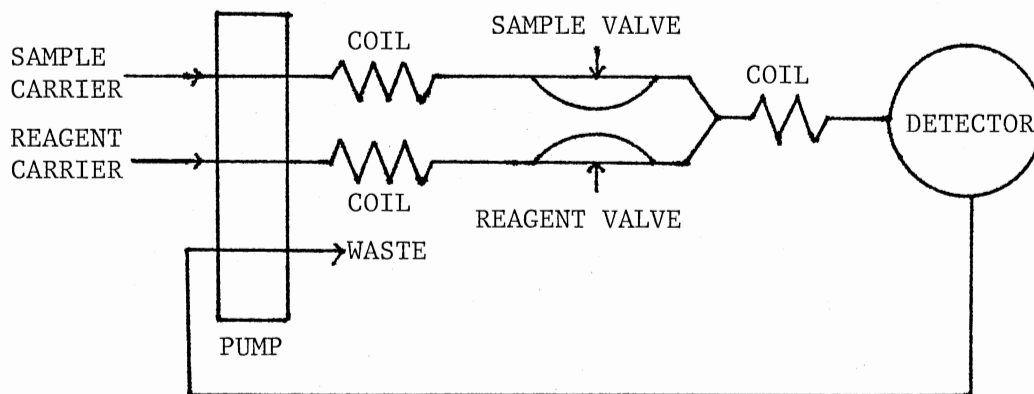
Figure 13. A Typical Merging-Zone FIA Set-Up
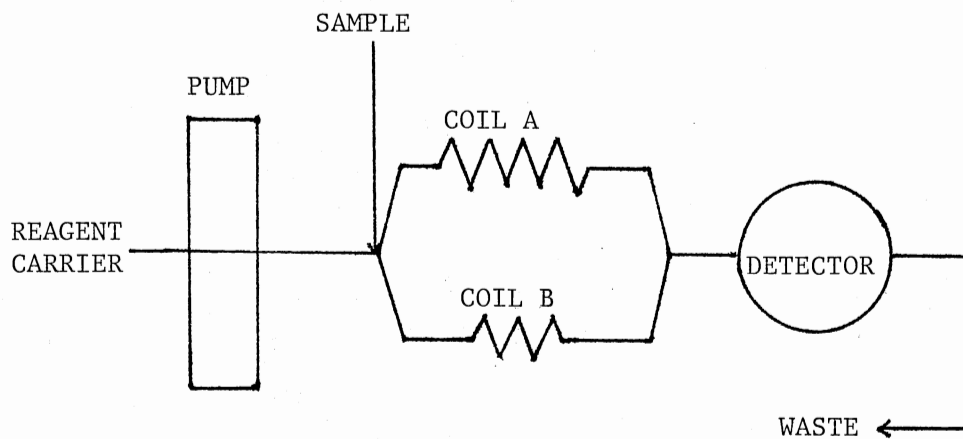
Figure 14. A Schematic Diagram for a Stream-Splitting
Process

lyzing highly concentrated samples.

A branched manifold in the immediate down stream from the sample injection port is used as shown in Figure 14. An injected sample plug is split into two streams each of which passes through a reactor of different size, then recombine just prior to the detector. The resulting peak is a split double peak; either peak height can be used for calibration.

Ruzicka et al. (100) claimed that the advantage of this technique is in providing expansion of the analytical range without loss of reproducibility. That is, it avoids the problem of lossing the analytical linearity at high concentrations.

Zone Sampling Process. A zone-sampling process achieves large dispersion by introducing a well-defined small portion of a dispersed sample zone into a second carrier stream. Figure 15 presents a general scheme of this process.
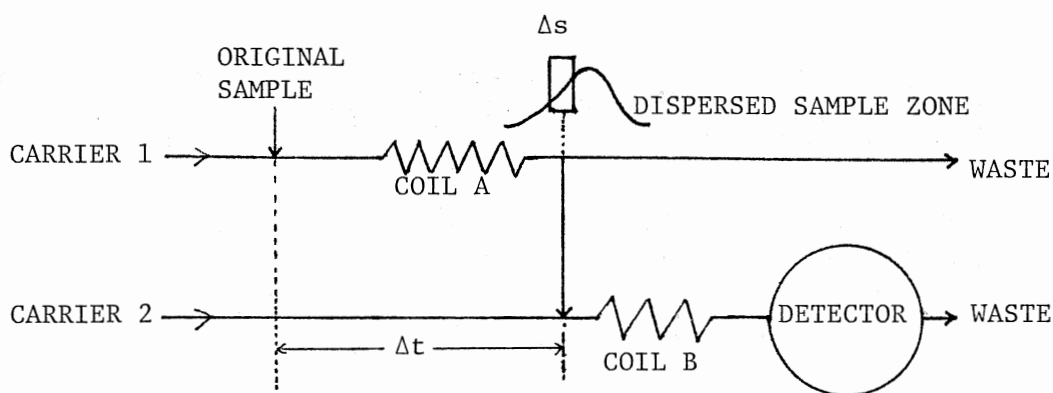
Figure 15. A General Scheme of Zone-Sampling Process

Reis et al. (101) discussed the applications of this process:

i. With two detectors set downstream of two carriers, this process can be used to simultaneously analyze two different species which require different degree of dispersion.

ii. Δs defines the size of the dispersed sample section that is injected into the second carrier stream, and Δt is the time elapsed between the introduction of the original sample and the transferring of the Δs to the second carrier stream. Using small Δs's and by varying Δt, as for a stepwise zone-sampling processes, a detailed study of the dispersed sample-carrier boundaries can be carried out.

By comparing with the stream-splitting process, the zone-sampling process seems to have the following two advantages:

i. It can be used for analyzing high concentration samples by providing a large dispersion without decreasing the sampling frequency, since only small portions of the injected sample plug are passed through the detector.

ii. It provides more flexibility in selecting the desired sample zones for different degrees of dispersion.

Dispersion Models

The dispersion models commonly adopted by FIA researchers are the Taylor's model, and the tanks-in-series model. Pungor et al. developed a model for use in a system where a mixing chamber is the primary contributor for the dispersion.

Taylor's Model. This model has the advantage of being the analog to the differential equation which describes a diffusion process in the

presence of convection. In the case of large L (tubing length) and small $\bar{u}$ (mean flow velocity), the solution for the concentration curve is a Gaussian type function, i.e.

$$C = (M/\pi a^2)(4\pi Dt)^{-\frac{1}{2}} \exp\{-(x - L)^2/4Dt\} \qquad (120)$$

Ruzicka and Hansen (102) have discussed FIA systems using the Taylor's model, and experimentally verified that

$$(C_o/C_{max}) \propto (t_m)^{0.5};$$

$$(C_o/C_{max}) \propto (L)^{0.5};$$

$$(C_o/C_{max}) \propto (a)^2$$

But Taylor's solution required the mean residence time, t_m, to be long in order to stabilize the radial concentration changes, i.e.

$$(t_m) \gg (a^2/14.4D)$$

or expressed in the reduced time

$$(\tau_m) \gg 0.07$$

where

$$(\tau_m) = (t_m)D/a^2$$

Lighthill (103), Ananthakrishnan et al. (36), and Golay et al. (51) all indicated that for Taylor's effect to develop, τ_m has to be larger than 0.8. For a normal FIA system with $D = 5\times10^{-5}(cm^2/sec)$ and a radius of 0.025(cm), the mean residence time has to be 100 seconds or more to satisfy this criterion.

Tanks-in-Series Model. Betteridge (86) recognized that the tanks-in-series model from chemical engineering is analogous to the concept of the height equivalent to a theoretical plate model for chromatography. It postulates that the reactor tube between the points of injection and detection consists of a number of well-stirred imaginary tanks of equal size in series. Thus

$$\frac{C}{C_o} = \frac{1}{\bar{t}_i} \left(\frac{t}{t_i} \right)^{N-1} \frac{1}{(N-1)!} \exp(-t/\bar{t}_i) \tag{121}$$

where $\bar{t}_i$ is the mean residence time in one hypothetical tank and N is the number of tanks containing the sample material.

The actual size of the imaginary tank is a function of tube dimensions and flow rate. Small N results in skewed concentration curves while very large N results in near Gaussian shape concentration curve with a variance

$$(\sigma_t)^2 = (t_m)^2/N \tag{122}$$

as given by van den Berg et al. (84).

The applicability of this model to a FIA system is best demonstrated by Figure 16 (95, 102, 104, 105). The longer a sample zone has travelled, the more spread out the sample zone becomes, and the resulting concentration curve is more Gaussian in shape which resembles the predictions of the tanks-in-series model shown in the same figure.

Comparing the two models just discussed, it becomes obvious that only for narrow and long reactor tubing and slow flow rate does Taylor's dispersion model provide an appropriate approximation. For other conditions the tanks-in-series model seems to provide a better theoretical
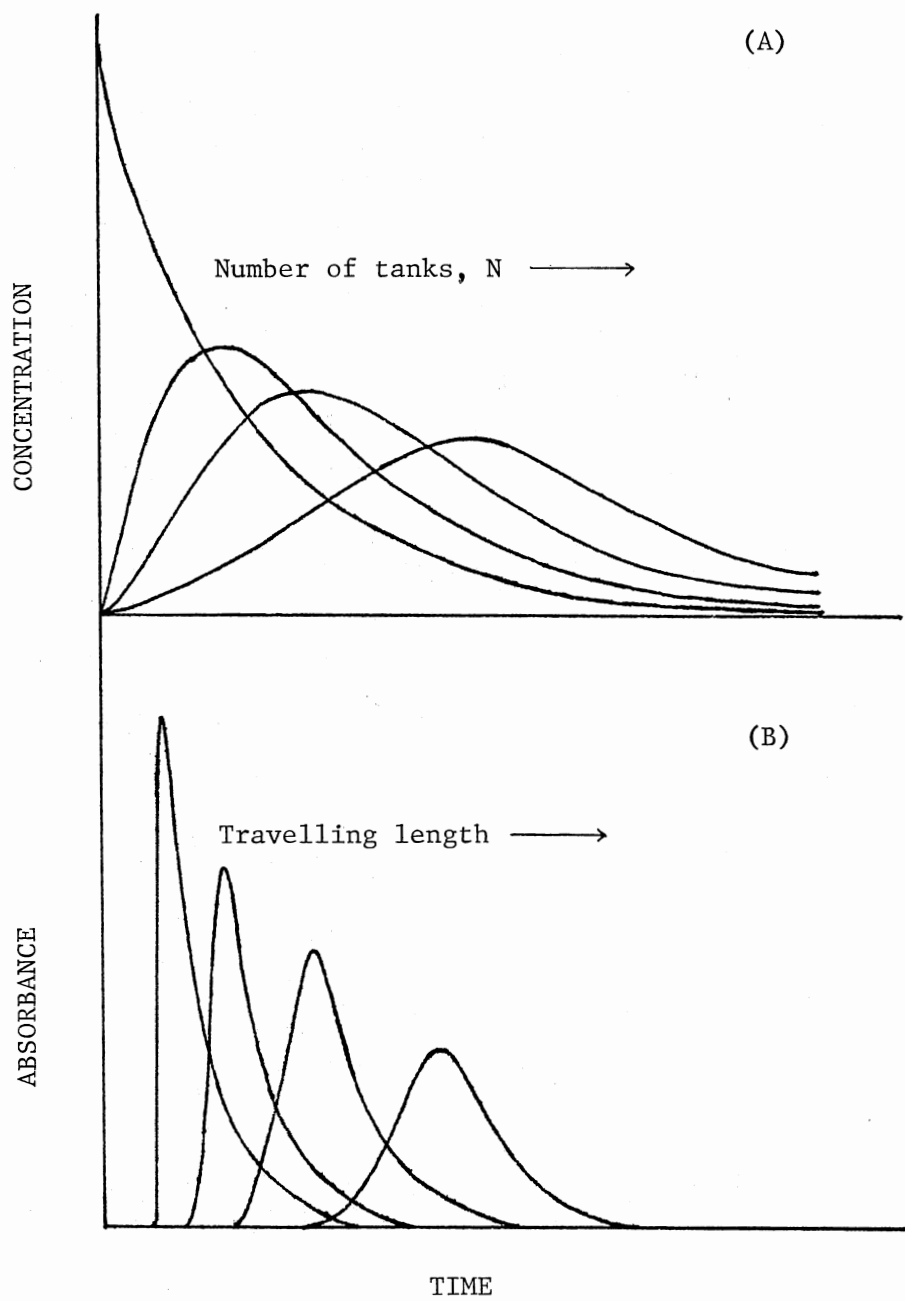
Figure 16. Comparison of Tanks–In–Series Model (A) and
Dispersion Signals in a FIA System (B)
(Adapted from References 79 and 106)

basis for the investigation of dispersion. Furthermore, the tanks-in-series model seems to be the best for use in a reactor vessel with uniformly repeated pattern of structure such as a jet mixer and a single-bead-string reactor.

Pungor's Model. Pungor et al. (107) derived the following equation to describe the concentration change with time as the result of sample dispersion caused by a mixing chamber:

$$\frac{d\Delta C}{dt} = \frac{F}{Vm} \left\{ \frac{M}{2A'(\pi D_{eff} \cdot t)^{\frac{1}{2}}} \exp\left(- \frac{1}{4D_{eff}} \left(\frac{L}{t^{\frac{1}{2}}} - \frac{Ft^{\frac{1}{2}}}{A'}\right)^2\right) - \Delta C \right\} \tag{123}$$

where V_m is the volume of the mixing chamber, and D_{eff} is the effective diffusion coefficient. D_{eff} is not a simple physical constant defined by one process only, but an effective parameter which describes the simultaneous effect of serveral processes, such as molecular diffusion, convection, etc. D_{eff} depends not only on the tubing radius and flow rate, but also on the microscopic properties of the injected and carrier solutions. The easiest way of determining D_{eff} is the fitting of model described by Equation 123 to experimental detector signal versus time curve, which is a time consuming process. In addition, the assumptions that a mixing chamber is used and the sample and carrier solution are homogenized in the mixing chamber instantaneously and completely have limited the use of this equation.

Simple Expressions for Dispersion

Table V lists the parameters that have been used for measuring sample dispersion in a simple, quantitative manner.

σ_t was derived from a chromatographic formula but with zero parti-

TABLE V

DISPERSION PARAMETERS IN FIA

Dispersion parameter	Symbol	Expression	Applications (A.) & limitation (L.)	Ref.
Standard deviation in time units	σ_t	$\left(\dfrac{\pi a^4 L}{24DF}\right)^{\frac{1}{2}}$	A. provide information for peak broadening L. axial diffusion is ignored, so can be applied only for rather symmetric curves	50
Practical dispersion	D	C_o/Cmax	A. can be used to determine limited, medium, and large dispersions A. extent of the dilution of a sample in carrier is known L. no information for the shape of the peak L. no information about the peak broadening	101
Travel time	t_A	$\dfrac{109a^2 D^{0.025}}{f}\left(\dfrac{L}{F}\right)^{1.025}$ f - correction factor	A. residence time measurement A. diffusion coef. determination L. no information for peak shape and peak sensitivity L. axial diffusion is ignored L. sample size restricted	108
Time for baseline to baseline	Δt_B	$\dfrac{35.4a^2 f}{D^{0.36}}\left(\dfrac{L}{F}\right)^{0.64}$ f - correction factor	A. provide information for peak broadening A. diffusion coef. determination L. no information for peak shape and peak sensitivity L. axial diffusion is ignored L. sample size restricted	108
The time to reach the peak maximum The time to return to baseline	tmax t_{bas}	$\dfrac{\ln k_2 - \ln k_1}{k_2 - k_1}$ $t_{bas} = \mathcal{T}/k_1$	A. can be used to estimate the reaction rate constants for either $\begin{cases} (A) + B \xrightarrow{k_1} C \\ C + (X) \xrightarrow{k_2} P \end{cases}$ or $\begin{cases} (A) + B \xrightarrow{k_1} C_D \\ C_D \xrightarrow{k_2} C' \end{cases}$ L. the original work involved direct injection into detection area	109

tion coefficient since a stationary phase is absent (in an open tube)
(78). From the expression of σ_t, it is clear that dispersion in FIA
can be significantly reduced by using smaller diameter tubing. In-
creasing the flow rate should also decrease the dispersion. However,
the ultimate decrease in tube diameter and increase in flow rate are
limited by the pressure drops that a FIA system can withstand.

In 1977, Ruzicka et al. (82) proposed a parameter called the di-
lution factor, , which is taken as the ratio of the peak heights ob-
tained at the detector and at the point of injection. A year later they
defined the reciprocal of this factor as the dispersion of an FIA system
(102), that is

$$\mathbf{D} = C_0/C_{max} = \{(\text{constant } 1)(H_0)\}/\{(\text{constant } 2)(H_{max})\} \qquad (124)$$

If Beer's law is obeyed in the concentration range of both C_0 and C_{max},
and the recorder's response is linear throughout the region of H_{max} and
H_0, then, $\mathbf{D}$ can be simplified to

$$\mathbf{D} = H_0/H_{max} \qquad (125)$$

where H_0 is the signal height obtained with undispersed original sample
and H_{max} is the signal height which corresponds to the peak maximum.
Thus $\mathbf{D}$ describes not only the degree of dilution of the original sample,
but also the ratio in which the sample has been mixed with the reagent
carrier stream. But it does not provide any information about the shape
of the signal nor the time for returning to baseline which is a primary
factor for determining the sample frequency and sample carry-over. For
the reasons that $\mathbf{D}$ can be measured easily and it provides an instan-
taneous information on the degree of dilution, $\mathbf{D}$ is more appropriate to

be named the "practical dispersion".

For an extraction-FIA system Karlberg et al. (110) adopted Ruzicka et al.'s D for the measurement of overall dispersion. They specified that in two-phase FIA (organic and aqueous phases), D must be regarded as an "apparent dispersion", since Cmax also depends on the extraction process in the reactor tubing.

The t_A and Δt_B expressions derived by Vanderslice et al. (108) were based on the Ananthakrishnan et al.'s numerical solution for the dispersion equation discussed previously. t_A is the time taken from injection to initial appearance of a peak at the detector. Δt_B is the total time for the observation of the peak which can also be referred to as t_{bas} (109). These two time-based expressions were derived under the conditions where the axial molecular diffusion is negligible, that is, for $0.1 < \tau < 0.5$ and $N_{pe} > 5\times10^4$.

The fact that Δt_B was found insensitive to the sample size is a surprising result since Ruzicka and Hansen have demonstrated in their work that both peak height and peak width increase with increasing sample size. However, the sample sizes used by Vanderslice et al. are less than 20% of the total reactor volume, without the contribution from axial molecular diffusion. There may not be significant increase in Δt_B while the sample size was increased from 5% to 20% of the total system volume.

The major limitation for these two expressions is the lack of correct estimation for the f value. a factor which corrects for different experimental conditions: either concentration or detector sensitivity. It has a range of $0.5 - 1.0$ [8]. From Vanderslice et al.'s experimental results, we see that f has a value 0.800 for 1.07 (mm) di-

ameter tubing while it increases to 0.932 for 0.46 (mm) diameter tubing,
thus f seems to be a factor that varies with any change in experiments.

Mottola and Hanna's (109) t_{max} and t_{bas} parameters for evaluation
rate proportionality coefficients of two consecutive first order re-
actions were based on chemical kinetics models. It seems to provide a
very useful tool for the kinetic application of FIA technique. The flow
rate needs to be optimized, which is common for any FIA system, in order
to obtain an optimized transient signal profile. The flow cell geometry
should also be constructed in such a way that it provides enough mixing
for the injected sample and reagent carrier stream.

As a summary, Ruzicka et al.'s **D** measures the degree of radial dis-
persion while Vanderslice et al.'s Δt_B, Snyder's σ_t and Mottola et al.'s
t_{bas} measure the degree of axial spreading in a tubular flow system.
Because the dispersion in FIA is such a complicated process the result-
ing signal output varies in its shape in ascending curve, descending
curve, peak height, peak width and even a double-humped peak is observed
under some experimental conditions. Use of any one of the parameters
listed in Table V for describing the whole dispersion process by itself
is oversimplifying the subject. With understanding of the limitations
and applications for each dispersion parameter, however, it is possible
to find out the necessary guidelines in designing a FIA system to suit
specific purposes.

---

[8]One of the authors, Stewart, K. K., stated that the f values are
always close to unity in practice, during the 1981 ACS meeting, N. Y.
August, 1981.

Influence of Sample Volume on Dispersion

Gine et al. (111) emphasized that the dispersion of the sample is related to the volume injected. Stewart et al. (112) also mentioned that sample dispersion is partly controlled by sample volume. Betteridge (86) recognized that sample volume is a parameter of analytical importance and has a marked effect on peak shape, consequently, he critized Taylor's theory for not taking account of sample size. Actually, Taylor's (19) theory discussed two type of injections: For constant flow injection where infinite sample is injected continuously, only one interfacing profile is predicted, there is no need to discuss sample size. For injection of a short "pulse" sample, sample size is also irrelevant since the length of sample is negligible in comparing with the length of reactor within the framework of Taylor's treatment.

Ruzicka and Hansen have derived an analytical expression to demenstrate the relationship of sample volume and the corresponding peak shape. For a model FIA system where a solution of a dye with concentration C_O is injected into a colorless carrier stream, the rising part of the curve can be described by the equation

$$C = C_O\{1 - \exp(-\beta V_S)\} \tag{126}$$

where

$$\beta = 0.693/(S_{\frac{1}{2}})$$

with $S_{\frac{1}{2}}$ being the volume of sample solution necessary to reach 50% of the steady state, and V_S being the injected sample volume. As V_S becomes larger, C approaches the value of C_O until a steady state plateau is reached ($C = C_O$). Thus larger sample size contributes to improving

sensitivity and reproducibility of a response curve. Bergamin F° et al. (113) suggested that dispersion can be decreased by using larger sample volume. Increasing sample size, however, not only cause larger sample consumption and decrease in sampling frequency, but may also result in a split peak or a large peak with a shoulder due to insufficient mixing of the sample plug with the carrier stream.

Influence of Injection System on Dispersion

Ruzicka and Hansen (102) used an equation

$$\mathbf{D}_t = (\mathbf{D}_i)(\mathbf{D}_f)(\mathbf{D}_d) \tag{127}$$

to include the contributions to dispersion arising from: the injection system, $\mathbf{D}_i$, the reactor manifold, $\mathbf{D}_f$, and the detector, $\mathbf{D}_d$. Ruzicka and Hansen thought that $\mathbf{D}_i$ is only due to variation in sample volume (102) and type of injector used (116). They neglected the dispersion that may arise from the manner of injection which, however, has been recognized by Caro (29) and Pungor et al. (107). Although Nagy et al. (3) found in their experiments that the area under the peak was practically unaffected by the rate of injection over a range of 1 - 30 sec, this does not indicate that the peak shape (dispersion pattern) was not affected by the rate of injection. Reijn et el. (105) pointed out that an exact specification of the injection devices used in experimental flow injection analysis systems is necessary. They replaced the general definition of injection process which states that "injection of a given amount of sample in a flow system with volume flow rate." with two types of injection process (105, p.106):

i. The time injection, which is similar to the constant flow injection, except the sample is injected during a finite time, ΔT. Reijn et al. suggested an ideal syringe which can inject sample at a constant flow velocity. Although an ideal syringe is not possible in reality, with a precise timing controlled by a microprocessor[9], sample injection may be close to ideal.

ii. The slug injection where an ideal sample loop is used with a finite length L. This is similar to the bolus injection discussed previously.

Precise sample volume injection ensures good reproducibility. Furthermore, a minimum dead volume and a precise injection timing should keep the effect of injection on dispersion to a minimum.

Relationship Between Detection System and Dispersion

Two types of detection system are commonly used in flow injection determinations, namely, electrochemical detector and spectrophotometric detector.

Electrochemical Detectors. Because the current intensity obtained with a amperometric sensor depends on the rate of mass transport to the sensor surface, Pungor et al. (107) found that under suitable hydrodynamic condition, the response current in streaming solutions may reach considerably higher values than in stationary solution. This results from a thinner diffusion layer and results in an increase in

---

[9]A commercial unit, FiAtron SHS-200 (Milwaukee, WI 53209) is an example.

sensitivity. A further advantage is that the noise is smaller under the conditions of convective mixing.

Spectrophotometric Detectors. Spectrophotometric detectors usually provide integrating signals, thus the homogeneity of the solution in the direction perpendicular to the flow is not very important. With a non-integrating detector, such as an electrochemical sensor, which follows the concentration profile at a single point in the vessel, the concentration gradient in the radial direction affects the reproducibility of the measurements. To ensure a good reproducibility we can either create a rapid and total homogenization of the injected analyte and the flowing supporting electrolyte (3) or position the sensor exactly in the center of the parabolic flowing stream where the highest concentration occurs (114, 115).

Reijn et al. (105) classified the spectrophotometric detector as a mean value detector with

$$Cm = \int_0^a C(r)2\pi rdr/\pi a^2 \tag{128}$$

where Cm is the average concentration over the cross section of a tube, and the electrochemical sensor as the cup-mixing value detector with

$$C_{cup} = \int_0^a C(r)u(r)2\pi rdr/\pi a^2 \bar{u} \tag{129}$$

where C_{cup} is the bulk concentration at the detection point.

In addition, Meschi et al. (117) concluded that the response of an amperometric detector also depends on d_o where

$$d_o = 1 - (\delta_d/a) \tag{130}$$

and δ_d is the thickness of the diffusion layer at the surface of a tubular electrode

In most of the FIA systems radial diffusion is not sufficiently rapid to maintain radial homogeneity of the analyte species in the flowing stream, thus the output signal obtained with an integrating detector may have quite different shape from that of a non-integrating one. In addition the hold-up volume of a detector cell, especially a electrochemical cell, should be kept much smaller than the total volume of the reactor to minimize the dispersion arising from the detector.

Other Factors that may Affect the Dispersion

Ramsing et al. (118) found out that more viscous sample zones cause less tailing due to the faster wash-out time. Betteridge and Ruzicka (119) experimentally proved that the degree of mixing is a function of the viscosity of the sample solution. Consequently, there is a need to ensure that the viscosities of sample and standard solutions for calibration purposes are equal, or at least are maintained constant throughout the experiment.

Betteridge et al. (120) reported a problem observed with slow flow rates in a refractometric determination using FIA technique. They found that at low flow rates the peak height depends on the diffusion coefficient. At fast flow rates, however, problems are also observed in FIA systems with voltammetric and amperometric detectors. Pungor et al. (107) pointed out that when the rate of mass transfer to the electrode surface approaches the rate of charge transfer at fast flow rate, the calibration curve may become non-linear and the measured signal heights may become independent of sample concentration.

Double-Humped Peaks

Double-humped peaks have been observed experimentally (29, 51, 108, 121) and also revealed in Mayock and coworkers' (122), and Gill and Ananthakrishnan's (123) numerically simulated concentration-time curves.

Karlberg et al. (110) and Krug et al. (121) explained that the formation of double-humped peaks is due to imcomplete mixing of the injected sample with the surrounding reagent stream. Nevertheless, Karlberg et al. only observed the "double-humped" peaks for a large sample volume. This indicates that one may confuse a split peak with a double-humped peak, in which the former is due to imcomplete mixing arising from a too large sample volume while the latter does not relate to the sample size used.

A typical double-humped peak is shown in Figure 17. Caro (29) explained that the first hump is due to fast moving cones of the sample zone while Bate et al. (16) suggested that it may be due to the method of detection employed. Both suggestions are unclear and lack convincing interpretation. Gill and Ananthakrishnan (123), and Vanderslice et al. (108) found out that a double-humped peak occurs only when the flow condition changes from pure convection to pure diffusion. Maylock et al. (122) provided the best and the most reliable explanation for the formation of double-humped peaks. Their view of the two humps are that: the first peak is a manifestation of convection dominating in the central region of the tube, while the "gentle" second peak is the evolution of the diffusion shoulder which indicates a strong diffusional influence in the tube wall region. For the same τ value, Reijn et al. (95) observed

a double-humped peak with a straight tubing while a coiled tubing and a single-bead-string reactor did not give any double-humped peaks. Their calculated axial diffusion coefficients were

7.50×10^{-7} (cm^2/sec) for a straight tubing at $\tau = 0.28$;

1.69×10^{-7} (cm^2/sec) for a coiled tubing at $\tau = 0.28$;

1.15×10^{-8} (cm^2/sec) for a s.b.s.r. at $\tau = 0.28$.

It is obvious from these values that the enhanced radial mixing in a coil and s.b.s.r. reactors diminished the axial diffusion, smoothed out the unbalanced influences induced by convection at the central region and by diffusion at the tubing walls.
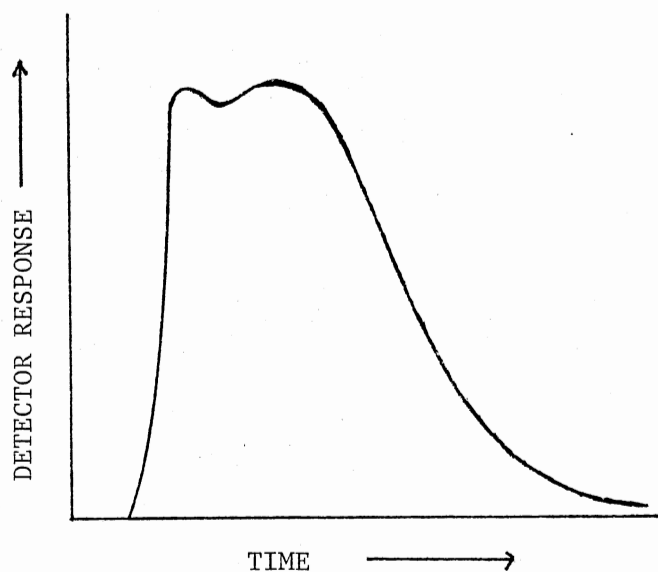
Figure 17. A Typical Double-Humped Peak

According to Vanderslice et al.'s (108) experimental observations slight pulsation or turbulence in the flow can smooth out the double humps, thus a reciprocating pump should be used rather than a syringe pump for a FIA system if a double-humped peak is not desirable.

Chemical Effect on Dispersion

Ruzicka and Hansen (79) have stated that

. . . the FIA response curve is a result of two processes, both kinetic in nature, the physical process of dispersion of the sample zone within the carrier stream and the chemical process of formation of chemical species (p.31)

The shape of a peak obtained in FIA which involves a chemical reaction should contain both information on physical dispersion of the injected sample zone into the carrier stream and information on the chemical re-action(s) taken place between the injected sample solution and the carrier reagent solution. In other words the nature of the chemistry involved should have some effects on the overall physical dispersion process. Experimental evidence about the kind of effects that a chemical reaction have on the shape of the peak (thus, dispersion) were provided by Painton and Mottola (126).

Pardue et al. (127) have discussed the chemical kinetic role in continuous flow titration. Rule and Seitz (128) discussed how the effect of flow rate on observed signal height and duration changes qual-itatively with slow and fast chemical reactions. Ranger (85) pointed out that the optimum response will be attained when a balance is reached between the degree of dispersion and reaction time for maximum sensitiv-ity. Hansen and Ruzicka (129) used the tanks-in-series model to demon-strate the difference in concentration profile with and without chemical

reaction contribution. Most of these works, however, were conducted in a rather qualitative manner.

A mathematical treatment of dispersion equations was presented in Ruzicka and Hansen's (79) book but no details of the chemical-dispersion kinetics interrelationship were discussed. Very recently, Reijn (130) described the influence of chemical kinetics on the FIA response curve in his thesis, yet, the entire work was based on a specific case, a single-bead-string reactor.

Reactor Geometry and Dispersion

Since large determination rates are the advantages of FIA, the use of straight tubing as the reactor may sometimes become impractical since it can cause peak broadening or provide insufficient residence time for chemical reaction(s) to take place as required by the method. Reijn et al. (95, p.1) stated that "the straight tubes are probably used for fast determinations of molecular dispersion coefficients only", this is, however, understating the use of straight tubing in FIA. Nevertheless, the use of other types of reactor geometry is rather common.

It has been mentioned that plug flow sets the upper limits for both analytical sensitivity and sample throughput rate. Thus, to improve the analytical efficiency of a method in FIA, the best way is to increase the plug flow characteristic in the flow. Levenspiel (106) pointed out that the classical advices for approaching plug flow are:

    i.   Turbulent flow;

    ii. Induce secondary flow by curving the flow path;

    iii. Disrupt the laminar flow by packing the reactor.

A general comparison for these three approaches with respect to a lami-
nar flow in straight cylindrical tubing is tabulated in Table VI. An in-
timate relationship between the radial dispersion enhancement and the
peak broadening inhibition is clearly illustrated in this table.

Dispersion due to Radial Diffusion. Radial diffusion is
the molecular displacement in radial direction. It counteracts the con-
vective spreading by trying to establish a uniform concentration distri-
bution of original sample and displacing it over a cross-section.
During the displacement a transition zone is formed in which the concen-
tration changes gradually, as shown in Figure 18. For slow radial dif-
fusion in a parabolic profile, the transition zone indicated by the 1%
and 99% equi-concentration surfaces extends to a long axial distance
which results in large peak spreading. For fast radial diffusion the
transition zone is much more flat, because concentration differences are
readily smoothed out. The sample zone "shrinks" down resulting in a
narrower signal.

Table VI indicates that the radial dispersion is not exclusively
enhanced by a turbulent flow, the axial dispersion is enhanced as well
and this opposes the decrease in peak broadening. In addition, turbu-
lent flow requires high pressure and results in large reagent consump-
tion. On the contrary, packed columns and curved channels offer more
advantage without paying the expenses of larger reagent consumption and
axial dispersion enhancement, thus are more frequently adopted by FIA
workers for improving analytical results.

Curved Channel Reactor - Open Coils. The use of coiled tubing to
decrease the peak spreading was discussed by many authors (50, 62, 132).

TABLE VI

COMPARISON OF TURBULENT FLOW AND CURVED CHANNEL, PACKED COLUMN
WITH RESPECT TO STRAIGHT TUBING IN A LAMINAR FLOW

Comparison / Approaches	Axial dispersion	Radial dispersion	Forces causing the enhanced dispersion	Required pressure drop	Reagent consumption	Residence time	Band broadening
Turbulent flow	Enhanced	Enhanced	Turbulence	Increased	Increased	--	Decreased
Curved channel	Not enhanced	Enhanced	Centrifugal force	Change is negligible	Less or no change	Change is negligible	Decreased
Packed column	Not enhanced	Enhanced	Eddy diffusion	Depends on the packing pattern	No change	Increased	Decreased

PARABOLIC FLOW PROFILE

99%   1%

SLOW RADIAL DIFFUSION PROFILE

99%   1%
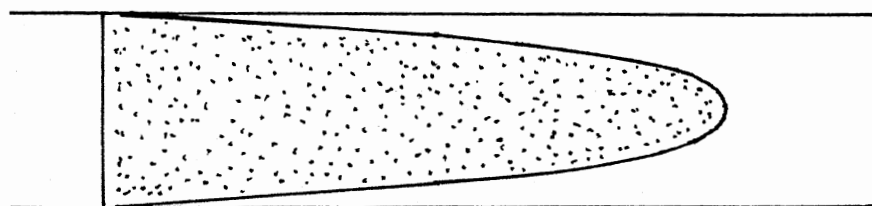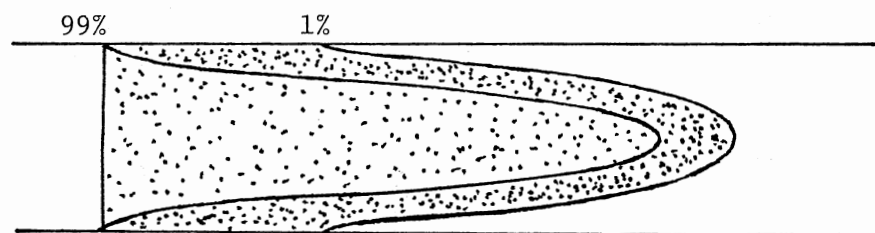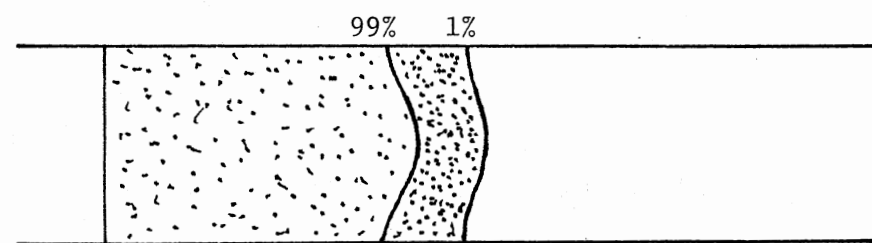
FAST RADIAL DIFFUSION PROFILE

Figure 18.   Influence of Radial Diffusion on the Para-
             bolic Flow Profile (Adapted from Refer-
             ence 131)

Experimental evidence has been provided by Tijssen (133), Painton and Mottola (126), and Stewart and Ruzicka (134).

Because of the centrifugal forces active in any curved flow channel a secondary flow which is perpendicular to the main flow is generated (133). In a laminar flow the secondary flow stimulates radial mass transfer and reduces velocity variation over the cross section. This results from forcing the central streamlines which are subject to greater centrifugal forces due to greater velocities to the outer walls (135). Consequently, peak spreading can be far less pronounced. This result is demonstrated in Figure 19. Because of the radial mixing enhancement the secondary flow is said to prevent sinking effects caused by molecules with higher specific gravity (29).
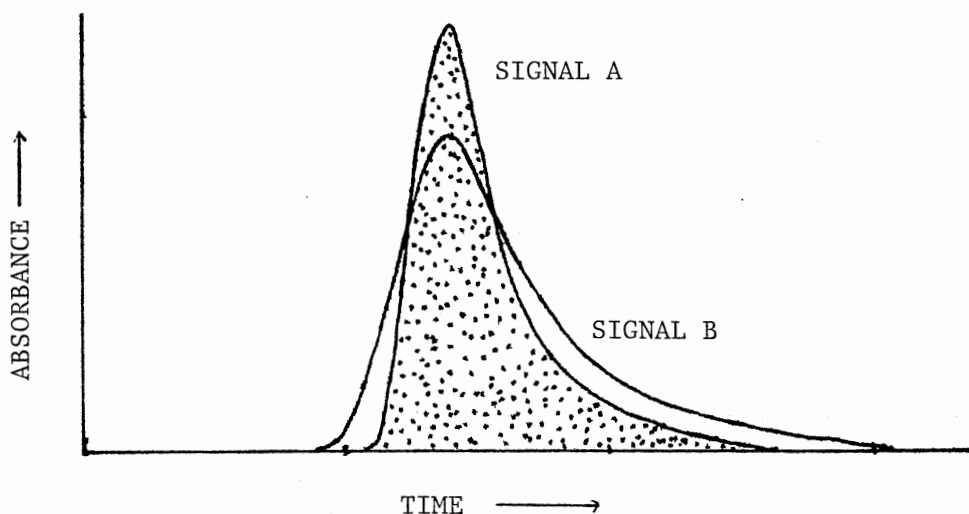
SIGNAL A: Obtained with a Coiled Tubing Reactor.

SIGNAL B: Obtained with a Straight Tubing Reactor.

Figure 19. Comparative, Superimposed Peaks Obtained with a
            Straight and a Coiled Tubing Reactors under
            Identical Experimental Conditions (Adapted
            from Reference 126)

Caro (29) has experimentally proved that the secondary flow effect is the largest at a flow with Reynolds number equal to 1000. Presumably because at Reynolds number smaller than 1000 the flow rate is too small to have effective centrifugal forces and induce a secondary flow, and at Reynolds number greater than 1000 the flow rate is too large to maintain its laminarity. However coiling tends to stabilize laminarity, the critical Reynolds number at which turbulence occurs is higher in coiled tubes than it is in straight tubes (59).

The secondary flow effect also depends on the tightness of the coil and the diameter of the tubing used to construct that coil. The secondary flow effect increases as the ratio of the coil diameter to the tubing diameter (curvature ratio) decreases (29, 84). Consequently, an effective coil is constructed tightly with a large diameter tubing[10].

The first theoretical study of flow in curved tubes was made by Dean (136, 137) who derived an approximate expression of the so-called dimensionless Dean number, Dn, for characterizing fluid flow in curved channel. That is

$$Dn = (\text{Reynolds number}) \times \left(\frac{\text{radius of the tubing}}{\text{radius of the coil}}\right)^{\frac{1}{2}} \tag{131}$$

A velocity parameter, $Dn^2 Sc$, was found related to the peak spreading in chromatography, and

$$Dn^2 Sc = 4a^3 \rho u^2 / \eta a_c D \tag{132}$$

---

[10]Too large diameter tubing causes larger axial dispersion, hence there is an upper limit within which the tubing diameter can be selected. Ruzicka and Hansen (102) concluded that only within the range of tube diameter smaller than 1.0 mm the dispersion is independent of the tube diameter for the same residence time.

where Sc is Schmidt number (Sc = $\eta/D\rho$), ρ is the density of the carrier stream, and a_c is the radius of coil (133). Let H be the plate height of a straight tubing, H_c be the plate height after coiling this straight tubing, σ_t^2 be the variance in time units for the straight tubing, and $(\sigma_t^2)_c$ be the variance in time units for the coiled tubing. Snyder defined a term, ξ, as the decrease in sample dispersion by coiling a straight tubing, that is

$$\xi = \{\frac{(\sigma_t)}{(\sigma_t)_c}\}^2 - 1 \simeq (\frac{H}{H_c}) - 1 \tag{133}$$

The change of (H/H_c) with Dn^2Sc was calculated by Tijssen (133). He concluded that at low Dn^2Sc value (< 10), $H = H_c$, and $\sigma_t = (\sigma_t)_c$, $\xi = 0$, and the coiling effect is negligible. At $Dn^2Sc > 10$, $H > H_c$, therefore $\sigma_t > (\sigma_t)_c$ and $\xi > 1$, the secondary flow develops gradually and is well established at $Dn^2Sc > 10^4$. At $Dn^2Sc = 10^9$, $H \simeq H_c \times 10^4$, $\xi \simeq 10^4$ which implies a substantial decrease in peak width by a factor of 100.

Snyder (50) found that the mass transfer coefficient for a solute of molecular weight 27, at 25°C in aqueous solution is four times higher in a coiled tubing than a straight tubing.

The use of coils has its limitations. White et al. (140) pointed out that the mixing coils function properly only when used in a horizontal position. This is probably because in a vertical position, the gravitational force in addition to centrifugal force would distort the radial mixing resulting from a curved channel.

Packed-Bed Reactor - a Special Case: Single-Bead-String Reactor.
Another approach for enhancing radial dispersion is to repeatedly disturb the streamline pattern by suddenly changing the direction of flow.

Packing a reactor tubing with an inert material of small spheres is the most practical way to obtain this effect (141).

Packed bed reactors have been used both by engineers and chromato-graphers. Usually very small particles are used for packing such that 5 < Pr < 50 where Pr is the packing ratio (the ratio of column diameter to particle diameter). Scott et al. (142), however, have used large size porous beads such that Pr is approaching unity, and called it " single-pellet-string reactor". Recently Reijn et al. (143) introduced a reactor packed with large size non-porous beads for FIA system and called it the "single-bead-string reactor" (s.b.s.r.).

The single-bead-string reactor is a device which provides efficient mixing (through enhanced radial diffusion) creating a longer residence time (by disturbing the parabolic profile). It retains the peak height but decreases the peak broadening. For a s.b.s.r. with an uniform size of packing beads, van den Berg et al. (84) derived an equation, based on Hiby's (139) experimental results, for evaluating the improvement in peak broadening and mean residence time. That is,

$$\left(\frac{\sigma_t}{t_m}\right)^2 = \frac{1}{L}\left\{\frac{2\gamma'D}{u} + \frac{2\upsilon\bar{a}_b}{1 + \upsilon'(D/2u\bar{a}_b)^{\frac{1}{2}}}\right\} \tag{134}$$

where γ' is the tortuosity factor, $\bar{a}_b$ is the average diameter of the packing beads, and υ and υ' are constants characterizing the geometry of the packed bed. Therefore for a given length of s.b.s.r. the efficiency of the reactor, which is directly proportional to the reciprocal of σ_t/t_m, depends on the particle size chosen. When optimizing σ_t/t_m ratio for the best performance of a s.b.s.r. the following criteria should be kept in mind:

i.   Bead diameter should be greater than 50% of the tubing diameter to ensure a single string packing.

ii.   Bead diameter should not be so large that back pressure becomes a problem.

iii.   A zig-zag pattern is preferable to ensure the uniformity of packing.

The Reynolds number of a single-bead-string reactor is calculated as follows (95):

$$(Re)_{s.b.s.r.} = 2\bar{a}_b F/\pi a^2 \nu \tag{135}$$

where ν is the kinematic viscosity.

Other Types of Reactors of Interest Not Used in FIA.   Band broadening can be reduced by disrupting the laminar nature of the fluid flow to induce instantaneous turbulence. This process can be achieved by interrupting the uniform geometry of the tube regularly. One of these reactors, the so-called jet mixer, has been constructed by Gaunce and D'Iorio (124) for use in the ordinary modules of the Technicon Auto-Analyzer and Halasz (125) for use in a liquid chromatography. The instantaneous turbulence caused by the liquid being forced through the constrictions results in very rapid radial mixing of reagents and decrease the axial band dispersion, which makes the jet mixer a good alternative of a single-bead-string reactor.

A secondary flow effect was also found in a straight tube with an elliptical cross section when the flow was pulsatd (29). However the secondary flow effect in an elliptical tubing is far smaller than in a coiled tubing.

Conclusion

When FIA was first developed in the mid-70's, there were doubts concerning the dilution effect of sample by the flowing stream and sample carry-over. These doubts prevented the calculation of the exact concentration of the reactants, and the system was considered unsuitable for detailed kinetic studies (5). It was also thought that only a single stream could be used in operating the system and reaction time was limited by the length of the reaction coil and the optimum flow rate that could be used.

Today, however, the development of the technique by numerous researchers allows us to recognize the high versatility of the system. The controlled dispersion of the sample zone, which takes place during its movement from the injection port to the detector, minimizes and/or maximizes the dilution to the desired extent. The stop-flow method (102) and the gradient chamber (79) method provide useful tools for detailed kinetic studies. The merging-zone method and the stream splitting method introduce two or more merging streams in the reaction flowing system. The zone-sampling method allows the flexibility in selecting the desired sample zones for different degrees of dispersion. Single bead-string reactor extends the residence time but does not affect the sample throughput rate. Furthermore, the FIA system is no longer limited to an all-liquid system, Ramasamy et al.'s (80, 150) work opens the door for developing FIA technique for an all-gas and gas-liquid systems.

Although the development of the theory of controlled diepsersion in FIA has drawn a great deal of attention, it is far from complete. From the review presented in Chapters II and III, it is obvious that the dispersion theory in FIA was mainly adopted from the dispersion models de-

veloped for physiological circulation research, chemical reactor engi-neering, and chromatographic band broadening. Nevertheless FIA is a totally different technique with its own analytical versatility. For each application in FIA, the dispersion should be controlled to suit its specific analytical needs. In addition, chemical effect has always been left out in dispersion studies of FIA. The guidelines set up by FIA workers for designing a FIA system are not complete and could even be misleading (102, 108). Consequently, the important task is to set up a chemical-physical dispersion model ideally to suit any chemical system used in FIA. The present study was aimed to do so.

CHAPTER IV

EXPERIMENTAL METHODS AND PROCEDURES

Apparatus

The peristaltic pump used throughout the study was a Minipuls II
(Gilson Medical Electronics, Inc., Middleton, WI). Photometric de-
tection was provided by a Beckman Model 25 spectrophotometer equiped
with a Beckman recorder / controller unit (Beckman Instruments,
Inc., Fullerton, CA). A Model E-178-Q-10 flow cell of 10 mm path length
and 80 µL chamber volume was used as the detection reservoir (Markson
Science, Inc., Del Mar, CA). The tubing used in the study was primarily
Tygon microbore, formulation S-54-HL for surgical and hospital use (Nor-
ton Plastics and Synthetics Division, Akron, OH). Two other types of
tubing were used for comparison purposes only, they were TFE tubing,
certified quality (Zeus Industrial Products, Inc., Raritan, N.J.), and
capillary glass tubing, drawn from PYREX Tubing Special Wall, 8 mm O.D.
x 48" (Corning Glass Works, Corning, N.Y.) by a Hupe + Busch 1045A cap-
illary drawing machine (Hewlett Packard, Loveland, CO). The glass beads
used for packing a single-bead-string reactor were "Borosilicate Shot"
solid glass beads (Propper Mfg. Co., Inc., Long Island, City 1. N.Y.).

In the study, samples were introduced with a custom-made rotary
valve constructed according to information available in the literature
(89). The details of the rotary valve are provided in Figure 20. Oc-

casionally, a gastight glass syringe was used for comparison to the rotary valve (Hamilton Company, Reno, NV). A block diagram of the entire instrumental set-up is shown in Figure 21.

<div align="center">Calibration of Rotary Valve</div>

<div align="center">Sample Injector</div>

Due to construction limitations there is an inherent dead volume at the center bore of the rotary valve. This dead volume is independent of the size of the interchangeable sample loops, but is additive to the volume of the each sample loop. That is

$$V_s = V_d + \pi a^2 L_s \tag{136}$$

where V_s represents the actual volume of the injecting sample (μL), V_d represents the dead volume of the rotary valve injector (μL), and L_s is the length of the sample loop tubing (mm) while a is the radius of the sample loop tubing (mm).

V_d can be determined by calibrating the rotary valve injector with clean mercury. The calibration has been performed with 0.5 mm i.d. sample loops of various lengths (35 mm - 98 mm). Figure 22 presents the results of the calibration. From the extrapolated intercept point, it has been determined that the value of V_d is 20.7 μL.

<div align="center">Chemical Model and Reagents</div>

A chemical reaction of moderate speed, the oxidation of L-ascorbic acid by dichromate ion, was selected as the model for the dispersion study. The overall chemical reaction is:
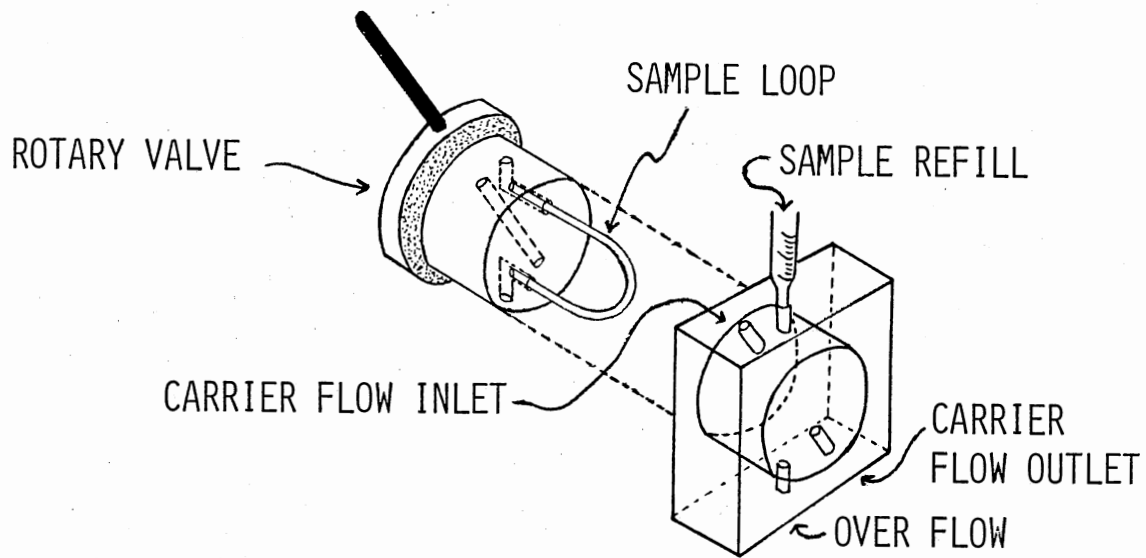
Figure 20. Rotary Valve for Sample Injection
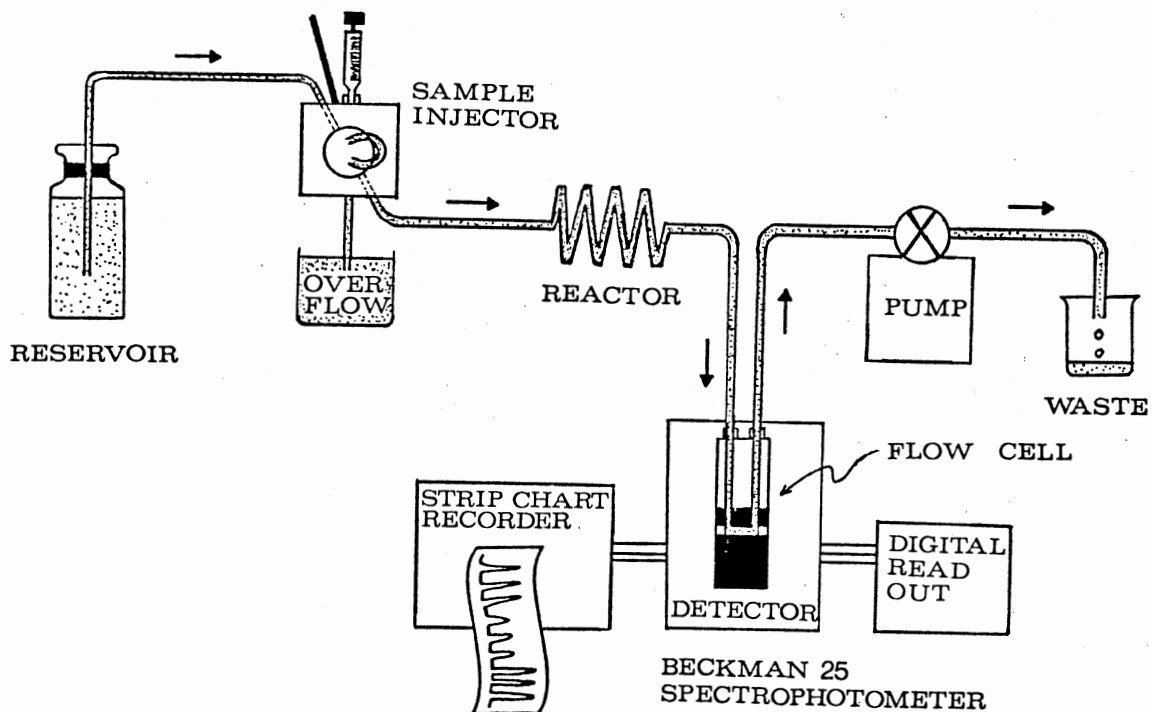
Figure 21. Instrumental Set-Up for Performing the Dispersion Study
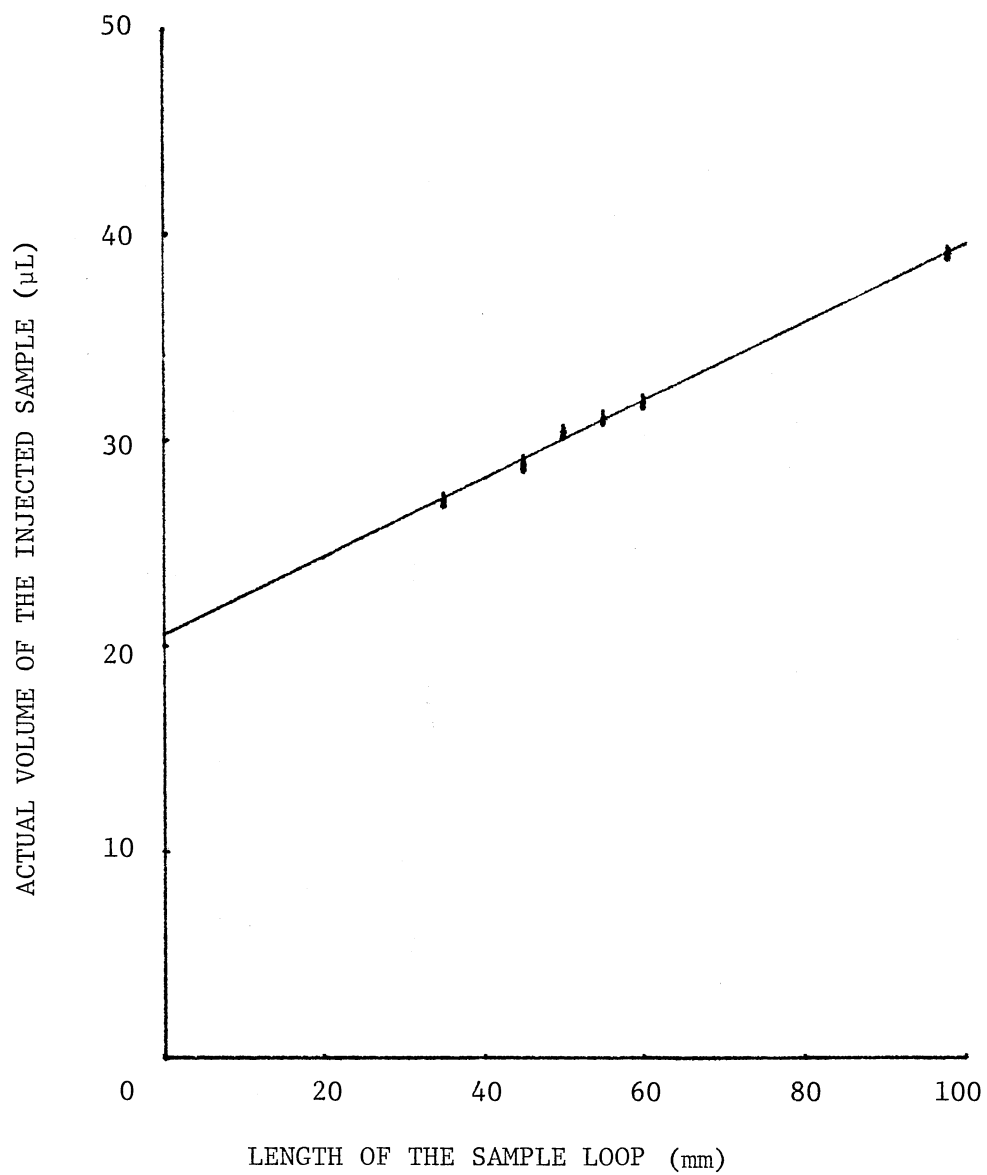
Figure 22. Calibration Plot for the Rotary Valve Injector

$$Cr_2O_7{}^{2-} + 3C_6H_8O_6 + 8H^+ \rightleftarrows 2Cr^{3+} + 7H_2O + 3C_6H_6O_6 \qquad (137)$$
(yellow)
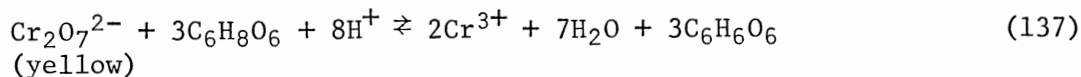
All chemicals used were of AR grade. The water used for solution preparation was deionized water that was further purified by distillation in an all-borosilicate still with a quartz immersion heater, Model Corning AG-1a (Corning Glass Works, Corning, N.Y.). Both reagent solutions, L-ascorbic acid (J. T. Baker Chemical Co., Phillipsburg, N.J.) and potassium dichromate (Fisher Scientific Company, Fair Lawn, N.J.) were prepared daily and kept in the dark or protected from direct exposure to light. The pH of the injected sample and that of the carrier stream were adjusted to the desired value with an Orion Research, Model 601A/digital IONALYZER, pH meter (Orion Research Incorporated, Cambridge, MA).

Experimental Procedure

The carrier stream was pumped from a closed dark reservoir at a constant flow rate. The flow rate was adjustable by varying either the size of the pumping tube or the pump revolutions per unit time. The sample was introduced by means of an injection device downstream from the reservoir and defining the start of the so-called "reactor". The injected sample, or "sample plug", experienced physical dispersion and/ or chemical reaction with the carrier stream as it was transported downstream. This dispersed or dispersed-reacted sample plug was monitored at the exit of the reactor as it passed through the flow cell. In the case of the reaction shown in Equation 137 the monitored species is the unreacted dichromate with a (λ_{max}) at 352 nm. The peristaltic pump was located either before the point of injection or after the point of

detection, and the stream was sent to waste.

The carrier stream was a 0.005 — 0.05 M solution of L-ascorbic acid (used in experiments to evaluate the chemical reaction effect) or aqueous solutions (HCl or $HClO_4$) of the same pH as the intercalated plug. All intercalated samples consisted of 0.00050 M potassium dichromate. The flow rate was varied in the range of 0.05 — 6.0 mL/min. The reactor tube diameters were 0.5, 0.8, 1.0, and 1.3 mm, corresponding to tube volumes of 1.96, 5.03, 7.85, and 13.3 μL/cm. Straight tube reactors had lengths between 30 — 600 cm and coiled tube reactors were composed of interconnected lengths of 30 cm (straight) — 120 cm (coiled) — 30 cm (straight) with coil diameter of 3.4, 6.7, 12.2, 15.6, and 22.3 mm. The single-bead-string reactor was of a comparable length tubing (with the straight or coiled tubing that was used for comparison) packed with glass beads, the average diameter of the glass beads was chosen so that a single string, zig-zag pattern would be obtained. The length of the sample loop was varied within the range 7 — 600 cm, corresponding to sample volumes of 33.7 — 1198 μL. All volumes were determined by calibration with mercury.

The chart speed and chart span were selected carefully in order to ensure adequate resolution of details in the recorded signal.

CHAPTER V

MATHEMATICAL ANALYSIS AND

COMPUTER SIMULATIONS

Dispersion Equation and Transformation

Intercalation of a dichromate solution into an aqueous stream of equal pH is assumed to lead to dispersion resulting solely from physical mass transport as a result of concentration gradients and velocity profiles. The dispersion in a laminar flow can be described in an equation discussed previously (Equation 19), that is

$$\frac{dC}{dt} + Umax(1 - \frac{r^2}{a^2})\frac{dC}{dx} = D(\frac{d^2C}{dx^2} + \frac{1}{r}\frac{dC}{dr} + \frac{d^2C}{dr^2})$$

where all of the variables have been defined previously (page 13).

This equation was transformed into a dimensionless equation because:

i. The dispersion of a sample of fluid into a carrier stream flowing in a tubular pipe is a dynamic phenomenon which is dictated by parameters such as the tube radius (a), flow velocity (u), and molecular diffusion coefficient (D). Thus, it is convenient to have flow parameters which would include the overall effect of reactor dimension and flow mechanics.

ii. Some parameters are normalized to simplify mathematical operations.

The transformation process is described in Appendix B. The transformed equation is

$$\frac{dC^*}{d\tau} + \{\frac{(1 - y^2)}{\sqrt{\tau}} - \frac{1}{2}\frac{\Omega}{\tau}\}\frac{dC^*}{d\Omega} = \frac{1}{\tau N_{pe}^2}\frac{d^2C^*}{d\Omega^2} + \frac{1}{y}\frac{dC^*}{dy} + \frac{d^2C^*}{dy^2} \tag{138}$$

where each variable has been defined in Appendix B.

However, with intercalation of a dichromate solution into an aqueous solution of L-ascorbic acid the chemical reaction contributes to the driving force for dispersion. Equation 19 is modified to account for the effect of a chemical reaction (the oxidation of dichromate by L-ascorbic acid) on the overall dispersion, this results in Equation 139,

$$\frac{dC}{dt} + U_{max}(1 - r^2/a^2)\frac{dC}{dx} = D(\frac{d^2C}{dx^2} + \frac{1}{r}\frac{dC}{dr} + \frac{d^2C}{dr^2}) - k(C)^n \tag{139}$$

where k is the rate coefficient. This equation implies that physical dispersions and the chemical reaction contribute simultaneously to the change of concentration-time profile in the flow system. The problem represented by Equation 139 can be regarded as a problem in dispersion in which some of the dispersing substance is chemically reacted as the dispersion proceeds, or as a problem in chemical kinetics in which the rate of chemical reaction depends on the rate of supply of one of the reactants by the dispersion. For the experimental condition studied here where the chemical reaction occurs when the sample molecules disperse into the carrier solution, or vice versa, from sample-carrier boundaries, it would seems appropriate to regard the dispersion problem as a problem in which some of the dispersing substance is chemically reacted as the dispersion proceeds. Therefore, Equation 139 has been regarded as two simultaneous equations, Equations 19 and 140, i.e.:

$$\begin{cases} \dfrac{dC}{dt} = D(\dfrac{d^2C}{dx^2} + \dfrac{1}{r}\dfrac{dC}{dr} + \dfrac{d^2C}{dr^2}) - U_{max}(1 - r^2/a^2)\dfrac{dC}{dx} \\[4mm] \dfrac{dC}{dt} = -k(C)^n \end{cases} \qquad (140)$$

For a first order (or a pseudo-first order) reaction, the change of concentration resulting from the chemical reaction follows the relation-ship:

$$C_{chem} = C_d\{\exp(-kt)\} \qquad (141)$$

where C_{chem} represents the concentration remaining from the chemical reaction and the physical dispersion, C_d represents the concentration resulting from physical dispersion alone. Equation 141 can be trans-formed into a dimensionless form, and becomes:

$$(C_{chem})^* = (C^*)\exp(-\kappa\tau) \qquad (142)$$

where $(C_{chem})^*$ represents the normalized concentration remaining from chemical reaction and physical dispersion, C^* represents the normalized concentration remaining from physical dispersion only, τ is the reduced time, and κ is the reduced rate coefficient ($\kappa = a^2k/D$).

Numerical Analysis

The method adopted for numerically solving the dispersion equation (Equation 138) is the alternating direction implicit finite difference approximation.

The basic principles of the implicit finite difference method is discussed thoroughly in Carnahan et al.'s (144) book. Ananthakrishnan et al. (36) adapted the method to solve for the dispersion occurring at

single sample-carrier boundary resulting from a constant flow injection. Vanderslice et al. (108) adapted Ananthakrishnan et al.'s solution to solve for the dispersion occurring at both sample-carrier boundaries resulting from a sample plug injection. Their solution, however, are limited to systems where no chemical reaction does occur. In the present study, Ananthakrishnan et al.'s solution was adapted to solve for the concentration-time profile resulting from the injection of a sample plug into a carrier stream, the plug physically disperses and chemically reacts with the carrier as it travels downstream. That is, Equation 138 and Equation 142 are solved alternately for each time step.

Equation 142 is a simple analytical expression, however, Equation 138 is a second order partial differential equation which requires a numerical solution. In this section, the numerical analysis for solving Equation 138 will be described briefly.

i. For a cylindrical tubing of uniform diameter the dispersion is assumed to be radially symmetrical with respect to the center origin axis. Consequently, a grid point network used in the numerical solution may be arranged using two dimensions as shown in Figure 23. In the radial direction (y), the grid points are bounded between the center origin (y_0) and the tubing wall. In the longitudinal direction (Ω), the grid points spread out from the entrance of the fluid (Ω_0) to a sufficiently distant point where only a negligible amount of sample is to be found.

ii. Replace the dispersion equation (Equation 138) by the following difference equation:

$$\frac{c^*_{i,j,2n+1} - c^*_{i,j,2n}}{\Delta\tau} + \{\frac{(1 - y^2)}{\sqrt{\tau}} - \frac{1}{2}\frac{\Omega}{\tau}\}\{\frac{c^*_{i+1,j,2n+1} - c^*_{i-1,j,2n+1}}{2\Delta\Omega}\}$$

A)

B)
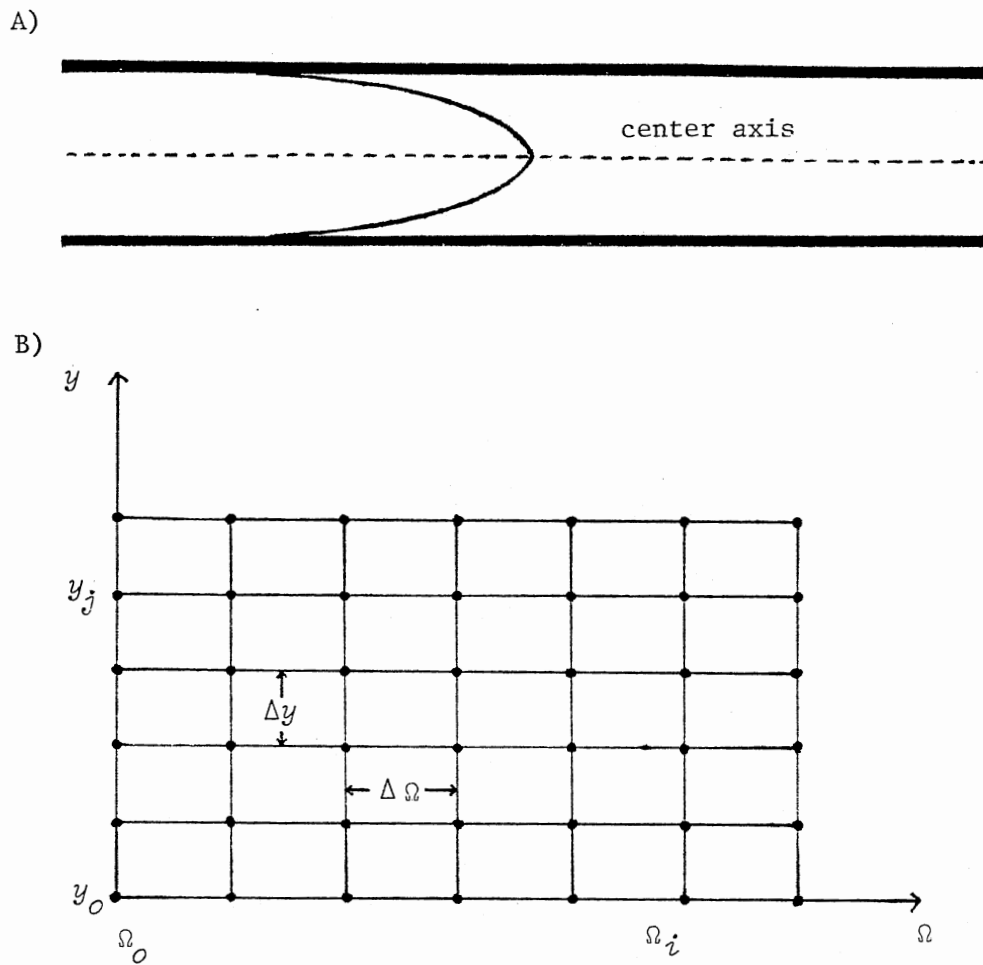
Figure 23. Laminar Flow Profile in a Cylindrical Pipe (A)
and Grid Point Arrangement in the Pipe for
Numerical Calculation of Flowing Fluid
Dispersion (B)

$$= \frac{C^*_{i,j+1,2n} - 2C^*_{i,j,2n} + C^*_{i,j-1,2n}}{(\Delta y)^2} + \frac{1}{y}\{\frac{C^*_{i,j+1,2n} - C^*_{i,j-1,2n}}{2\Delta y}\} +$$

$$\frac{1}{\tau N_{pe}^2}\{\frac{C^*_{i-1,j,2n+1} - 2C^*_{i,j,2n+1} + C^*_{i+1,j,2n+1}}{(\Delta\Omega)^2}\} \qquad (143)$$

iii. Set up the initial and boundary conditions for $\tau = 0$.

iv. Time is advanced by one time step, $\Delta\tau$.

v. Proceeding along the Ω direction, solve Equation 140. Assuming that the total grid points in the longitudinal direction is M. This treatment will lead to a set of M simultaneous equations whose coefficients alone are called the tridiagonal matrix.

vi. The tridiagonal matrix system is readily solved by a Gaussian elimination method (144).

vii. Step v and step vi are applied to the y direction as well.

viii. Because an injected sample bolus has two boundaries, steps i through vii will be performed twice, once for the leading and once for the trailing boundaries.

ix. Finally, the total concentration at a fixed longitudinal position is integrated over the cross section.

x. The sequence of steps iv through ix is repeated until the accumulated time reaches a preset limit.

Equations are diagonally dominant, hence Gaussian elimination is completely stable. However, by Douglas' (145) analysis the prime error is due to the discretization introduced by the choice of grid mesh sizes. This error is an unavoidable consequence of using a successive approximation method.

The stability and the convergence of the solution have been discussed by Carnahan et al. (144) and Ananthakrishnan et al. (36). Mesh

sizes which are too large result in divergence and instability of the solution. Too small mesh sizes, however, result in excessive time expense. Consequently, the mesh sizes used in the present study were selected via a meticulous trial-and-error process.

Computer Algorithm and Programming

The computer algorithm used in this study is described by the following series of steps:

i. Carefully choose the mesh sizes for the longitudinal distance, radial distance, and time, i.e. $\Delta\Omega$, Δy, and $\Delta\tau$. Thus, the total number of grid points in each direction and the total time elapsed can be determined.

ii. The initial condition is set by assigning computer memory locations to each of the grid points.

iii. Both the leading section and the trailing section of the sample plug dispersion are calculated simultaneously. For the leading section, the sample ($C_0^* = 1$) disperses into the carrier ($C_0^* = 0$) while for the trailing section, the carrier ($C_0^* = 0$) disperses into the sample ($C_0^* = 1$).

iv. The time is increased by $\frac{1}{2}\Delta\tau$.

v. Coefficient arrays for the tridiagonal matrix and the solution for grid point concentration are computed for the Ω-implicit equations.

vi. The time is increased by another $\frac{1}{2}\Delta\tau$.

vii. Coefficient arrays for the tridiagonal matrix and the solution for grid point concentrations are computed for the y-implicit equations.

viii. The Ω- and y-implicit equations are applied alternately by

repeating steps iv to vii for the various time steps. The entire procedure is repeated until the desired value of τ is reached.

ix. The grid point concentration distribution for the sample plug at the end of each $\Delta\tau$ step is calculated by subtracting the distribution of the trailing portion from the distribution of the leading portion.

x. The total concentration within the dimension of the flow cell is then intergrated and the resulting concentration-time data becomes a printed out-put.

xi. For the system where a chemical reaction is occurring in addition to the physical dispersion, Equation 143 is used to calculate the final point concentrations at the ends of each v and viii steps.

The FORTRAN/WATFIV program incorporating the above algorithm was run on an IBM/370 computer at Oklahoma State University. A listing of the program is contained in Appendix C.

<div align="center">

Comparing Taylor's Model with the

Numerical Solution Model

</div>

The following section is devoted to a comparison between Taylor's model and the dispersion model based on the numerical solution described in the preceding section, for a system without chemical reaction, with emphasis on their capability to simulate dispersion signals in FIA.

Recalling Equations 30 and 31 which describe dispersion by the Taylor model:

$$C = \frac{1}{2} Ma^{-2} \pi^{-\frac{3}{2}} (Kt)^{-\frac{1}{2}} \exp\{-(x - \frac{1}{2}(Umax)t)^2/4Kt\}$$

where

$$K = \frac{a^2(U_{max})^2}{192D}$$

and also recalling that the derivation of these equations was under two assumptions;

(i) the material of mass M was originally concentrated at a point $x = 0$, at the time $t = 0$, thus the volume of the sample is negligible in comparison with the volume of the reactor tubing, and

(ii) $(L/Umax) \gg (a^2/3.8^2D)$, where L represents the total length of the reactor tubing.

With these assumptions in mind a computer program was written, based on Equations 30 and 31, for simulating signals obtained in FIA experiments. The computer program was written for a HP-9825A desk-top calculator. A listing of the program is provided in Appendix D. With input data corresponding to the desired experimental condition the resulting dispersion profile can be calculated. The output data was then plotted with a HP-9862A plotter. Some generated simulated curves are shown in Figures 24 - 26. These figures were generated with different values of L/Umax which are typical values used in FIA experiments. The value of $\{a^2/(3.8)^2D\}$ is 8.7 sec for all three figures. By comparing the value of $\{a^2/(3.8)^2D\}$ with the values of L/Umax listed in the figures, i.e. 11.4 sec, 18.8 sec, and 29.8 sec, it is obvious that the second assumption, $(L/Umax) \gg \{a^2/(3.8)^2D\}$, is not exactly satisfied. Therefore it is not surprising that discrepancies exist when comparing the simulated curves with the experimental curves. As shown in Figures 24 - 26 the closer the value of L/Umax is to the value of $\{a^2/(3.8)^2D\}$, the larger is the discrepancy. These discrepancies indicate that Equations 30 and 31 from Taylor's model are not suitable for describing the dis-
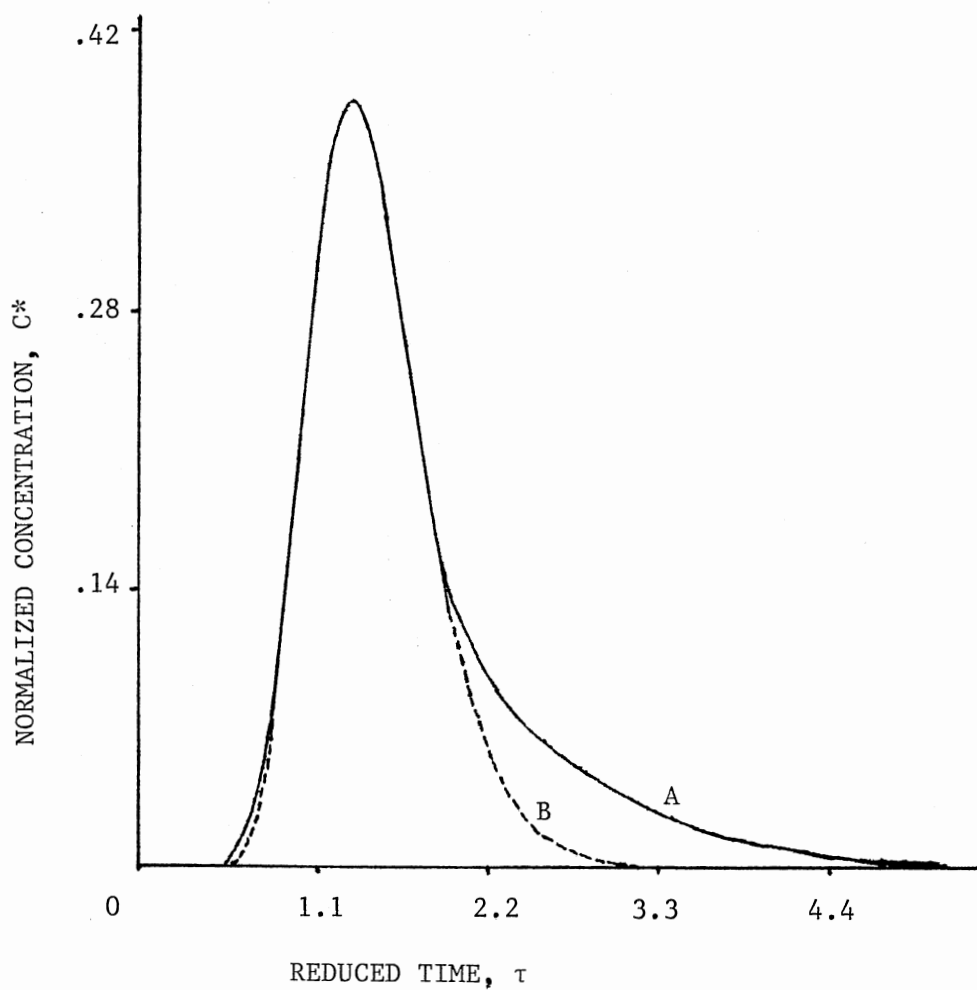
Experimental Conditions: Radius, a = 0.025 cm; Reactor,
Straight Open Tube with Length, L = 405 cm; Flow Rate,
F = 0.80 mL/min; Sample Volume, V_S = 62 µL; pH 4.76.

Figure 24. Comparison of Experimental Concentration-Time
Curve (A) with Simulated Curve Obtained from
Taylor's Model (B) (L/Umax = 29.8 sec)
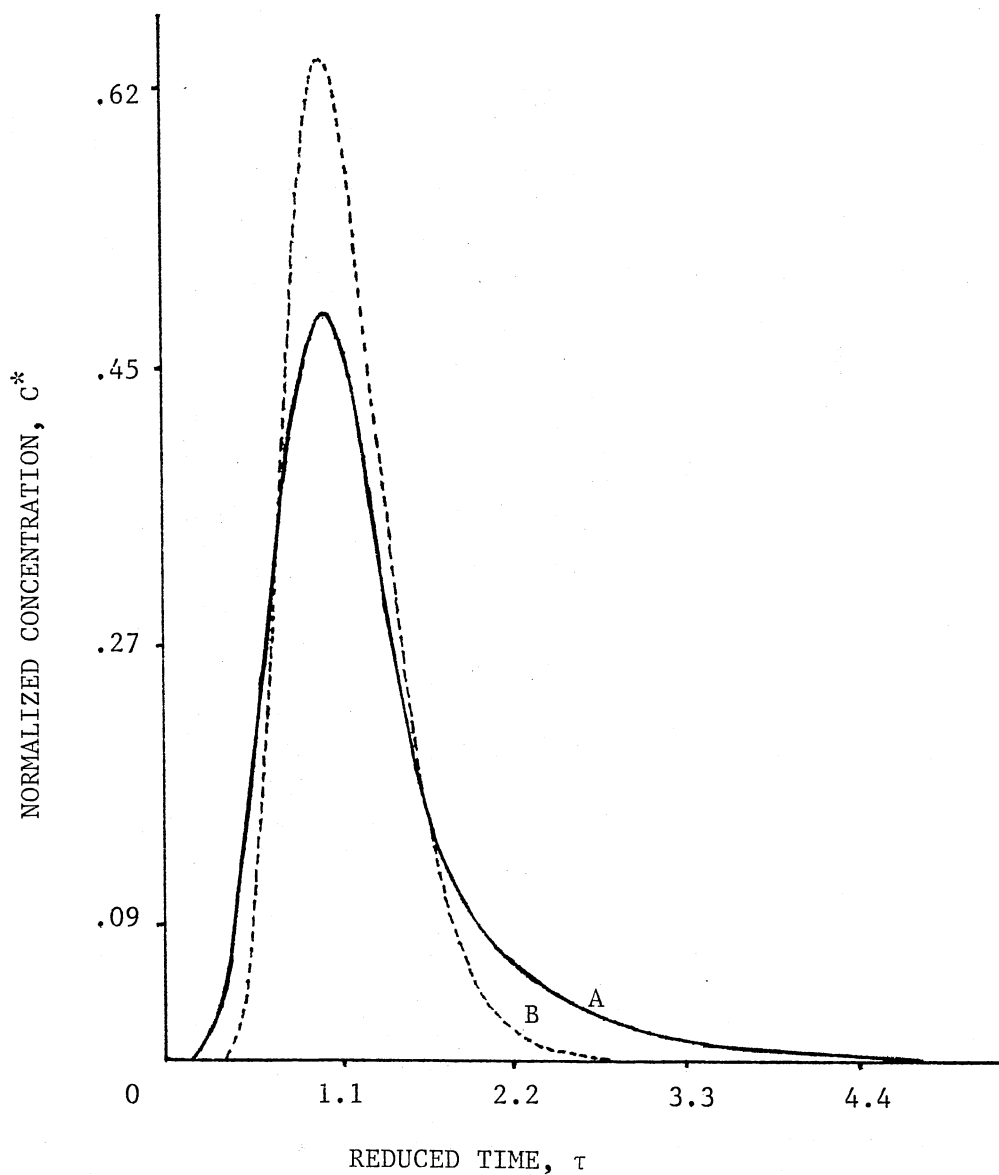
Experimental Conditions: Radius, a = 0.025 cm; Reactor,
Straight Open Tube with Length, L = 255 cm; Flow Rate,
F = 0.80 mL/min; Sample Volume, V_S = 62 µL; pH 4.76.

Figure 25. Comparison of Experimental Concentration-Time
Curve (A) with Simulated Curve Obtained from
Taylor's Model (B) (L/Umax = 18.8 sec)
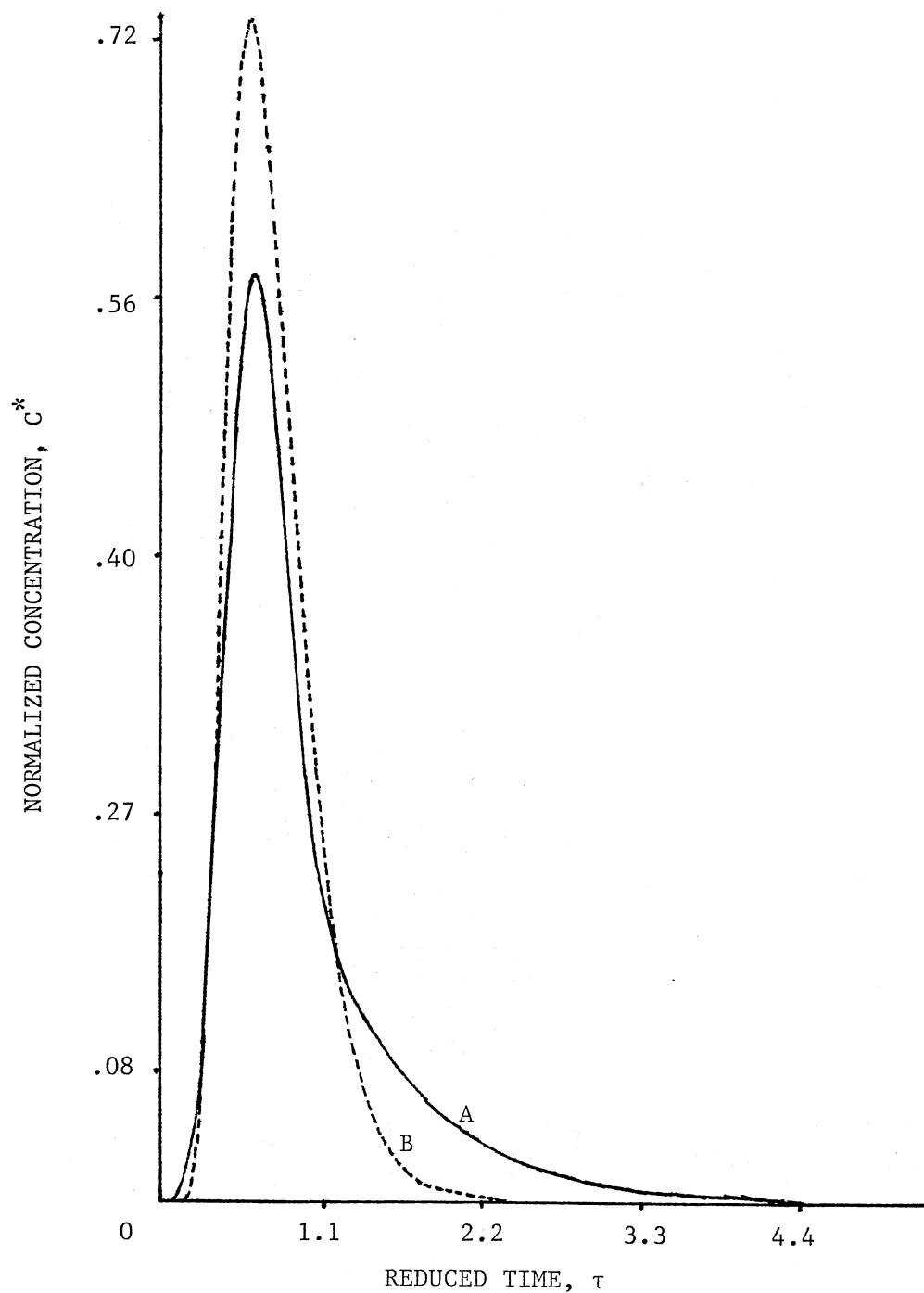
Experimental Conditions: Radius, a = 0.025 cm; Reactor,
Straight Open Tube with Length, L = 155 cm; Flow Rate,
F = 0.80 mL/min; Sample Volume, V_s = 62 μL; pH 4.76.

Figure 26. Comparison of Experimental Concentration-Time
Curve (A) with Simulated Curve Obtained from
Taylor's Model (B) (L/Umax = 11.4 sec)

persion resulting from a typical FIA experiment. It does have, however, the advantages of simplicity and easy programming. The first assumption of the model can be satisfied without much effort. The same, however, can not be said of the second assumption. To satisfy the second assumption, either very long tubing or a very slow flow rate is required. Yet, neither option is practical for flow injection experiments. Consequently, it appears that Taylor's model fails in describing the physical dispersion for experimental conditions commonly used in flow injection analysis.

On the other hand, the use of the numerically solved dispersion equation for simulating dispersion curves of the same kind was more satisfactory. Figures 27 - 29 demonstrate the agreement between simulated curves generated from the numerical solution of Equation 19 and the corresponding experimental curves. Even at low values of L/U_{max} the agreement was satisfactory. However, the theoretically generated curves would be subjected to tail correction due to the nonideality of the experimental conditions. This correction is discussed in the next section.

<div align="center">

Correction Factors for Numerically

Simulated Curves

</div>

Vanderslice et al. (108) have provided analytical expressions, based on Ananthakrishnan et al.'s (36) numerical solution of Equation 19, for two time factors that are frequently used to represent a concentration-time curve, that is

$$t_A = \frac{109a^2D^{0.025}}{f}\left(\frac{L}{F}\right)^{1.025} \tag{144}$$
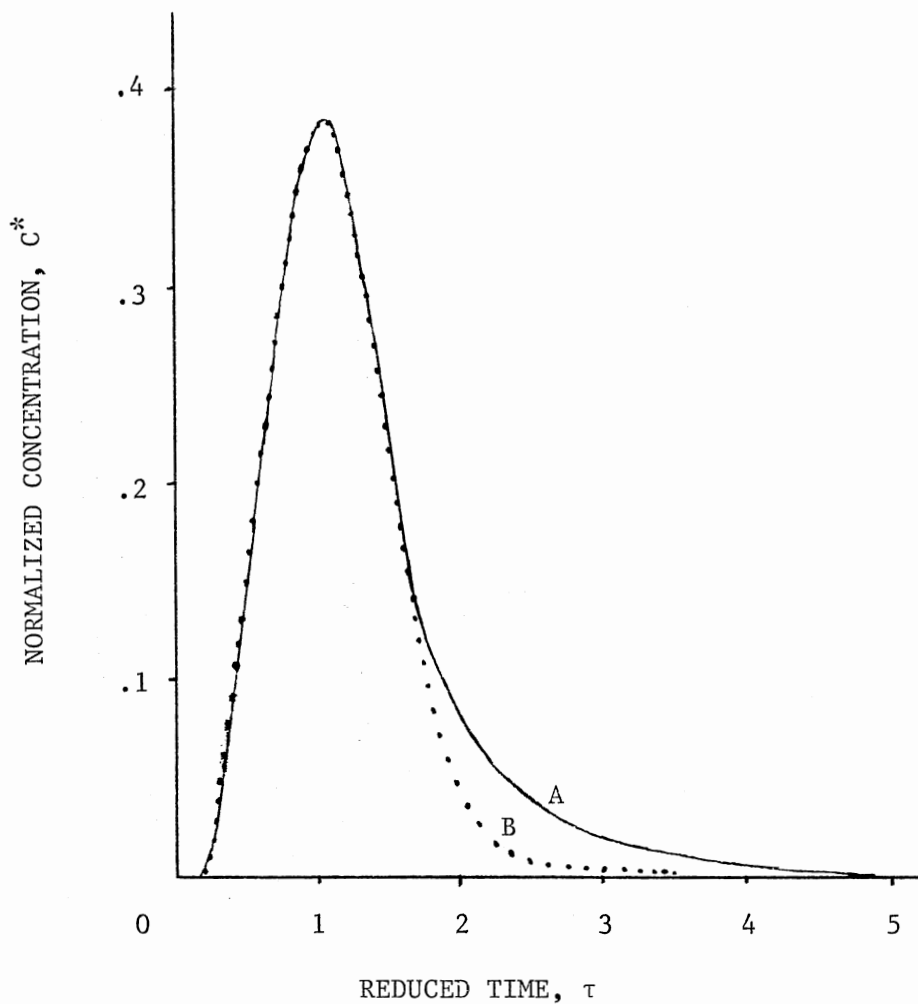
Experimental Conditions: Radius, a = 0.025 cm; Reactor, Straight Open Tube with Length, L = 405 cm; Flow Rate, F = 0.80 mL/min; Sample Volume, V_s = 62 µL; pH 4.76.

Figure 27. Comparison of Experimental Concentration-Time Curve (A) with Simulated Curve Obtained from Numerical Solution of Equation 19 (B), L/Umax = 29.8 sec
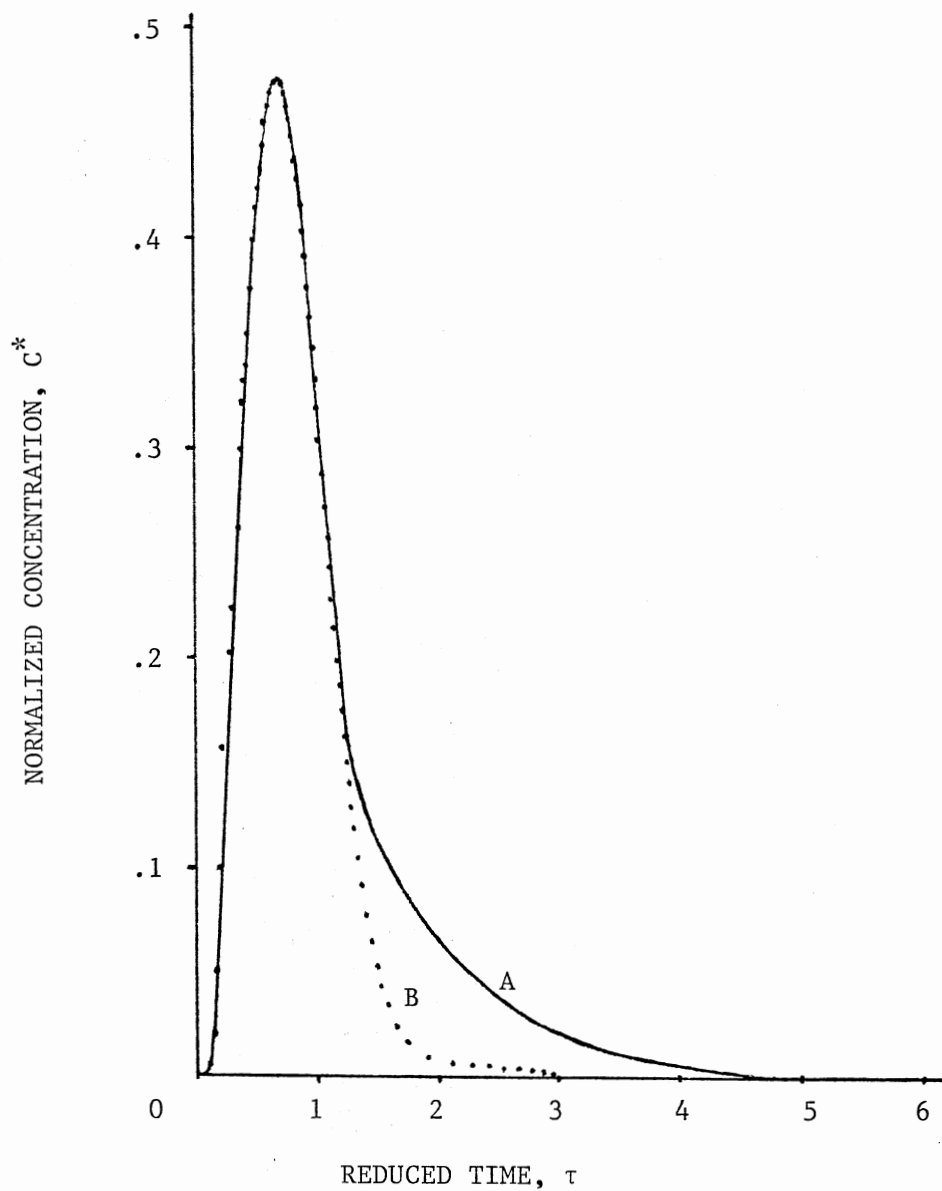
Experimental Conditions: Radius, a = 0.025 cm;
Reactor, Straight Open Tube with Length, L =
255 cm; Flow Rate, F = 0.80 mL/min; Sample
Volume, V_S = 62 µL; pH 4.76.

Figure 28. Comparison of Experimental Concentration-
Time Curve (A) with Simulated Curve Ob-
tained from Numerical Solution of Equa-
tion 19 (B), L/Umax = 18.8 sec
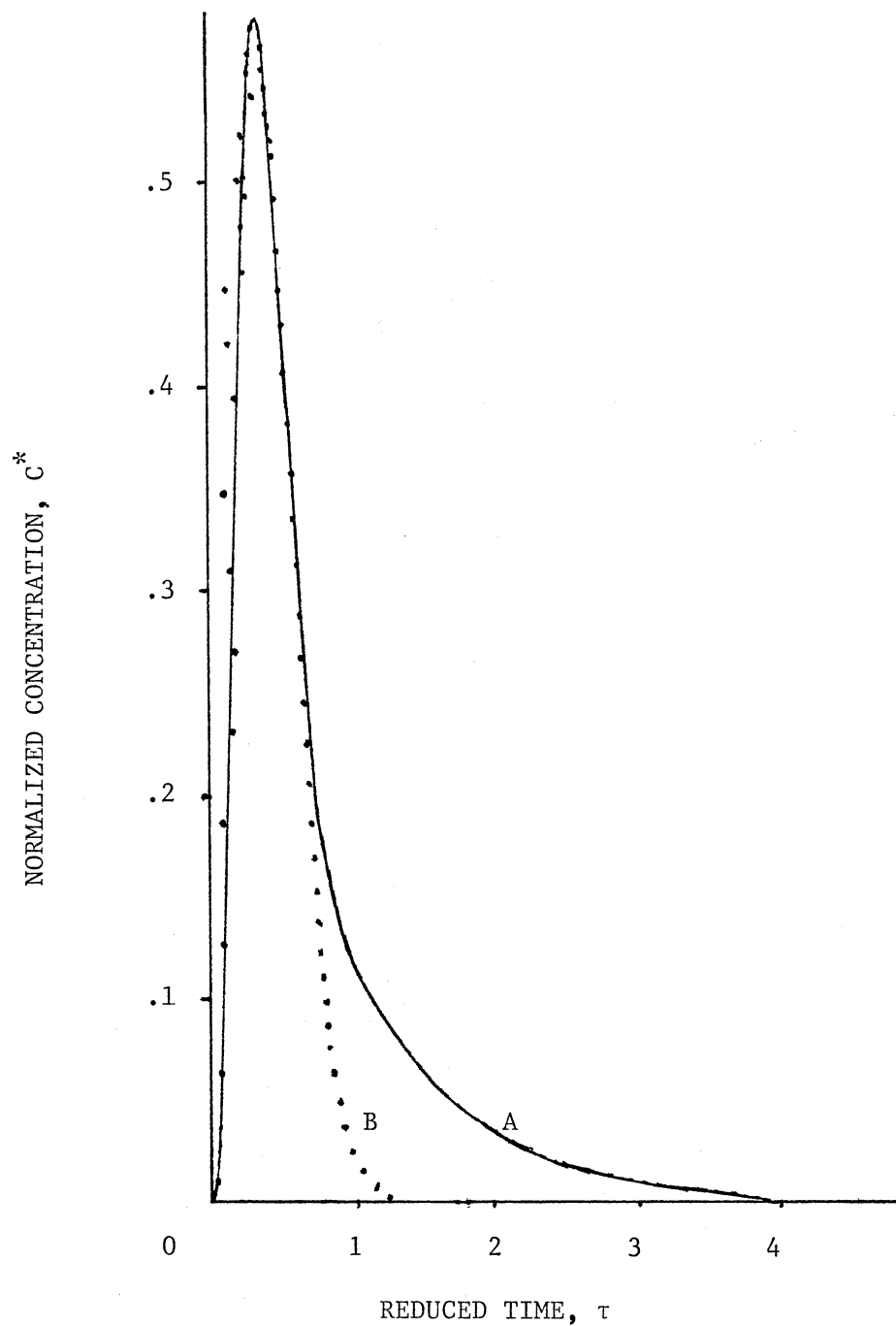
Experimental Conditions: Radius, a = 0.025 cm;
    Reactor, Straight Open Tube with Length, L =
    155 cm; Flow Rate, F = 0.80 mL/min; Sample
    Volume, V_S = 62 μL; pH 4.76.

Figure 29. Comparison of Experimental Concentration-
            Time Curve (A) with Simulated Curve Ob-
            tained from Numerical Solution of Equa-
            tion 19 (B), L/Umax = 11.4 sec

$$\Delta t_B = \frac{35.4a^2f}{D^{0.36}}(\frac{L}{F})^{0.64} \tag{145}$$

where t_A is the initial appearance of a peak at the detector (travel
time), and Δt_B is the total time of observation of the peak (baseline to
baseline). A correction factor, f, is present in both expressions.
Δt_B is proportional to f, and t_A is proportion to the reciprocal of f.
f takes on values from 0.5 to 1.0 depending on either concentration or
detector sensitivity.

The experiments that were performed in the present study, however,
have suggested a correction factor that is also influenced by nonuni-
formity of the reactor-connector diameter, the injector inner path dia-
meter, and the detector flow cell diameter. As shown in Figure 30 the
front end of the injected sample plug travels through d, e, f, and g
manifold, and finally is monitored while it passes through h. The lar-
gest portion of the manifold is e, consequently it is expected to con-
tributed the most to the dispersion of the sample plug travelling in the
system. Thus the diameter of section e was chosen as the manifold dia-
meter when performing the numerical calculation of concentration profile
for the dispersed sample plug. However, the deviations in the inner
diameter of d, f, g, and h also distort the shape of detected
concentration-time curves. It would seem appropriate to include all
these deviations in diameter for use in the numerical calculation of
dispersion signals. But previous attempts to do so did not provide sat-
isfactory results. Presumably the variations of the radial mesh size Δy
(which corresponds to the different inner diameters of the manifold)
produced a mathematical instability in the succesive approximation proc-
ess. Therefore, no convergence was obtained for the numerical results.
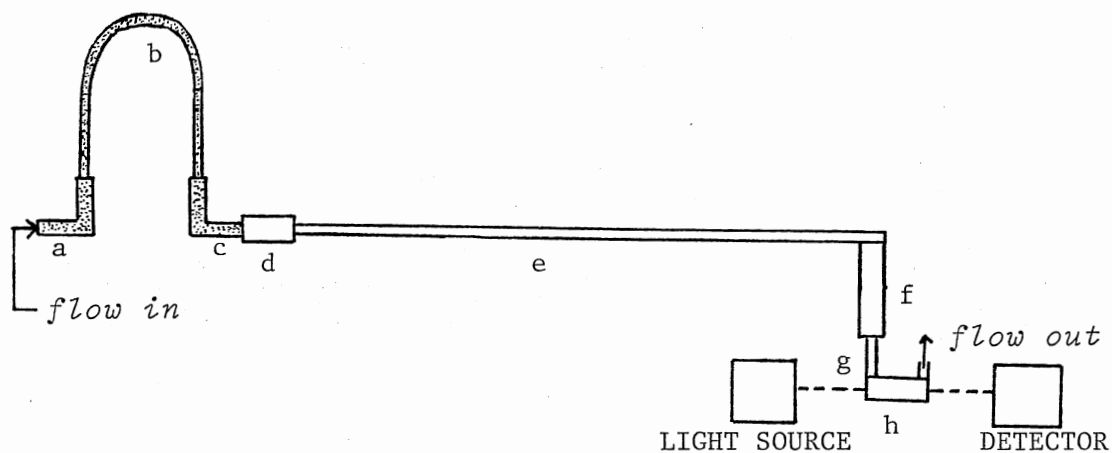
MANIFOLD	DESCRIPTION
a	Sample Loop (Trailing Portion), 1.2 cm Long, 0.1 cm i.d.
b	Sample Loop (Center Portion), Various Length, 0.05 i.d.
c	Sample Loop (Leading Portion), 1.2 cm Long, 0.1 cm i.d.
d	Sample Chamber Built-In Path, 0.5 cm Long, 0.13 cm i.d.
e	Reactor Tubing, Various Length Which Forms the Main Portion of the Entire Manifold, 0.05 cm i.d.
f	Flow Cell Entrance Connector, 2.8 cm Long, 0.2 cm i.d.
g	Flow Cell Inner Path, 0.8 cm Long, 0.28 cm i.d.
h	Flow Cell Detecting Area, 1.0 cm Long, 0.32 cm i.d.

(Shaded Area Represents the Sample Region at the Time t = 0)

Figure 30. Detail Measurements of the Flow Manifold Used as Input Data for the Numerical Simulation of Concentration-Time Curves

Although using the diameter of section c alone eliminates the mathematical instability, the simulated result does not sufficiently match the experimental signal. The addition of correction factors to the time scale, however, has been found to substantially improve the simulation. Equations 144 and 145 were used in this process. It should be noted that Equations 144 and 145 imply that the correction factor has the same value for both equations, and do not suggest any dependence of its value on the construction of the manifold. This failure limits the usefulness of both equations.

In practice, the path between the points of injection and detection is frequently not of absolute uniform dimension (Figure 30 is a typical example). Thus, the overall variance of the signal obtained at the detector can be shown to be (106):

$$(\sigma_{overall})^2 = (\sigma_{injector})^2 + (\sigma_{flow\ cell})^2 + (\sigma_{connectors})^2$$

$$+ (\sigma_{reactor})^2 \tag{146}$$

The magnitude of each component in this equation is directly proportional to the residence time that the sample spends in each section of the manifold. Furthermore, for a fixed flow rate, residence time is indirect proportion to the volume of the vessel. Because of

$$V_{overall} = V_{injector} + V_{flow\ cell} + V_{connectors} + V_{reactor} \tag{147}$$

where V represents the volume, the closer the volume of the reactor approaches the overall volume, the larger the proportion of the overall dispersion that is contributed by the reactor. Thus, the calculated dispersion, assuming an uniform diameter for the manifold (the diameter

of reactor), is more close to the experimental result. That is, the correction factor is closer to unity.

The preceding text was intended to point out that the manifold has substantial influence on the value of the correction factor added to the time scale. However, the present study has indicated that there are two correction factors associated with Equations 144 and 145 designated f_A and f_B respectively, but only one of them, f_A, is influenced by the manifold. f_A is the correction factor associated with Equation 144. The influence of reactor length on f_A is plotted in Figure 31. As the reactor tubing length increases from 100 cm to 600 cm, f_A increases from 0.23 to 0.58. Because t_A in Equation 144 depends on the linear flow velocity which varies with the variation of the manifold diameter, the longer reactor tubing will diminish the variation in the linear flow velocity. Consequently, the calculated t_A should have a value that is closer to the experimental t_A value, therefore, f_A is closer to unity. Thus, Equation 144 may be rewritten as follows:

$$t_A = \frac{109(a)^2(D)^{0.025}}{f_A}(\frac{L}{F})^{1.025} \tag{148}$$

where f_A is a variable depending on the length of the reactor, which should be recalibrated whenever the injector, the flow cell, or any one of the connectors are changed.

On the other hand, the correction factor for Δt_B in Equation 145 (f_B), was found to be constant as long as the injector, flow cell, and all connectors remain the same. The fact that f_B does not depend on the length of the reactor as does f_A, indicates that Δt_B is independent of the variation of the reactor tubing length in the range studied. This
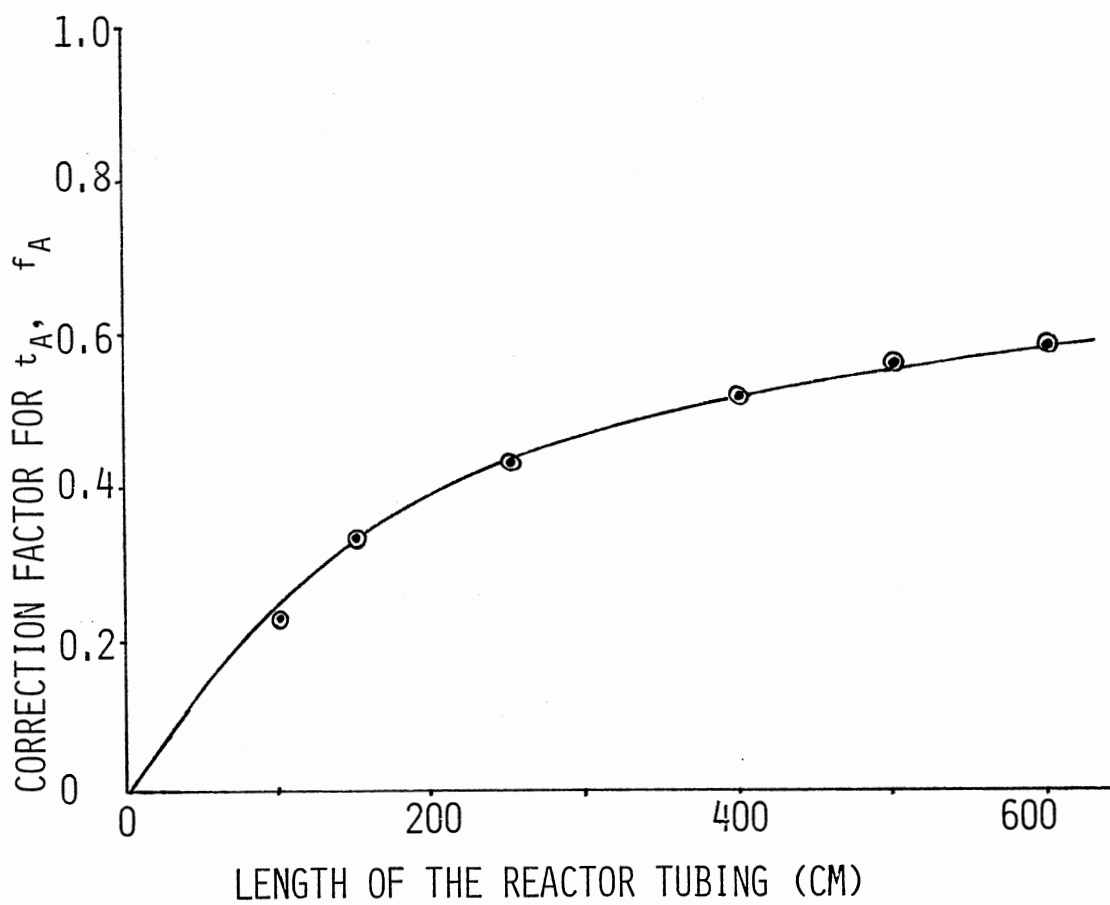
Figure 31. Variation of the Correction Factor for Travel Time (t_A) with Respect to the Length of Reactor

is not a surprising result since the factor, f_B, is correcting for the total difference on the diameters of the injector, the flow cell, and connectors, which does not change with the reactor tubing length. The present study demonstrates that f_B has a value of 0.86 for a reactor tubing of 100 cm to 600 cm in length. Thus, Equation 145 may be re-written as follows:

$$\Delta t_B = \frac{35.4(a)^2 (f_B)}{D^{0.36}} \left(\frac{L}{F}\right)^{0.64} \tag{149}$$

where f_B is a constant for a defined flow system.

The use of the correction factors, f_A and f_B, substantially improves the fit of the simulation curve, however, an additional problem exists. In the present study the simulated concentration data were obtained by integrating over the entire cross section of the monitoring flow cell. In reality, however, the ligth path may not cover the entire cross section of the monitoring flow cell. Consequently, a correction factor must be applied to the integrated concentration data in order to improve the fit of the simulation to the experimental data. A factor of 2.3 was found to be appropriate for the present study. Thus, the experimental concentration data can be expressed as:

$$(C_{experimental})^* = (C_{theoretical})^* / (f_C) \tag{150}$$

where f_C is the correction factor for the calculated concentration data.

A summary of all the correction factors that may be used in the numerical simulation of a concentration-time curve is presented in Table VII.

TABLE VII

CORRECTION FACTORS FOR THE NUMERICALLY SIMULATED
CONCENTRATION-TIME CURVES

Symbol	What does it correct	Expression for the use of the correction factor	Dependence on the variation of the reactor tubing length
f_A	t_A (the travel time)	$t_A = \dfrac{109a^2 D^{0.025}}{f_A}(\dfrac{L}{F})^{1.025}$ $0 < f_A < 1$	Approaching unity as the reactor tubing length increases
f_B	Δt_B (the time for baseline to baseline)	$\Delta t_B = \dfrac{35.4a^2 f_B}{D^{0.36}}(\dfrac{L}{F})^{0.64}$ $0 < f_B < 1$	Does not depend on the reactor tubing length
f_C	c^* (the concentration)	$c^* = (C_{theo.})^*(\dfrac{1}{f_C})$ $f_C > 1$	Does not depend on the reactor tubing length

CHAPTER VI

CHEMICAL EFFECT ON DISPERSION

Chemical Effect on Dispersion

Intercalation of a dichromate solution into an aqueous stream of
equal pH leads to the dispersion resulting solely from physical
mass transport as a result of concentration gradients and velocity pro-
files. On the other hand, intercalation of similar samples into aqueous
streams containing L-ascorbic acid adds the effect of the overall chem-
ical reaction that has been described in Equation 137.

The analytical implications in both cases have been demonstrated by
means of the practical dispersion, D, as defined by Ruzicka and Hansen
(126), previously. Figure 32 clearly identifies the chemical effect on
the practical dispersion value with respect to flow rate and pH gra-
dient. This figure provides an example of the kind of effect on dis-
persion that may be introduced by a chemical reaction. However, it must
be recognized that the dependence between the chemical reaction and
physical dispersion is reciprocal. Sample-carrier solution boundaries
induce physical dispersion, while the mixing of the sample and carrier
solutions triggers a chemical reaction. The chemical reaction causes a
new concentration gradient, which becomes a driving force for increased
dispersion. The fact that the chemical reaction facilitates further
physical dispersion can be observed clearly by examining Figures 33 and
34. Figure 33 was obtained from the numerical calculation of Equation
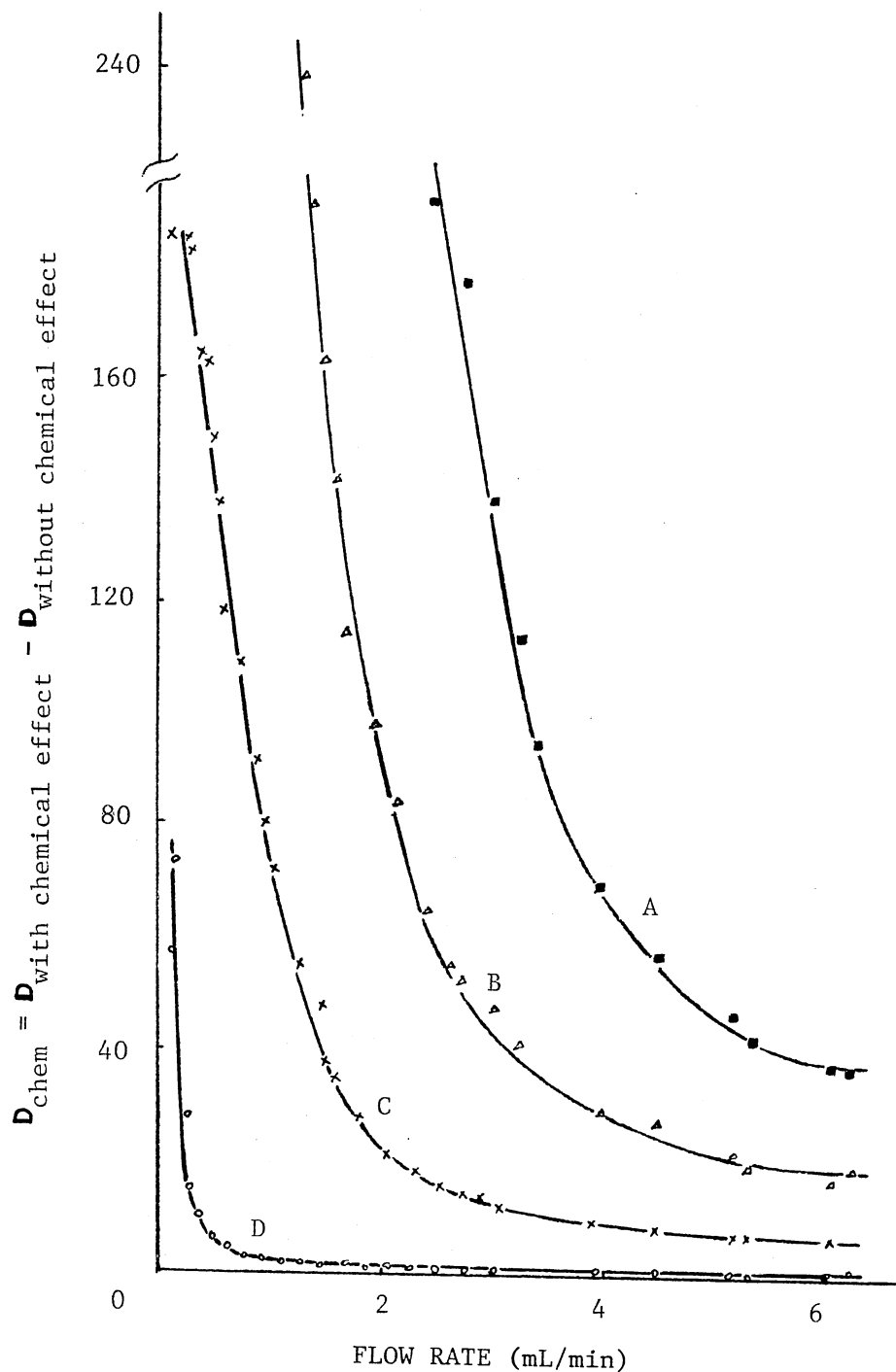
Experimental Conditions: Radius, a = 0.025 cm; Reactor,
Straight Open Tubing with Length, L = 155 cm; Sample
Volume, V_S = 33.7 µL; .5 mM Dichromate Sample with
pH Values of (A) 5.01, (B) 4.58, (C) 3.33, and (D)
2.54; 5 mM L-Ascorbic Acid Carrier Stream with a pH
Value of 5.55.

Figure 32. Variation of D_{chem} with Flow Rate (Adapted from
Reference 126)
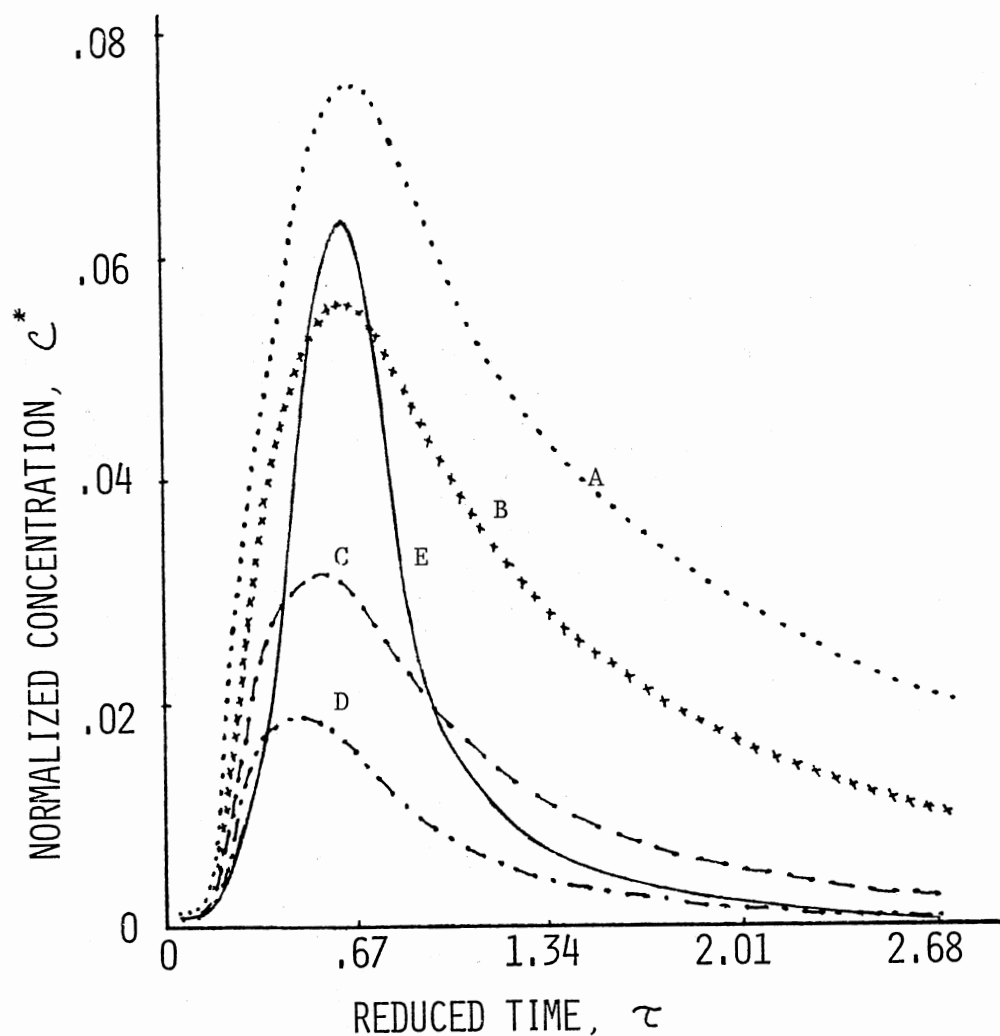
Experimental Conditions: Radius, a = 0.025 cm; Reactor,
Straight Open Tube with Length, L = 405 cm; Flow Rate,
F = 0.80 mL; Sample Volume, V_S = 62 μL; pH 4.76.

Theoretical Curves were Numerically Calculated Under the
Simulated Reaction Rate Coefficients: (A) 0.16 sec^{-1};
(B) 0.20 sec^{-1}; (C) 0.28 sec^{-1}; (D) 0.40 sec^{-1}.

Figure 33. Comparison of the Experimental Curve (E) with Nume-
rically Calculated Curves (A – D) at Simulated
Reaction Rate Coefficients
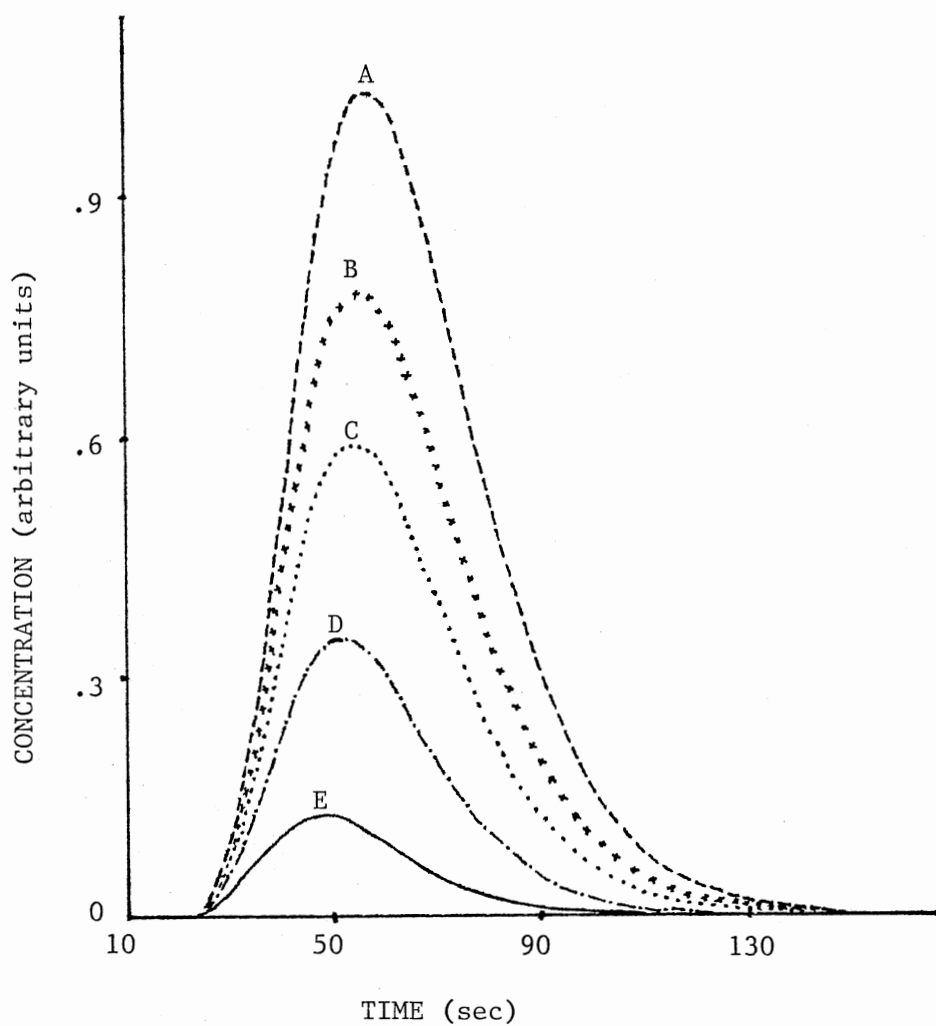
Simulated Conditions: Radius, a = 0.025 cm; Reactor,
Straight Open Tube with Length, L = 405 cm; Flow
Rate, 0.80 mL/min; Reaction Rate Coefficients:
(A) 0 sec^{-1}; (B) .005 sec^{-1}; (C) .01 sec^{-1}; (D)
.02 sec^{-1}; (E) .04 sec^{-1}.

Figure 34. Theoretically Generated Curves from Taylor's
Model (Equations 30 and 31) with Chemical
Contribution at Simulated Reaction Rate
Coefficients

19 with chemical contribution at simulated reaction rate coefficients. Figure 34 was obtained in the similar manner by using Equation 30 and 31 of Taylor's model. In both figures it is noticeable that the time at where the peak maximum appears is shorter the larger the rate coefficient is. Thus it becomes evident that while the sample is transported by the carrier reagent stream from the injection point to the detection point, dispersion and chemical processes are facilitating each other continuously, and "pushing" the sample molecules forward. The monitoring signal reflects the result of both processes. Knowing information from one process may permit us to extract more information from the other process. Since physical dispersion is a well-known subject, the interest lies in extracting kinetic data from the simulation models.

Curve Fitting to Experimental Results

Figure 33 illustrates the numerically simulated curves obtained under the assumption that the rate coefficient is constant throughout the entire body of the sample plug. Comparison with the experimental curve in the figure, however, shows that the above assumption did not reflect the actual chemical behavior within the plug. In fact the kinetics involved within the sample plug seemed to have a dynamic characteristic. In this figure the experimental curve, E, intersects theorectical curves, B – D, at different times, this observation suggests that the rate coefficient changes with time. Following this rationale, a number of trial-and-error studies were performed to refine the fit of the simulation to the experimental curve. The experimental curve has been adequately simulated by varying the rate coefficient through out the entire calculation process. Part (A) of Figure 35 illustrates

(A)

(B)
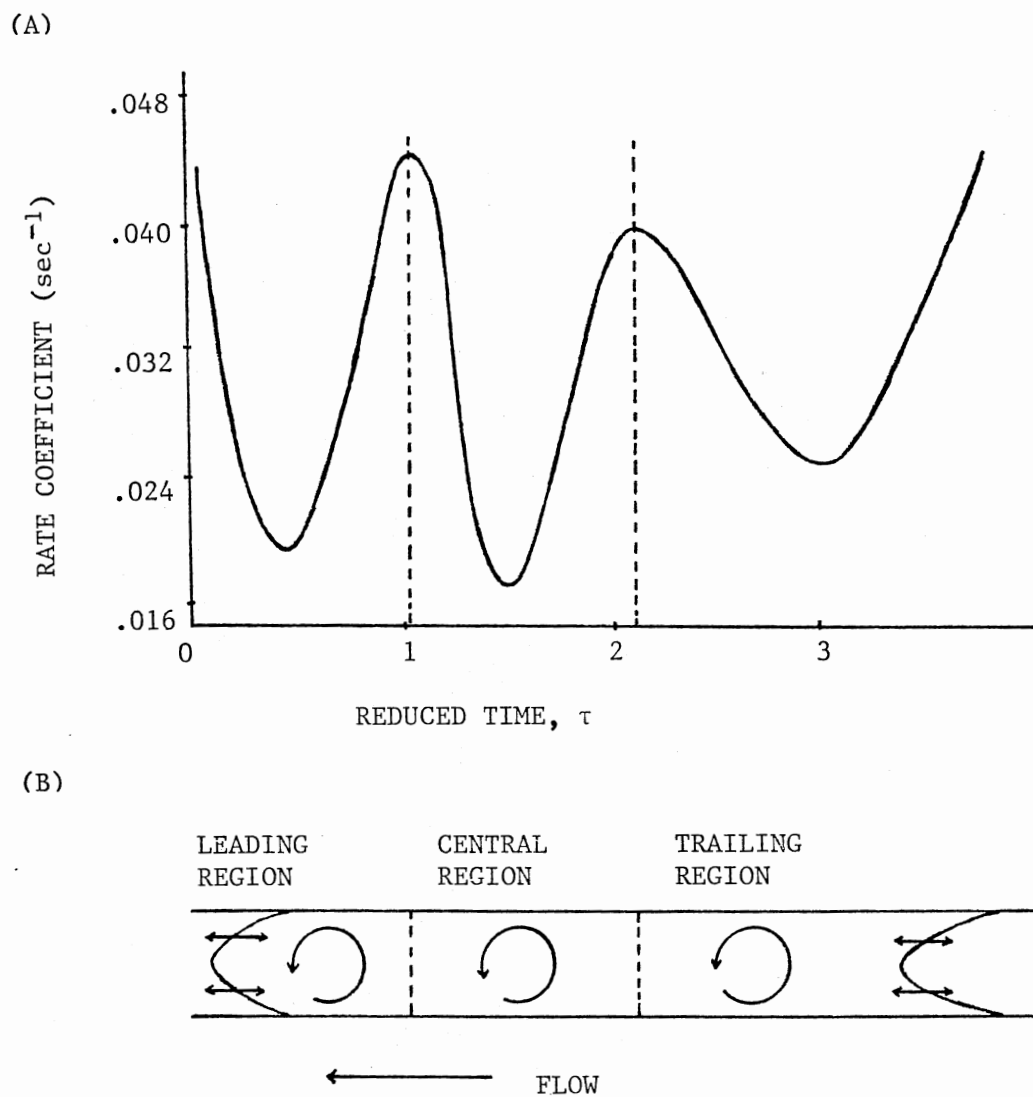
Figure 35. Variation of the Rate Coefficient with Time (A)
and the Corresponding Dispersing Sample Plug
(B)

the variation of rate coefficients as the time elapsed. There are three cyclic fluctuations which appear throughout the body of the sample plug. This result is reasonable if each of the three fluctuations is assumed to correspond with one of three regions within a sample plug, namely, the leading region, the central region, and the trailing region. Consider a dispersing sample plug which is subdivided into three regions as shown in the part (B) of Figure 35. In both the leading and trailing regions the carrier-sample boundaries induce molecular diffusion, while the velocity profile induces convection. In the central region no sample-carrier boundary exists, convection becomes the primary dispersion force. Because the physical dispersion in these three regions of the sample plug differ from one another, the rate coefficients along the length of the plug are expected to have a dynamic variation and a wave pattern. The wave pattern of the variation in rate coefficients implies that a concentration gradients of sample and carrier reactants dictate the chemical behavior within a travelling sample plug. And the results of chemical behavior localize the dispersion pattern within the sample plug. The fact that the reaction rate varies throughout the entire sample plug may imply also that the kinetic order is not constant within the sample plug.

The result in Figure 36 implies that as the sample plug travelled a longer distance (L increased from 405 cm for Figure 35 to 605 cm for Figure 36) the molecular diffusion at the leading and trailing regions are more developed, the variation of rate coefficients eased off at both regions. An opposite result is observed in Figure 37 which is obtained from a system of shorter reactor tubing (L = 305 cm). However, the overall pattern remained the same.
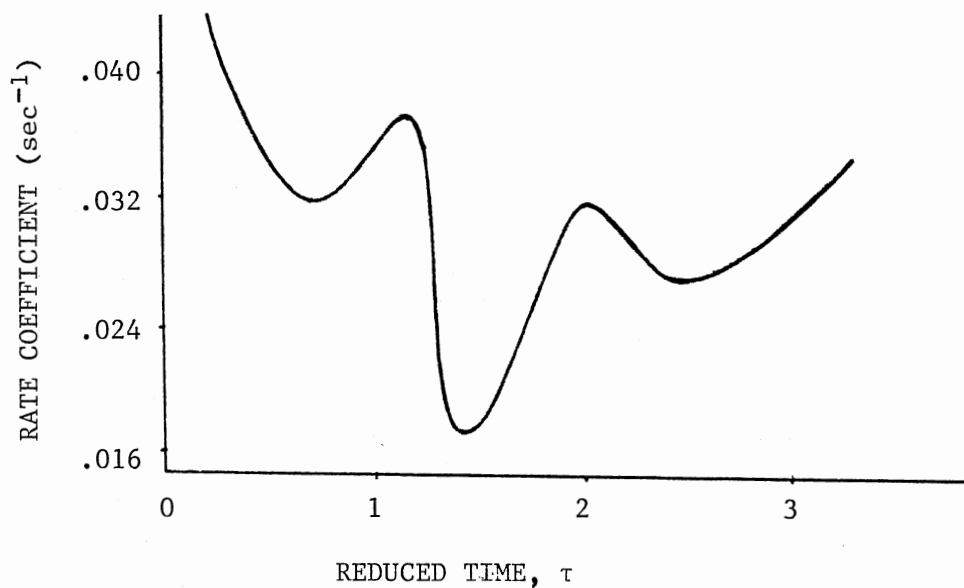
Figure 36. Variation of the Rate Coefficient with Time as the Length of Reactor Tubing Increased ∿ 50% from that of Figure 35
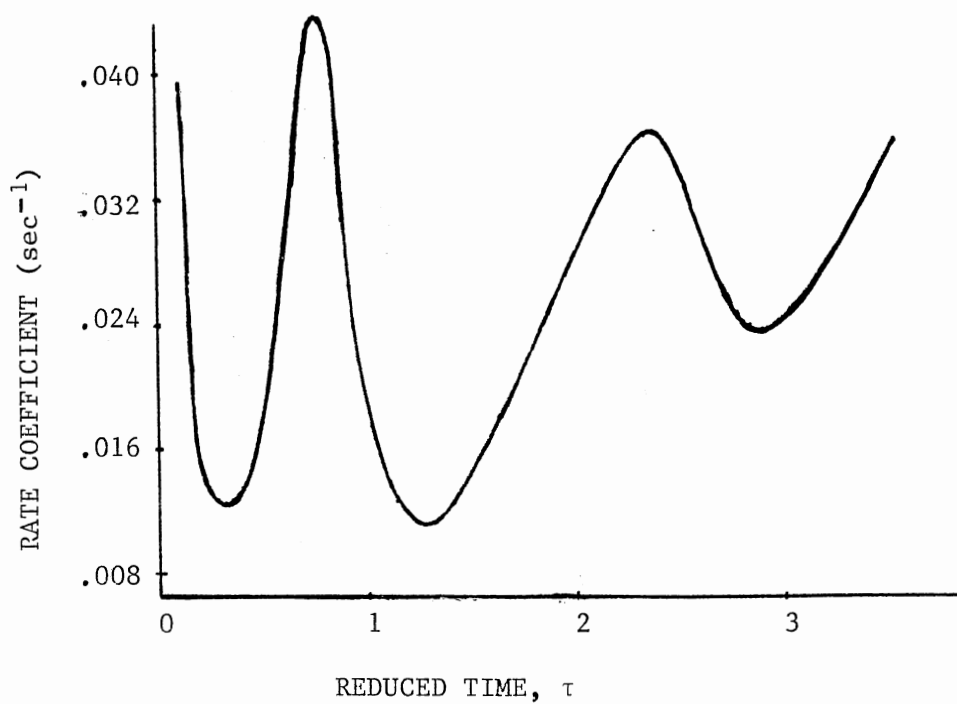
Figure 37. Variation of the Rate Coefficient with Time as the Length of Reactor Tubing Decreased ∿ 25% from that of Figure 35

Kinetic Data Extraction

Although the simulated curves shown in Figure 33 do not account for the variation on chemical kinetics, which is the result of chemical reaction occurring as physical dispersion proceeds, surprisingly they seem to provide satisfactory results for use to extract kinetic data of the chemistry involved.

First order kinetics allow a straight line relationship for the variation of ln(concentration) with rate coefficient. It was found that a straight line relationship also exists between the time at the peak maximum and the rate coefficient. By fitting the data of ln(concentration) and time at the peak maximum obtained from the experimental curve into the above two straight line relationships, the rate coefficient of the reaction can be estimated. Curves for the ln(concentration) and the time at the peak maximum versus rate coefficients, based on the numerical solution of Equation 19 (Figure 33), are plotted in Figures 38 and 39. The extracted rate coefficients are listed in Table VIII. For comparison purpose, the same processes for extracting kinetic data have been performed with the dispersion with chemical contribution curves simulated from Equations 30 and 31 of Taylor model (Figure 34), and Figures 40 and 41 are the resulting curves with the extracted rate coefficients also listed in Table VIII. In this table the rate coefficient obtained from the batch experiment (described in Appendix E) was used as a standard to evaluate the accuracy of the predicted rate coefficients by the above theoretical models. It was found that the data extracted from the numerically simulated curves is far superior with $\leq$ 2.69% error relative to the batch experiment.

Kinetic data extraction processes by using the numerical simulation
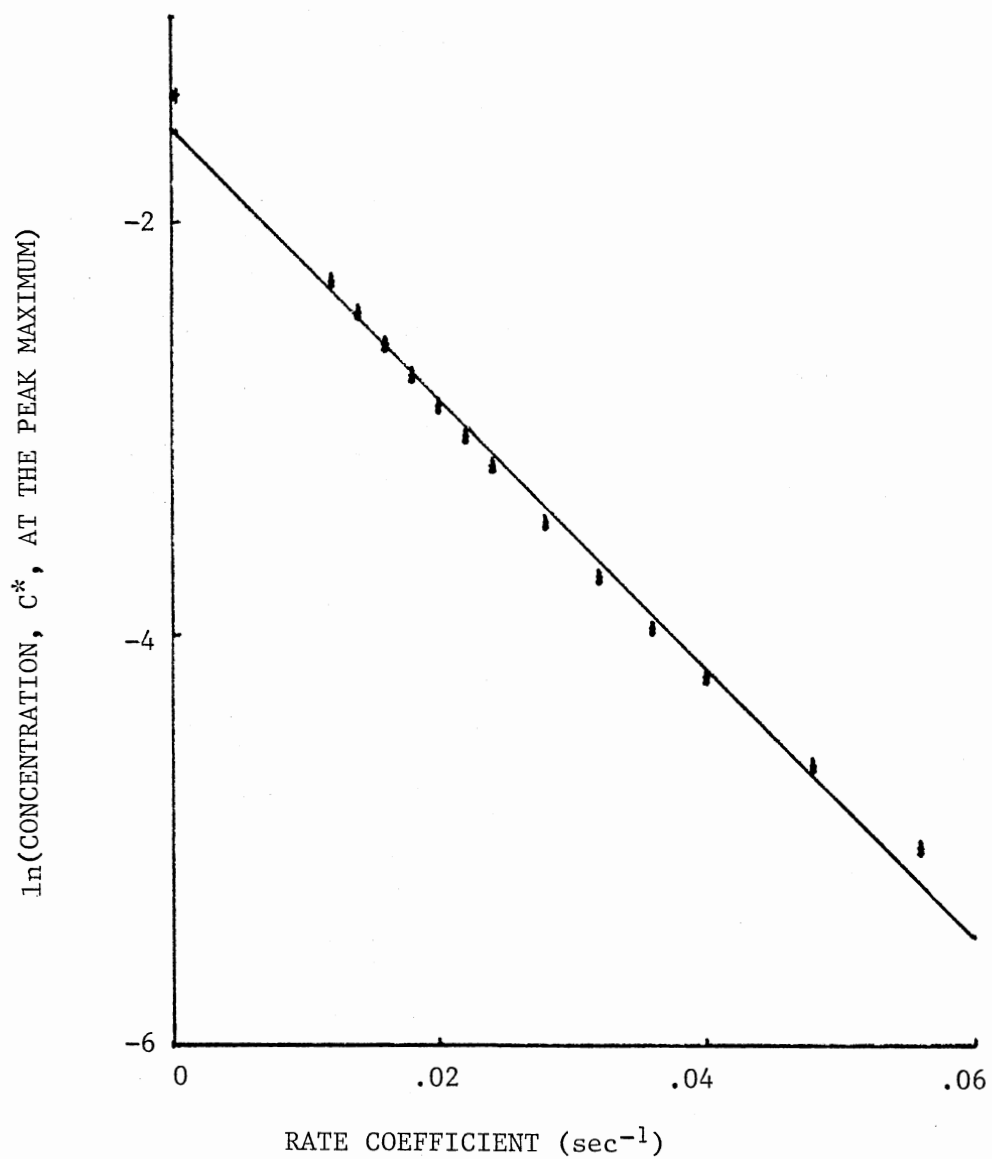
Figure 38. Variation of ln(Peak Maximum Concentration)
with Simulated Rate Coefficient — Data
Extracted from Figure 33
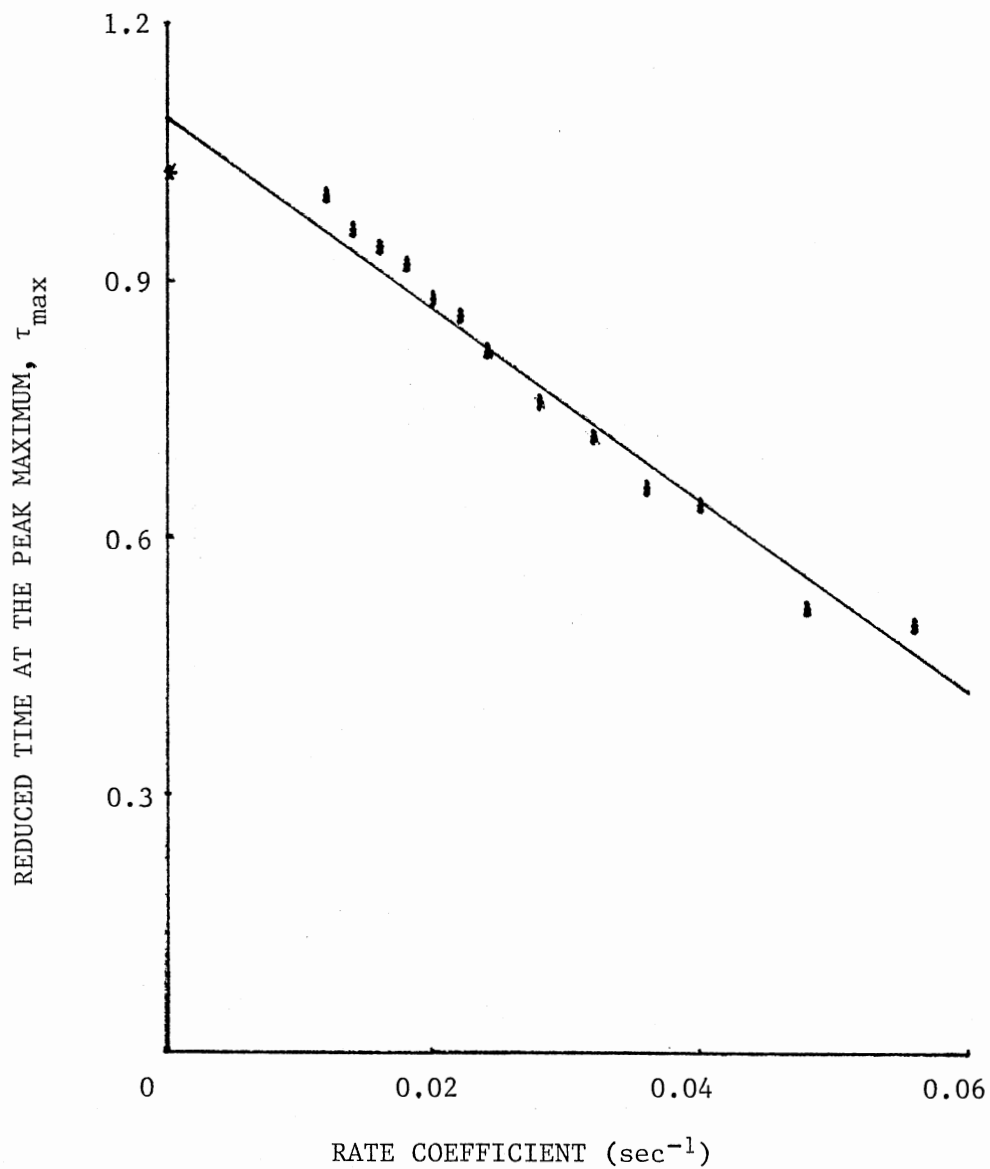
Figure 39. Variation of the Reduced Time at Peak Maximum
with Simulated Rate Coefficient – Data
Extracted from Figure 33
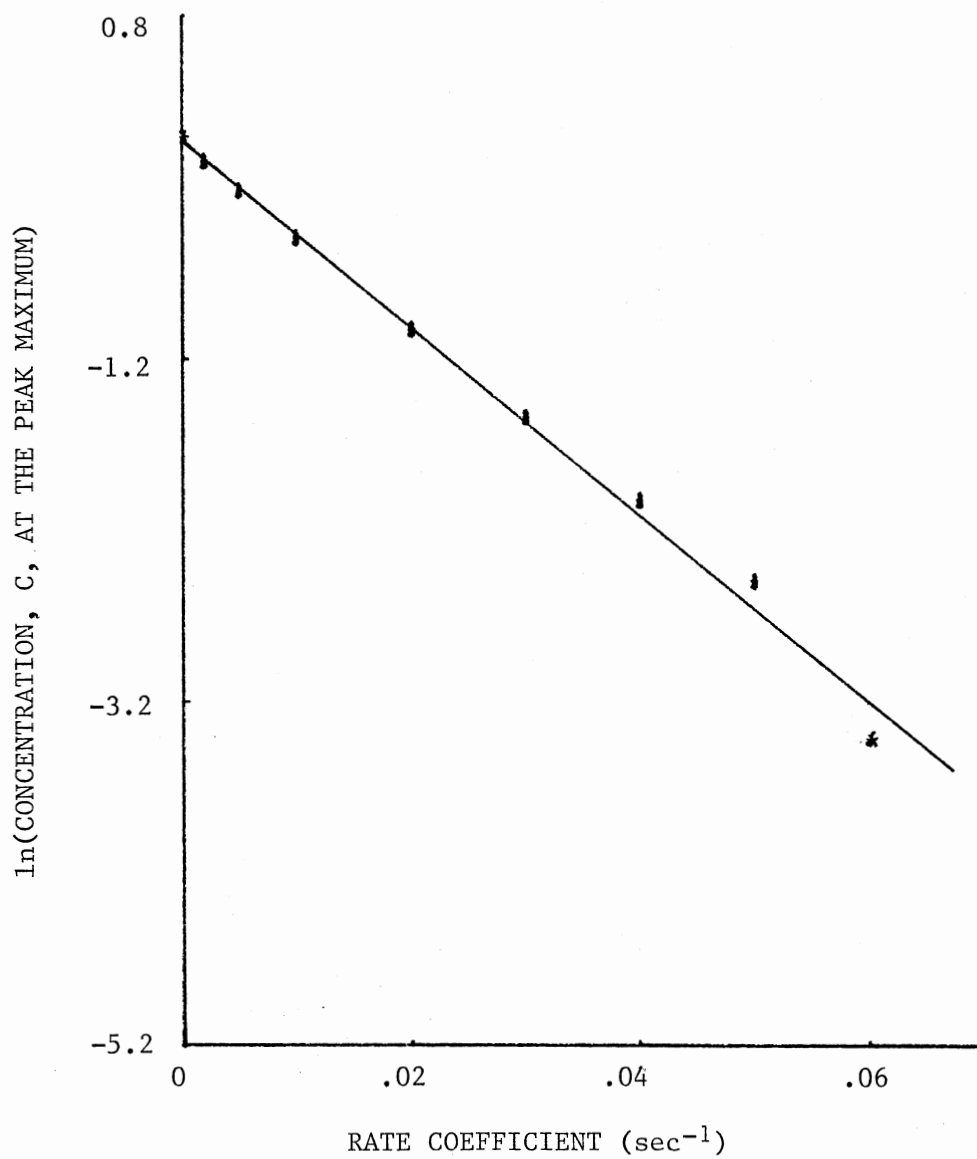
Figure 40. Variation of ln(Peak Maximum Concentration) with Simulated Rate Coefficient - Data Extracted from Figure 34
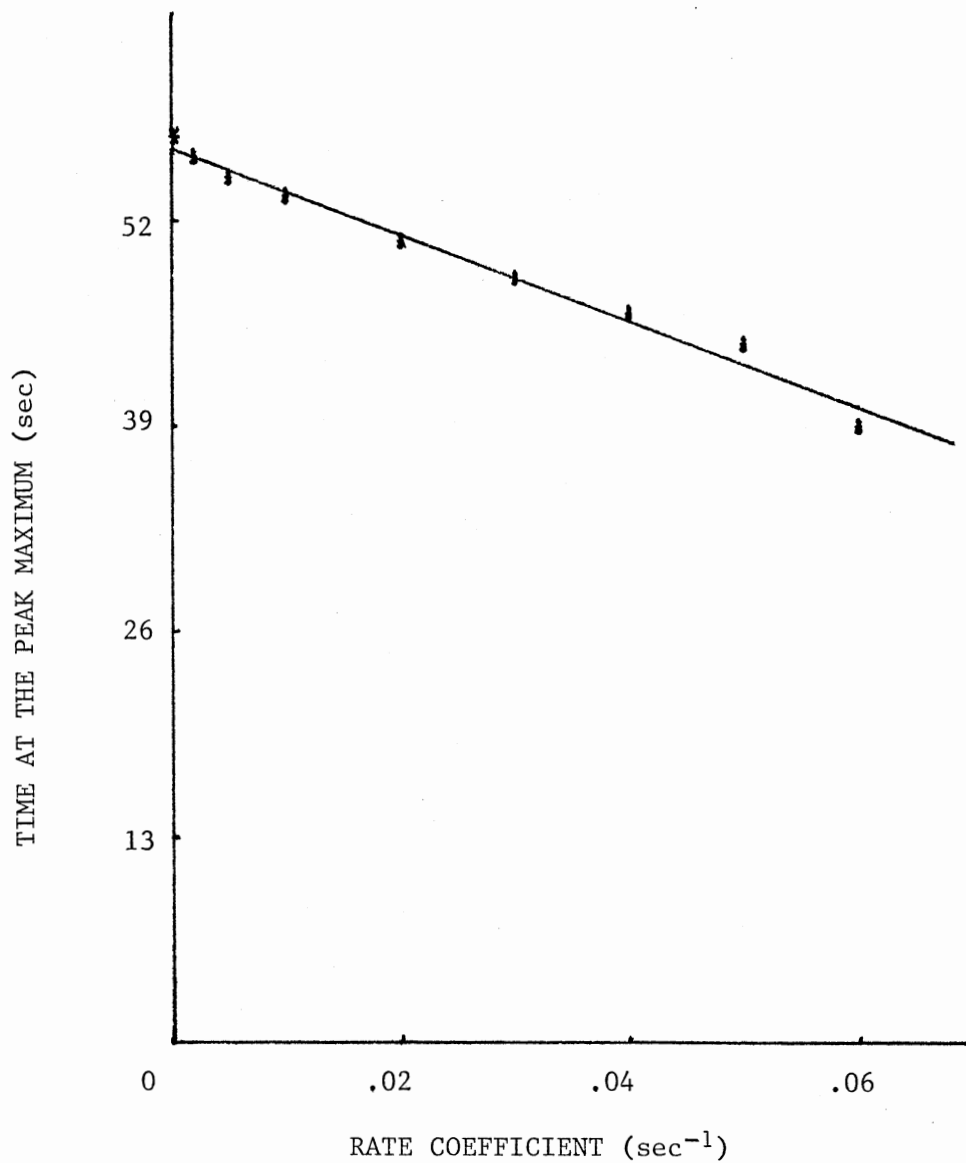
Figure 41. Variation of the Time at the Peak Maximum
with Simulated Rate Coefficient - Data
Extracted from Figure 34

TABLE VIII

EVALUATION OF RATE COEFFICIENTS PREDICTED
FROM THEORETICAL MODELS

THEORETICAL MODEL	RATE COEFFI-CIENT DETER-MINED FROM THE BATCH EXPERIMENT	RATE COEFFI-CIENT PRE-DICTED FROM ln(concen-tration) PLOT	%ERROR RELA-TIVE TO BATCH EXPERI-MENT	RATE COEFFI-CIENT PRE-DICTED FROM time at peak maximum PLOT	%ERROR RELA-TIVE TO BATCH EXPERI-MENT
Numerical Simulation Model	0.0186 (sec^{-1})	0.0186 (sec^{-1})	0.00%	0.0181 (sec^{-1})	2.69%
Simulation from Taylor Model	0.0186 (sec^{-1})	0.0251 (sec^{-1})	34.9%	0.0251 (sec^{-1})	34.9%

TABLE IX

PERCENT ERRORS FOR THE EXTRACTED RATE COEFFICIENTS
FROM NUMERICALLY SIMULATED CURVES WITH RE-
SPECT TO THE EXPERIMENTAL RATE CO-
EFFICIENTS OBTAINED FROM
BATCH STUDIES

pH of the System	% Error
3.22	9.24%
3.64	5.09%
3.81	3.43%
4.76	1.08%
5.25	1.16%

model have also been performed to systems of different pH values. Table IX is a list of the error produced in the above processes. The result in this table suggests that the deviation of the extracted rate coefficient from that of the batch experiment increases as pH of the system decreases (the reaction rate increases as pH decreases). Presumably lower pH complicated the mechanism of the reaction, and the system was deviated from the assumed pseudo-first order kinetics, resulting in larger error.

Double-Humped Peak Induced by Chemical Effect

In Chapter III it was pointed out that a double-humped peak appears when the nature of the dispersion of a flowing sample plug shifts from pure convection to pure diffusion. The experimental results shown in Figure 42 imply that the chemical effect induced this situation. Figure 42 was obtained while the sample volume was substantially larger than the reactor volume (this condition, however, is not a realistic one for flow injection determinations). The steady state plateau is disrupted by the contribution of the chemical effect. The chemical reaction introduces a new concentration gradient, enhances the diffusional force, and thus changes the dispersion pattern. The greater the chemical contribution, the greater the transitional change and more pronounced the hump is. The data in Table X supports this rationale by demonstrating a more pronounced "hump" at larger sample concentrations, due to increased amount of chemical reaction.
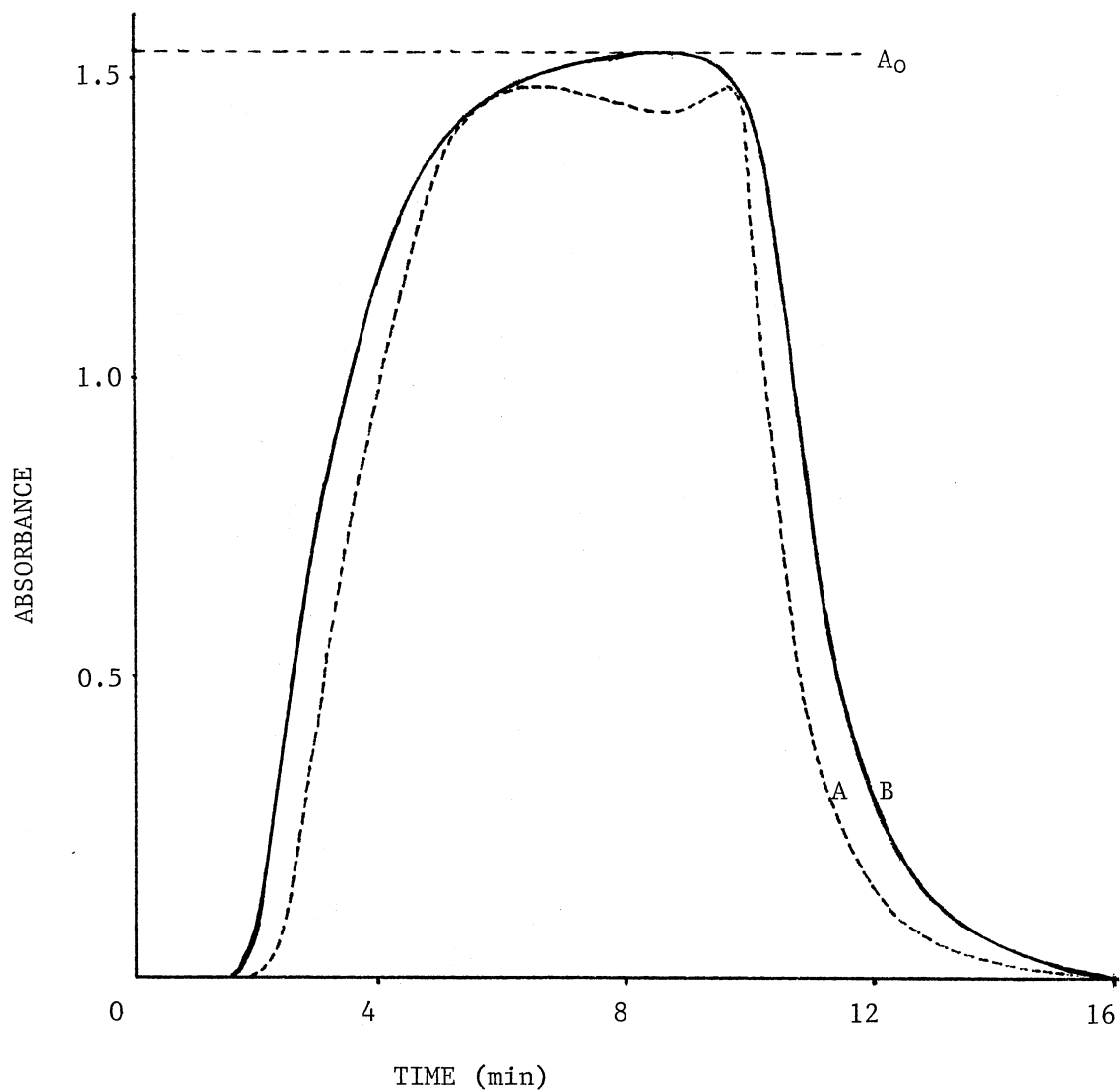
Experimental Conditions: Radius, a = 0.025 cm; Reactor, Straight Open Tube with Length, L = 95 cm; Flow Rate, F = 0.14 mL/min; Sample Loop Length, L_S = 600 cm; pH 5.40; Absorbance of the Original Sample, A_O = 1.56.

Figure 42. Steady State Signals with (A) and without (B) Chemical Effect

TABLE X

VARIATION OF THE INJECTED SAMPLE CONCENTRATION WITH
THE HEIGHT OF THE FIRST HUMP MEASURED FROM THE
LOWEST POINT OF THE STEADY-STATE SIGNAL

CONCENTRATION OF THE IN-JECTED SAMPLE (mM)	HEIGHT OF THE HUMP AT PEAK MAXIMUM (absorbance units)
0.300	3.2×10^{-2}
0.400	4.4×10^{-2}
0.500	6.0×10^{-2}

CHAPTER VII

EFFECT OF SOME EXPERIMENTAL CONDITIONS

ON CHEMICAL CONTRIBUTION

TO DISPERSION

The effect of a chemical reaction on the dispersion of an injected
sample solution in a flowing stream has been discussed extensively in
Chapter VI. In many cases, the chemical contribution to dispersion
changes its characteristics when the experimental conditions change. The
effect of some experimental conditions on the chemical contribution to
dispersion will be discussed in the present chapter under separate head-
ings, namely, injection method, sample volume, reactor geometry, reactor
tubing material, and carrier stream concentration.

Sample Injection Method

There are two types of injection devices which are commonly adopted
in flow injection systems, rotary valve and syringe injection. Because
of the nature of these injection methods, the flow pattern is inter-
rupted transiently during injection into the flow.   However, the
type of injection method used may influence the signal profile and the
chemical effect on dispersion. The present section will be devoted to a
comparison of the effects of the syringe "push-in" injection with the
rotary sliding valve "insert-in" injection.

The construction of the sliding rotary valve has been previously

described in Chapter IV. The attached sample loops used in the valve are 0.5 mm i.d. Tygon tubing of 15.3 cm, 40.7 cm, 66.2 cm, 91.6 cm, and 117.0 cm in length which correspond to 50 μL, 100 μL, 150 μL, 200 μL, and 250 μL respectively. The syringe injector was a Hamilton gas tight syringe (#750, Lure Tip, Hamilton Company, Reno, Nevada).

Figure 43 represents the typical signal profile obtained from the two injection methods. Sample injection by means of a syringe pushes the flowing stream forward, creating a transient convection turbulence. This turbulence acts to maintain the sample plug integrity, preventing the sample plug from spreading, therefore, reducing the interaction between sample and carrier streams. On the other hand, the rotary valve intercalates the sample plug into the carrier stream, no turbulence is generated, consequently, molecular diffusion and laminar convection are the main driving forces for the sample-carrier interaction. From Figure 43 it can be seen that the signal obtained by rotary valve injection has a 50% longer travel time, t_A (20 sec versus 10 sec), a 15% longer time for returning to baseline, Δt_B (172 sec versus 146 sec), and a 17% larger signal height (0.63 absorbance versus 0.52 absorbance) than the signal obtained by syringe injection. The transient reduction of mixing between sample and carrier at the time of injection becomes a disadvantage for the syringe injection system when the analytical output relies on an effective mixing. Only sufficient residence time can minimize this effect. Figure 44 and Figure 45 indicate that the rotary valve injection and the syringe injection perform equally well at low values of sample/reactor volume ratio. The rotary valve injection, however, becomes superior as the value of sample/reactor volume ratio exceeds 0.48.
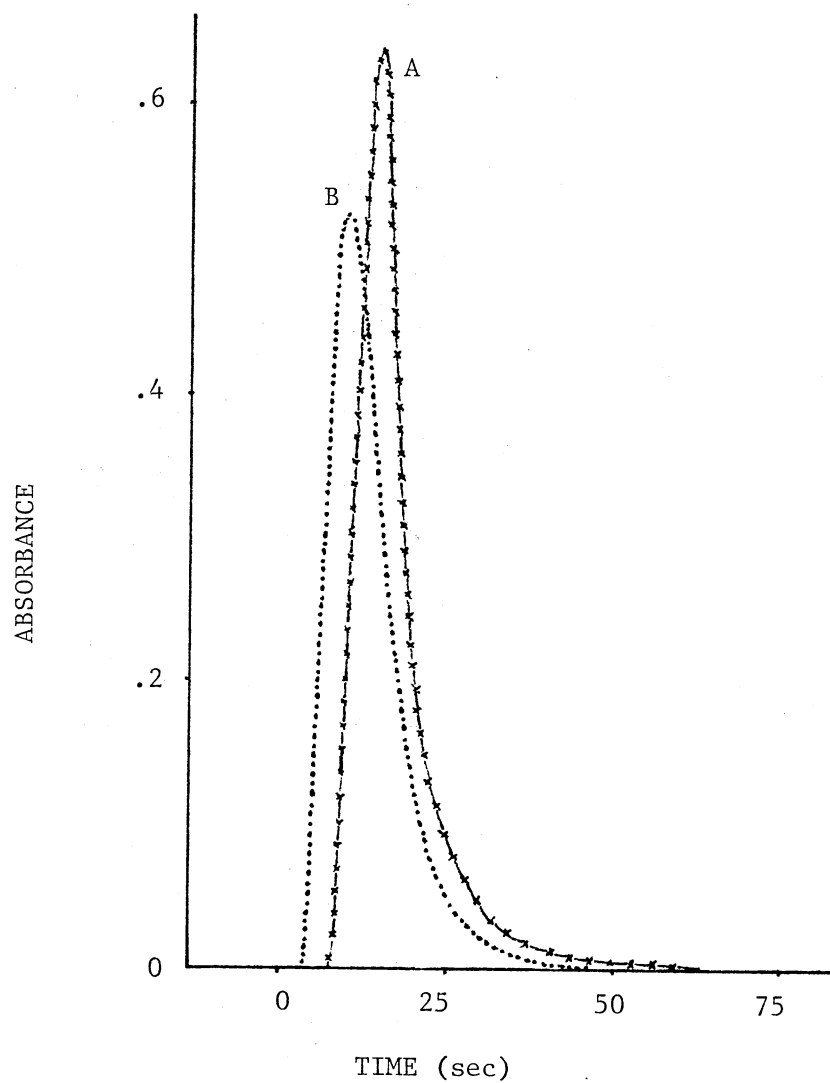
Experimental Conditions for Both Signals:
  Radius, a = 0.025 cm; Reactor, Straight Open
  Tube with Length, L = 105 cm; Flow Rate, F =
  0.8 mL/min; Sample Volume, V_S = 50 µL; pH
  4.2.

Figure 43. A Comparison of the Typical Signal Profiles
            Obtained with a Rotary Valve Injection
            System (A) and a Syringe Injection
            System (B)
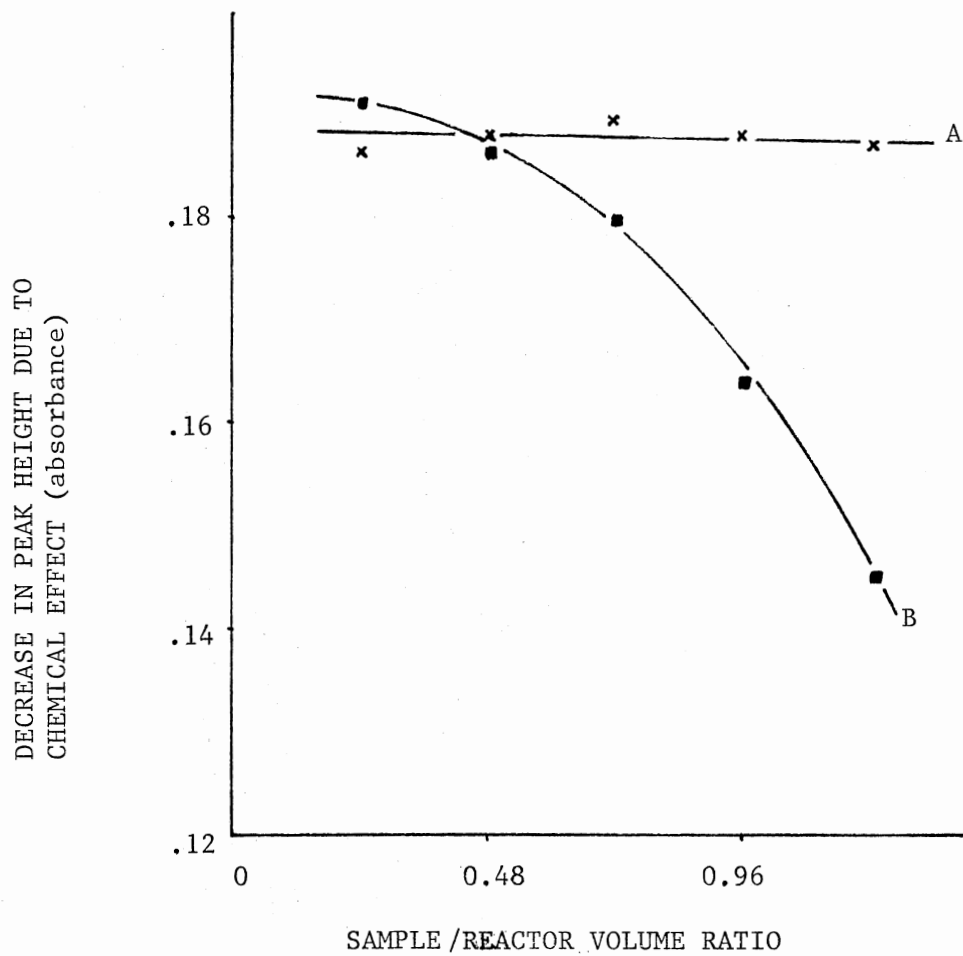
Experimental Conditions for Both Injection Systems:
Radius, a = 0.025 cm; Reactor, Straight Open Tube
with Length, L = 105 cm; Flow Rate, F = 0.80
mL/min; pH 4.2.

Figure 44.   A Comparison of Chemical Contribution to Peak Height
for a Rotary Valve Injection System (A) and a
Syringe Injection System (B)
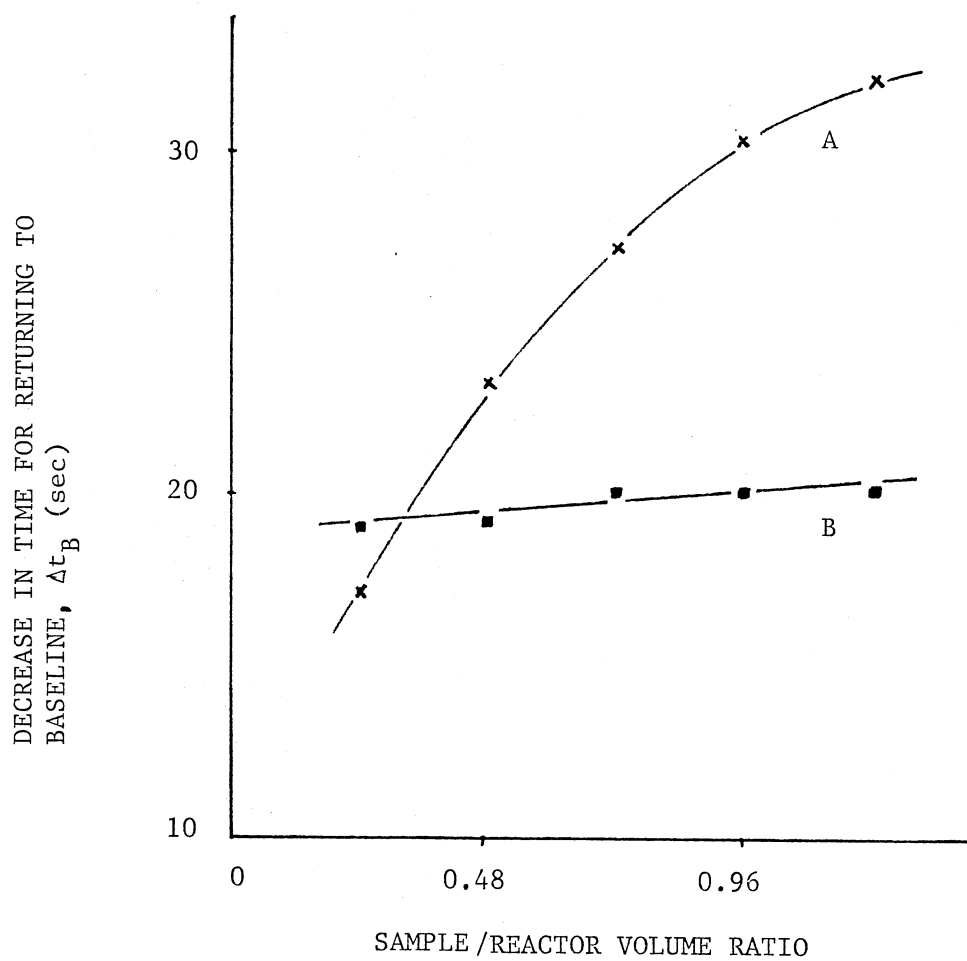
Experimental Conditions for Both Injection Systems:
  Radius, a = 0.025 cm; Reactor, Straight Open
  Tube with Length, L = 105 cm; Flow Rate, F =
  0.80 mL/min; pH 4.2.

Figure 45. A Comparison of the Chemical Contribution to Time
            for Returning to Baseline for a Rotary Valve
            Injection System (A) and a Syringe Injection
            System (B)

In addition, syringe injection causes a momentary increase of the linear flow velocity, upon injecting a sample into the flow. This increase is manifested by a typical negative or positive peak on the baseline. Consequently, a relatively large volume reactor is required for effective control of dispersion. This is another disadvantage in using the syringe injection method.

Effect of Sample Size on Dispersion

Because the volume of the injected sample may constitute a substantial part of the volume of the entire flow manifold, the sample size is important when discussing the dispersion.

Recall the expression that describes the relationship of sample size and the corresponding peak shape (Equation 126),

$$C = C_0\{1 - \exp(-\beta V_s)\}$$

where

$$\beta = 0.693/(S_{\frac{1}{2}})$$

with $S_{\frac{1}{2}}$ representing the volume of sample solution necessary to reach a 50% of the steady state signal height. This equation implies that the sensitivity of the system depends on the magnitude of $S_{\frac{1}{2}}$. Therefore when the available sample size is small, such as in clinical analysis, the flow manifold should be designed in such a way to keep $S_{\frac{1}{2}}$ as small as possible.

Table XI presents the experimental results which can be used to examine the validity of Equation 126. The experimental conditions used for obtaining the data in the table were: Radius, a = 0.025 cm; Re-

TABLE XI

A COMPARISON OF THE VALIDITY OF EQUATION 126 FOR SYSTEMS
WITH AND WITHOUT CHEMICAL CONTRIBUTION

SYSTEM WITHOUT A CHEMICAL EFFECT				SYSTEM WITH A CHEMICAL EFFECT			
SAMPLE VOLUME (μL)	EXPERI-MENTAL SIGNAL HEIGHT (absorbance)	SIGNAL HEIGHT CAL-CULATED FROM EQ.126 (absorbance)	% ERROR	SAMPLE VOLUME (μL)	EXPERI-MENTAL SIGNAL HEIGHT (absorbance)	SIGNAL HEIGHT CAL-CULATED FROM EQ.126 (absorbance)	% ERROR
34	.276	.279	1.09	34	.210	.257	22.4
48	.401	.390	2.73	48	.315	.352	11.8
61	.481	.478	.62	61	.393	.441	12.2
75	.578	.568	1.73	75	.480	.526	9.6
89	.670	.665	.81	89	.565	.605	7.1
103	.742	.733	1.21	103	.641	.681	6.2
155	.980	.973	.70	155	.880	.930	5.7
185	1.111	1.119	.72	185	1.068	1.049	1.8
389	1.619	1.633	.86	389	1.530	1.560	2.0
805	1.920	1.919	.05	805	1.888	1.867	1.1
1198	1.970	1.961	.50	1198	1.930	1.918	.6

actor was a straight open tube of a length, L = 105 cm; Flow rate, F = 0.8 ml/min; pH of the system was 4.5. In this table, the calculated signal heights were obtained by applying Equation 126. Interpolated $S_{\frac{1}{2}}$ values are different for systems with and without a chemical contribution, i.e. 153 μL for a system with no chemical contribution, and 163 μL for a system with chemical effect. The calculated error indicates that Equation 126 holds well in systems with solely physical dispersion, and it fails in systems with a chemical effect only at sample sizes below 185 μL.

Larger samples which take a longer time to pass through the detecting area, result in a wider signal baseline. This is illustrated in Figure 46. Figure 46 presents a plot of linear variations of the signal baseline width with the sample size. The slope of the curve representing the system of no chemical effect is 0.84, while the slope of the curve representing the system with a chemical effect is 0.78. The difference in slopes indicates that the increase in signal baseline width with the increase in sample size is smaller when a chemical effect is present in the system.

The Effect of Reactor Geometry
on Dispersion

It is well-established that the dispersion can be manipulated by modifying the geometry of the reactor. The use of coils and a single-bead-string reactor are examples of the reactor geometry modifications. In the present section, several subjects will be discussed concerning the effect of reactor geometry on the chemical contribution to the dispersion, namely, coiling, single-bead-string packing, a comparison of
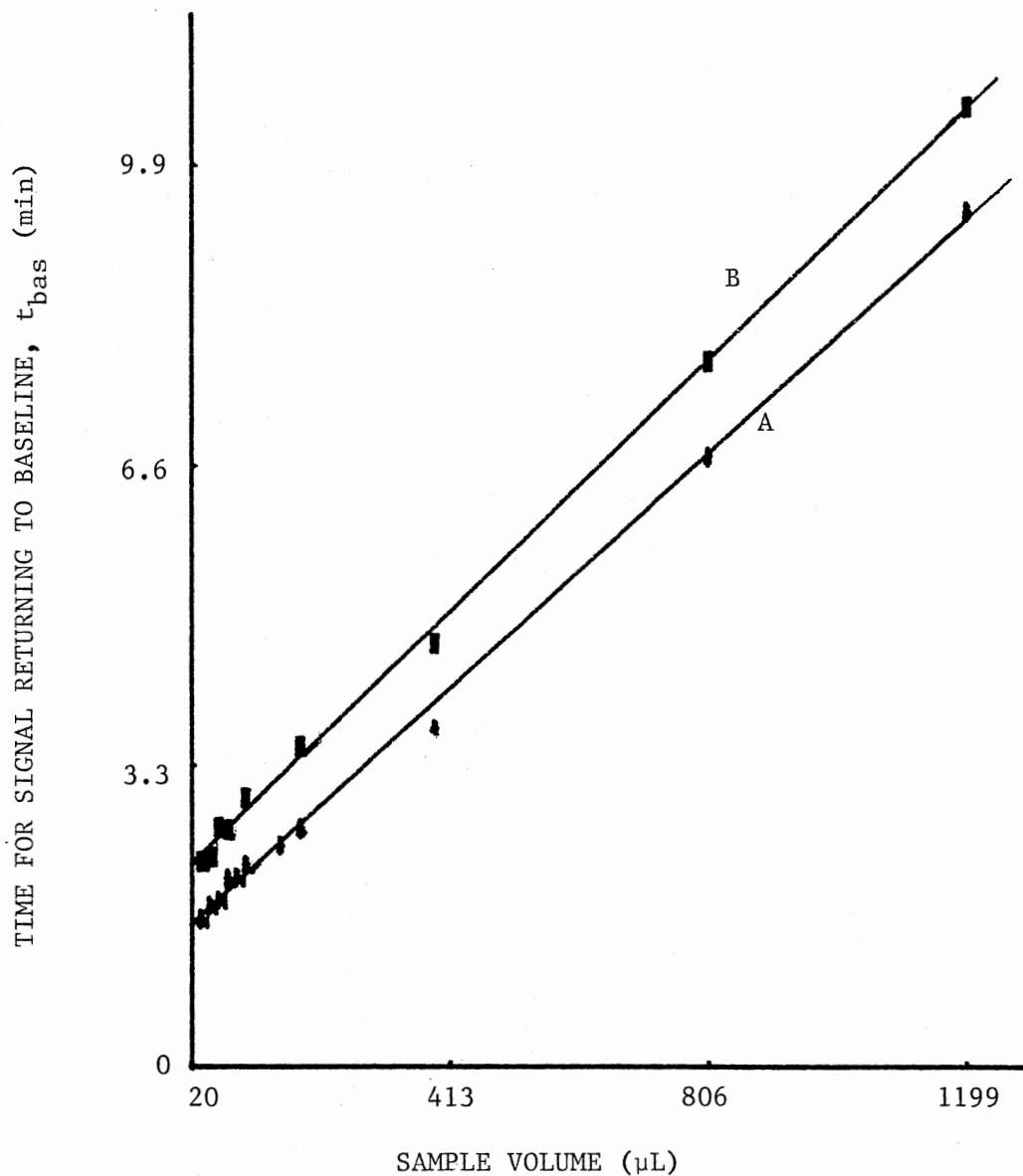
Experimental Conditions: Radius, a = 0.025 cm; Reactor, Straight Open Tube with Length, L = 105 cm; Flow Rate, F = 0.8 mL/min; pH 4.5.

Figure 46. The Variation of the Signal Baseline Width with the Volume of the Injected Sample for Systems with Chemical Effect (A) and Without Chemical Effect (B)

these two, and the combined effect of coiling and single-bead-string packing.

The Effect of Coiling on Chemical Contribution
to the Dispersion

The secondary flow effect in a coiled tubing has been found to enhance the radial mixing. Therefore for a system where the flowing sample plug undergoes physical dispersion as well as chemical reaction in a coiled reactor, the secondary flow effect must have some influence on the output signal profile. The effect of secondary flow on the chemical contribution to dispersion is illustrated in Table XII, and is discussed in the following. Let H_{max} and t_{bas} denote the signal height and time for returning to baseline obtained from a system with solely physical dispersion respectively, and $(H_{max})'$ and $(t_{bas})'$ denote the signal height and time for returning to baseline obtained from the same system with an additional chemical effect. Therefore, values of $|H_{max} - (H_{max})'|$ and $|t_{bas} - (t_{bas})'|$ should be proportional to the amount of chemical effect on the dispersion. For a straight tubing reactor, a larger diameter tubing offers a longer residence time and the corresponding values of $|H_{max} - (H_{max})'|$ and $|t_{bas} - (t_{bas})'|$ are larger. This increase in the values of $|H_{max} - (H_{max})'|$ and $|t_{bas} - (t_{bas})'|$ are even more pronounced when a part of these reactors are coiled and secondary flows are present, which implies an enhancement of chemical contribution to dispersion. Table XII also domonstrates that the enhancement of chemical contribution to the dispersion is dependent upon the tubing diameter, and the greatest enhancement occurred with tubing of the smallest diameter.

TABLE XII

A COMPARISON OF THE CHEMICAL EFFECT IN A STRAIGHT OPEN TUBING
AND A COILED OPEN TUBING OF THE SAME LENGTH

TYPE OF REACTOR	STRAIGHT OPEN TUBE REACTOR (150 cm) F =.33 mL/min, pH 4.5				COILED OPEN TUBE REACTOR (150 cm, coiled portion is 90 cm) F =.33 mL/min, pH 4.5			
INNER DIAMETER OF THE TUBING (mm)	0.5	0.8	1.0	1.3	0.5	0.8	1.0	1.3
H_{max} (mm)	208	146	99	63	249	179	105	64
$(H_{max})'$ (mm)	199	113	65	28	198	123	59	19
$H_{max} - (H_{max})'$ (mm)	9	33	34	35	51	46	46	45
t_{bas} (mm)	46	65	80	98	32	53	70	92
$(t_{bas})'$ (mm)	40	58	72	90	20	40	55	76
$t_{bas} - (t_{bas})'$ (mm)	6	7	8	8	12	13	15	16

The Effect of Single-Bead-String Packing on the

Chemical Contribution to Dispersion

Because of the difficulty in finding beads of the proper sizes for
packing tubing of different diameter, the only tubing used in this study
was 1.3 mm i.d. Teflon tubing. The single-bead-string reactor studied
was packed with 1 mm glass beads, which amounts to 77% of the tubing
diameter. The signal profiles obtained by using this straight single-
bead-string reactor, and a comparable straight open tube reactor, are
presented in Figure 47, while a quantitative comparison of the chemical
effect on peak height and peak width for the two reactors are presented
as Table XIII. From the table, it can be seen that the straight single-
bead-string reactor produces a 1.5 times larger chemical effect on peak
height, and 2.6 times larger chemical effect on the peak width than the
comparable straight open tube. These comparisons imply that the eddy
diffusion generated in a packed reactor provides more effective mixing.
Effective mixing promotes the chemical reaction, thereby increasing the
chemical contribution to the dispersion.

A packed reactor can sometimes be disadvantageous to chemical con-
tribution to the overall dispersion. Since the packed glass beads take
over a part of the reactor inner space, the linear flow velocity is
greater in a single-bead-string reactor than in its counterpart, the
straight open tubing, at the same flow rate. Therefore in a single-bead-
string reactor, the time available for chemical reaction shortens. If
a chemical reaction requires a longer reaction time than can be provided
by travelling through a specified length of a single-bead-string reactor,
then a longer length of single-bead-string reactor will be necessary.
But a longer packed reactor will mean an increased back pressure which
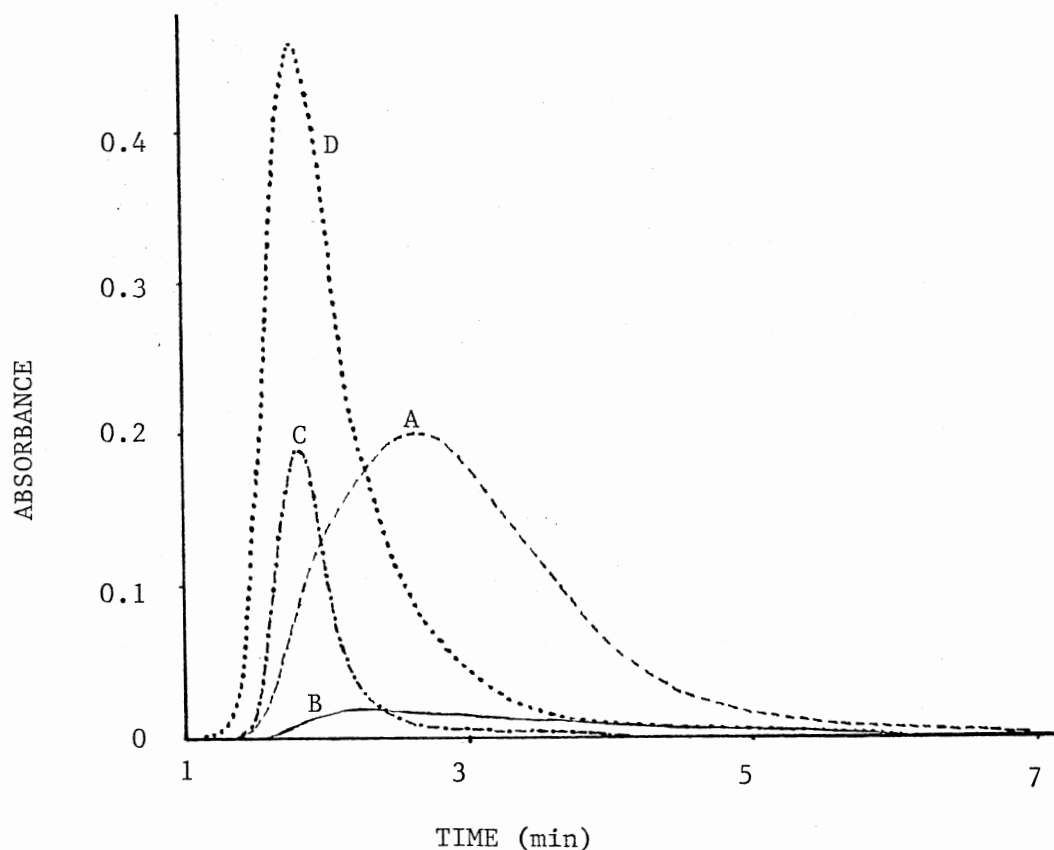
Experimental Conditions for the Both Reactors:
  Radius, a = 0.065 cm; Reactor Length, L = 66 cm;
  Flow Rate, F = 0.33 mL/min; Sample Volume,
  V_S = 62 µL; pH 4.5.

The Signals Were Obained Under the Following
  Conditions: Straight Open Tube Reactor in a
  System Without Chemical Effect (A), and With
  Chemical Effect (B); Straight Single-Bead-
  String Reactor in a System Without Chemical
  Effect (D), and With Chemical Effect (C).

Figure 47. A Comparison of the Signal Profiles Obtained in
           a System Containing a Straight Open Tube
           Reactor and a System Containing a Straight
           Single-Bead-String Reactor

TABLE XIII

A COMPARISON OF CHEMICAL EFFECT ON PEAK HEIGHT AND
PEAK WIDTH FOR STRATGHT OPEN TUBING REACTOR
AND SINGLE BEAD STRING REACTOR

REACTORS COMPARISON	STRAIGHT OPEN TUBE REACTOR	SINGLE BEAD STRING REACTOR
Hmax (mm)	53.8	128
(Hmax)' (mm)	5.0	51
Hmax $-$ (Hmax)' (mm)	48.8	72
W_{bas}[11] (mm)	140.0	125
(W_{bas})'[12] (mm)	115.0	60
$W_{bas} - (W_{bas})$' (mm)	25.0	65

----

[11]W_{bas} denotes the signal baseline width obtained from a system with solely physical dispersion.

[12](W_{bas})' denotes the signal baseline width obtained from a system with both physical and chemical dispersions.

may not be desired by the user. If this should cause a problem, another means of mixing, such as a mixing chamber, should be added to the reactor rather than extending the length of the single-bead-string reactor.

A Comparison of a Coiled Open Tube Reactor and a
Straight Single-Bead-String Reactor

In a coil the mixing across the stream is enhanced by the secondary flow effect, which tends to oppose the dilution of the injected sample by a longitudinal dispersion. Consequently, high and narrow signals may be expected.

In a single-bead-string reactor eddy diffusion provides effective mixing in both directions, i.e. across and along the flowing stream, which facilitates the chemical reaction(s) which may occur between the sample and the carrier solutions. Consequently, the chemical effect on dispersion can be enhanced by the use of a single-bead-string reactor.

A comparison may be made between the chemical effects that are achieved by either coiling or packing a reactor tubing. The data which are listed in Table XII and Table XIII are taken for this comparison. The original experiments that were conducted to produce the data listed in these two tables are comparable, and both the open coil and the straight single-bead-string reactor are constructed with a 1.3 mm i.d. Teflon tubing, but the length of the coil is 2.3 times that of the length of the single-bead-string reactor. The chemical effect measured by the decrease in signal height relative to a straight open tube reactor, is 1.48 for the single-bead-string reactor and 1.29 for the open coil. Obviously, a single-bead-string reactor provides a larger chemical effect on dispersion than an open coil even at a shorter length of the

bead reactor. However, if a very long single-bead-string reactor is required to provide a sufficient residence time and mixing, such that back pressure due to packing may be a problem, then an open coil may be used as an alternative. Furthermore, the construction of an open coil is easier than the construction of a single-bead-string reactor.

From the preceding discussion it appears that no conclusion may be reached regard to the overall superiority of either the open coil or straight single-bead-string reactors. Although Tijssen (148) claimed that his experiments show that both axial and radial dispersion in strongly coiled open tubes are more favourable than in the single-bead-string reactor with the same reactor volume, a much longer single-bead-string reactor would be required in order to have the same reactor volume as the open coil. Longer length reactors are expected to be unfavorable for both axial and radial dispersions.

The Effect of a Coiled Single-Bead-String Reactor on the Chemical Contribution to Dispersion

Mottola (146) has found that a coiled single-bead-string reactor surpasses an open coiled reactor of equal length by several times (see data in Table XIV) in a system where signal heights depended on the amount of chemistry involved. The reactors that were used in Mottola's study are those whose inner reactor surface has been physically as well as chemically modified. These kinds of reactor have not been used in the course of the present study, however, the data suggest that a coiled single-bead-string reactor have a promising positive effect on the dispersion.

TABLE XIV .

COMPARISON OF SIGNAL CHARACTERISTICS OBTAINED WITH AN OPEN
TUBE WALL REACTOR AND A SINGLE-BEAD-STRING REACTOR WITH
PENICILLINASE A IMMOBILIZED ON THE WALL OF THE TUBE
AND ON THE BEADS (ADOPTED FROM REFERENCE 146)[a]

Penicillin determined: Penicillin V (phenoxymethylpenicillinic acid; potassium salt obtained from Sigma Chemical Company, St. Louis, Missouri, USA).

Carrier stream: 5.0×10^{-4} M phosphate, pH 7.037

Sample size injected: 1.00 mL, 8.0×10^{-4} M penicillin.
Flow rate: 1 mL/min

	OPEN TUBE REACTOR	SINGLE-BEAD-STRING REACTOR
Peak height, mV	17.6	44.0
Width at half peak height, arbitrary units (b)	9	6
Area under the peak, arbitrary units (c)	330	585

(a)
  Coils were both 7 turns of 6 cm diameter (1.3 mm i.d., capillary . Glass beads were 1 mm nominal diameter from Propper Mfg. Co. Inc., Long Island City, NY.)

(b)
  Although the amount of penicillinoic acid released in the single-bead-string reactor is about twice that released in the open tube reactor, the control of dispersion provided by the beads obviates a decrease of sampling rate which, even though not optimized, is about 50 samples/h in this case.

(c)
  Graphical integration with an OTT planimeter, A. OTT, Kempten, Federal Republic of Germany.

In the present study the investigation of a coiled single-bead-string reactor without wall-modification was conducted. Table XV presents the comparison between a coiled single-bead-string reactor and a straight single-bead-string reactor of the same size. The coiled single-bead-string reactor provides a 1.44 times greater chemical effect on the peak height than the straight single-bead-string reactor, while the former also results in a 1.07 times greater chemical effect on the signal baseline width than the latter.

All of the previous discussion about reactor geometry suggests that

TABLE XV

A COMPARISON OF THE CHEMICAL CONTRIBUTION TO THE PEAK HEIGHT
AND THE PEAK BASELINE WIDTH FOR A STRAIGHT SINGLE-BEAD-
STRING REACTOR AND A COILED SINGLE-BEAD-STRING
REACTOR OF THE SAME LENGTH

REACTORS / COMPARISON	STRAIGHT SINGLE-BEAD-STRING REACTOR $a = 0.065$ cm $L = 66$ cm $F = 0.33$ mL/min $V_S = 62$ μL pH 4.5	COILED SINGLE-BEAD-STRING REACTOR $a = 0.065$ cm $L = 66$ cm $F = .33$ mL/min $V_S = 62$ μL pH 4.5
H_{max} (mm)	125	156
$(H_{max})'$ (mm)	55	55
$H_{max} - (H_{max})'$ (mm)	70	101
W_{bas} (mm)	87	76
$(W_{bas})'$ (mm)	59	50
$W_{bas} - (W_{bas})'$ (mm)	28	26

a coiled single-bead-string reactor approaches an ideal reactor. The combined effect of secondary flow and eddy diffusion, is very beneficial in obtaining a high and narrow signal provided that back pressure is not a problem. In addition, the effective mixing in a coiled single-bead-string reactor makes it very analytical sound for flow injection determinations.

The Effect of Reactor Tubing Material
on the Dispersion

Because of the difference in dragging force on the walls, reactor tubings of different material generate different velocity profiles for the same flow rate, results of different chemical effect are therefore expected.

In the present study the primary part of the reactor tubing had an inner diameter of 0.05 cm, a length of 573 cm, and was made of three selected materials: glass, Teflon, and Tygon. The flow rate was measured as 0.40 mL per minute, and the sample size used was 62 μL.

The experimental results presented in Figure 48 imply that there is no significant difference in the peak height and width for the three different material reactors in the system without chemical reaction. But the fact that the three signal maxima appear at different times illustrates the different amount of "dragging" effect observed in each of the materials tested. Teflon tubing seems to have a greater dragging force on the walls than the glass and Tygon tubings, which promotes the mixing of the sample and the carrier and thereby increases the chemical effect on dispersion.

Tubing Materials: Tygon (····); Glass (-x-x-x-x);
Teflon (----).
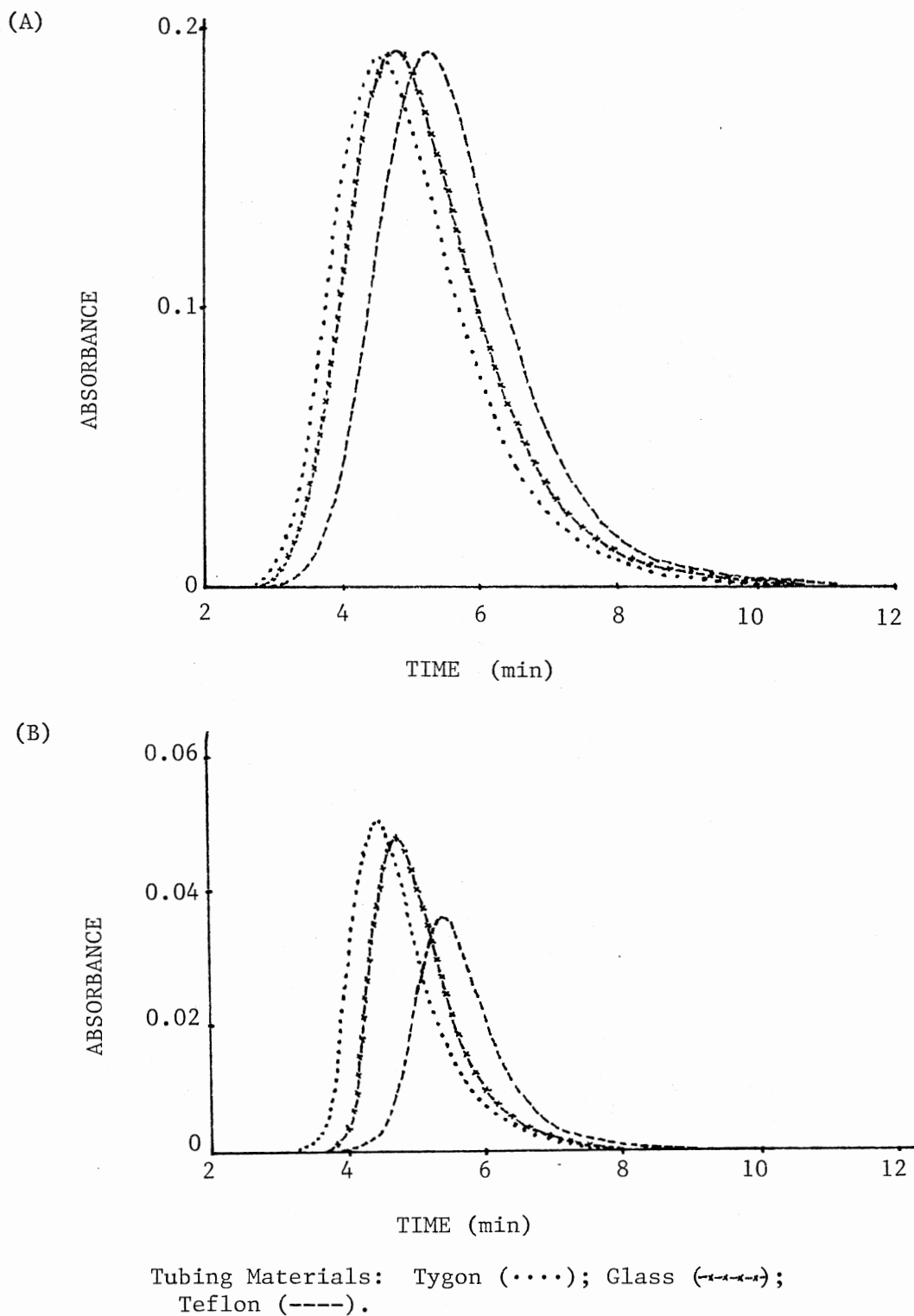
Figure 48. A Signal Profile Comparison for three Equal-Length
Reactor Tubings of Different Material in a
System without a Chemical Effect (Part A) and
a System with a Chemical Effect (Part B)

The Effect of the Carrier Stream Concentration

on the Dispersion

In order to have pseudo first order kinetics, the concentration of the background carrier stream is made sufficiently large (such as 100:1 to the sample solution). The concentration of the background carrier has an effect, however, on the analytical readout, and this effect depends on the flow rate of the flowing stream. Figure 49 demonstrates the change in signal height due to changing concentrations of the carrier.

The experiment which provided the result for Figure 49 was carried out in a straight, 155 cm long, 0.05 cm i.d. reactor. The concentration of the injected dichromate sample, 62 µL, was 0.50 mM, while the concentration of the L-ascorbic acid carrier stream was in the range of 0.50 mM to 45.0 mM, and the pH of the system was 4.5. Four flow rates were selected for use in the experiments; 0.28, 1.24, 1.68, and 2.19 mL/min.

Figure 49 shows that the chemical effect contributes to the signal height only when the carrier/sample concentration is beyond the stoichiometric ratio. At a flow rate of 2.19 mL/min, it takes a 12 mM carrier to double the practical dispersion number, D, defined by Ruzicka and Hansen (see Table V). But at a flow rate of 0.28 mL/min, it takes only a 6 mM carrier to double the value of D. By the same token a 10 mM carrier would maximize the contribution of chemistry (i.e. peak maximum no longer decreases with increasing carrier stream concentration) to dispersion at the flow rate of 0.28 mL/min, while a 40 mM carrier is required for maximization at the flow rate of 2.19 mL/min.

It has been known that a small flow rate reduces the number of de-
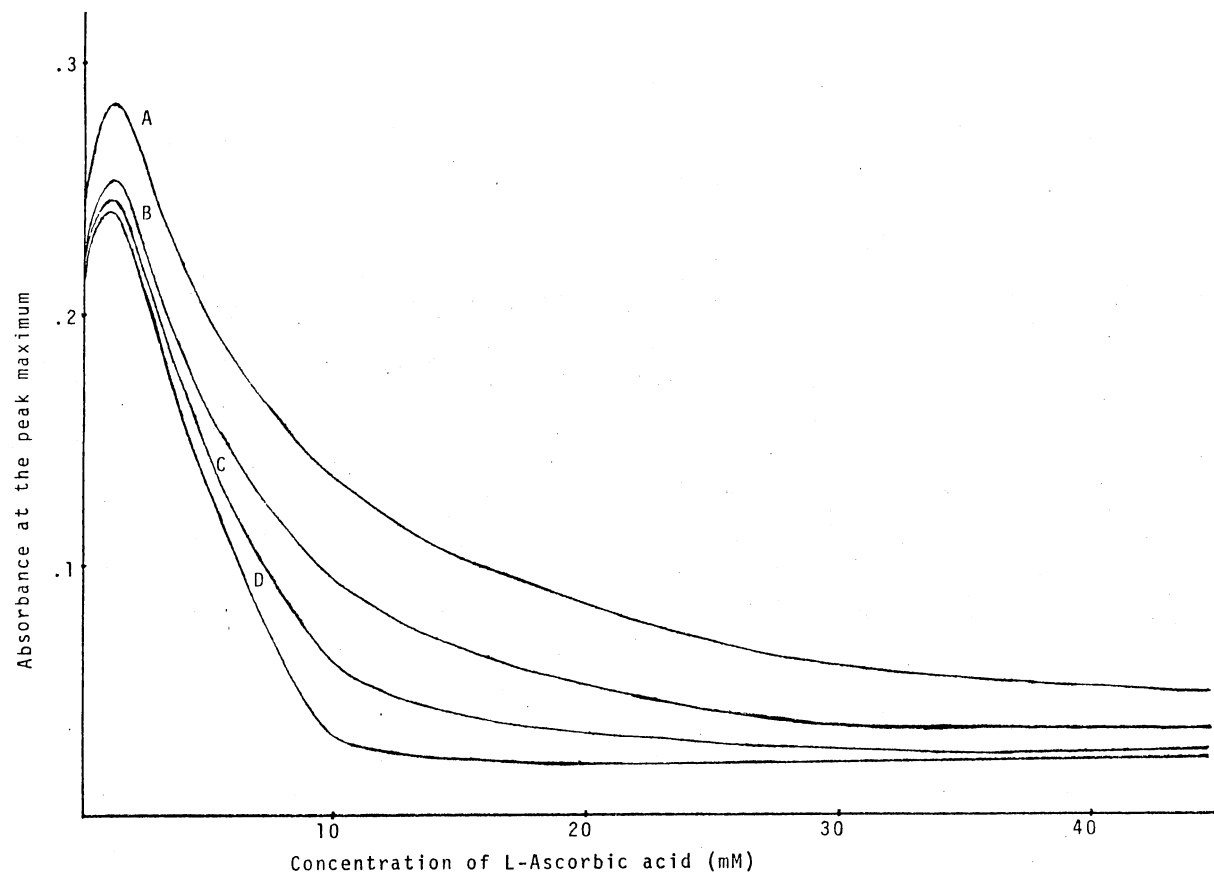
Flow Rates for each Curve: 2.19 mL/min (A); 1.68 mL/min (B);
     1.24 mL/min (C); 0.28 mL/min (D).

Figure 49.   Variations of Absorbance at the Peak Maximum with Concentrations
             of the Background Carrier Stream

terminations per unit time, therefore, the preceding observations made from Figure 49 imply that a trade off exists between determination rate and cost per determination. To achieve a specified signal height which carries a desired amount of chemical contribution, a small flow rate may be used at the expense of the determination rate or a higher carrier concentration may be used but this may result in an increased cost per determination.

CHAPTER VIII

CONCLUSION

As demonstrated in Chapter V, the numerical model, based on the laminar dispersion equation, is more effective for simulating signals typically obtained in flow injection analysis. The model requires not only the knowledge of time-dependence for the dispersion, but also precise measurements of the reactor vessel dimensions. The model calls for a straight open cylindrical reactor; different reactor geometries are not accommodated by the model. The effects of different flow geometries on the dispersion, however, have been discussed in Chapter VII.

Correction factors are necessary a system for which manifold does not have a uniform diameter. These correction factors are unique for a specific experimental set-up. Therefore, recalculation of the correction factor(s) is necessary for any change made in the flow manifold unless values of these factors are very close to unity.

Laminar dispersion with a simultaneously occurring chemical reaction was expressed mathematically as Equation 139, Chapter V, that is

$$\frac{dC}{dt} + U_{max}(1 - \frac{r^2}{a^2})\frac{dC}{dx} = D(\frac{d^2C}{dx^2} + \frac{1}{r}\frac{dC}{dr} + \frac{d^2C}{dr^2}) - k(C)^n$$

Because of the unknown nature of the chemical dynamics, the above equation was solved by regarding it as the following two processes (Equations 19 and 140):

$$\begin{cases} \dfrac{dC}{dt} = D\left(\dfrac{d^2C}{dx^2} + \dfrac{1}{r}\dfrac{dC}{dr} + \dfrac{d^2C}{dr^2}\right) - U_{max}\left(1 - \dfrac{r^2}{a^2}\right)\dfrac{dC}{dx} \\[3em] \dfrac{dC}{dt} = -k(C)^n \end{cases}$$

The total time elapsed was divided into very small subdivisions. By solving the two equations consecutively for each time step, the physical dispersion (Equation 19) and chemical reaction (Equation 140) were treated as virtually two simultaneous processes as it is expected to be experimentally.

The fact that the extracted rate coefficient, from simulated curves resulting from the above treatment, closely resembled the rate coefficient obtained from the batch study suggests the validity of the treatment.

In the present study, the model was restricted to systems in which chemical reaction takes place upon the mixing of the sample and the carrier solutions. For a system in which the chemical reaction depends on the mass transfer of the sample molecules to the reactor walls, then the wall retention capability will make the dispersion phenomenon more complicated than systems discussed in the present study.

It should be mentioned that the primary goal of the present study was not the simulation of FIA curves, but to open a door for the investigation of chemical dynamics involved in a flow injection process. The computer simulation of FIA curves was a tool used for the accomplishment of the above goal in the present work. Understanding chemical dynamics in a flow injection system, is not only essential to controlling dispersion for the desired quality of analytical readout (high sensitivity, large number of determinations per unit time), but also contributes to

the optimization of the system parameters such as the sample size, the reactor volume, the reagent concentration, etc.

The observed wave pattern of rate coefficients for a, physically dispersed, chemically reacted, injected sample plug suggests a dependence of reaction rate on the physical dispersion. Extensive mathematics and computer calculations will be required to further study the kinetics/dispersion interrelated phenomenon.

BIBLIOGRAPHY

(1)   Skeggs, L. T. Jr. Amer. J. Clin. Pathol., 1957, 28, 311-322

(2)   Margoshes, M. Anal. Chem., 1977, 49, 17-19

(3)   Nagy, G.; Feher ZS; Pungor, E. Anal. Chim. Acta, 1970, 52, 47-54

(4)   Ruzicka, J.; Hansen, E. H. Anal. Chim. Acta, 1975, 78, 145-157

(5)   Stewart, K. K.; Beecher, G. R.; Hare, P. E. Anal. Biochem., 1976,
         70, 167-173

(6)   Westhaver, J. W. Industri. Eng. Chem. (Industri. Ed.), 1942, 126-
         130

(7)   Hamilton, W. F.; Moore, J. W.; Kinsman, J. M.; Spurling, R. G.
         Am. J. Physiol., 1928, 84, 338-344 (Quoted from this paper)

(8)   Stewart, G. N. J. Physiol., 1897, 22, 159-173

(9)   Hamilton, W. F.; Moore, J. W.; Kinsman, J. M.; Spurling, R. G.
         Am. J. Physiol., 1932, 99, 534-551

(10) Allen, C. M.; Taylor, E. A. Mech. Eng., 1924, 46, 13-16

(11) Meier, P.; Zierler, K. L. J. Appl. Physiol., 1954, 6(12), 731-744

(12) Hamilton, W. F.; Remington, J. W. Am. J. Physiol., 1947, 148,
         35-39

(13) Lane, D. A.; Sirs, J. A. J. Physics E Sci. Instru., 1974, 7, 51-
         55

(14) Spalding, D. B. Chem. Eng. Sci., 1958, 9, 74-77

(15) Gronzalez-Fernandez, J. M. Circulation Res., 1962, 10, 409-427

(16) Bate, H.; Rowlands, S.; Sirs, J. A. J. Appl. Physiol., 1973, 34
         (6), 866-872

(17) Rossi, H. H.; Powers, S. H.; Dwork, B. Am. J. Physiol., 1935,
         173, 103-108

(18) Harris, T. R.; Newman, E. V. J. Appl. Physiol., 1970, 28(6), 840-
         850

(19) Newman, E. V.; Merrell, M.; Genecin, A.; Monge, C.; Milonso, W. K.; McKeeves, W. P. Circulation, 1951, 4, 735-746

(20) Bassingthwaighte, J. B.; Ackerman, F. H.; Wood, E. H. Circulation Res., 1966, 18, 398-415

(21) Conrad, W. A.; Broncato, R. W.; Pallini, C. A. J. Appl. Phys., 1965, 36, 861-863

(22) Taylor, G. Proc. Roy. Soc. London, Ser. A, 1953, 219, 186-203

(23) Taylor, G. Proc. Roy. Soc. London. Ser. A. 1954, 223, 446-468

(24) Levenspiel, O.; Bischoff, K. B. Adv. Chem. Eng., 1963, 4, 95-198

(25) Goresky, C. A. Am. J. Physiol., 1963, 204, 626-640

(26) Perl, W.; Chinard, F. P. Circulation Res., 1968, 22, 273-298

(27) Bate, H.; Rowlands, S.; Sirs, J. A.; Thomas, H. W. Brit. J. Appl. Phys. (J. Phys. D), 1969, Ser. 2, 2, 1447-1456

(28) Carnahan, B.; Luther, H. A.; Wilkes, J. O. "Applied Numerical Methods", John Wiley & Sons, Inc., N.Y. 1969, p.431

(29) Caro, C. G. J. Physiol., 1966, 185, 501-519

(30) Aris, R. "Elementary Chemical Reactor Analysis", Prentice-Hall Inc., Englewood Cliffs, N.J. 1969, p.306

(31) Danckwerts, P. V. Chem. Eng. Sci., 1953, 2, 1-13

(32) Levenspiel, O. "Chemical Reaction Engineering", 1st ed., John Wiley & Sons, Inc., N.Y. 1967

(33) Wen, C. Y.; Fan, L. T. "Models for Flow Systems and Chemical Reactors", Marcel Dekker, Inc., N.Y. 1975

(34) Gatsev, V. A.; Zaitsev, A. I. Theor. Found. Chem. Eng., 1977, 11(1), 65-69

(35) Gill, W. N. Proc. Roy. Soc. London, Ser. A, 1967, 298, 335-339

(36) Ananthakrishnan, V.; Gill, W. N.; Barduhn, A. J. A. I. Ch. E. Journal, 1965, 11(6), 1063-1072

(37) Aris, R. Proc. Roy. Soc. London, Ser. A, 1956, 235, 67-77

(38) Aris, R. Proc. Roy. Soc. London, Ser. A, 1959, 252, 538-550

(39) Wissler, E. H. Chem. Eng. Sci., 1969, 24, 527-539

(40) Wehner, J. F.; Wilhelm, R. H. Chem. Eng. Sci., 1956, 6, 89-93

(41) Taylor, G. Proc. Roy. Soc. London, Ser. A, 1954, 225, 473-477

(42) Philip, J. R. Aust. J. Phys., 1963, 16, 287-299

(43) Philip, J. R. Aust. J. Phys., 1963, 16, 300-310

(44) Bournia, A.; Coull, J.; Houghton, G. Proc. Roy. Soc. London, Ser. A, 1961, 261, 227-236

(45) Geankoplis, C. J. "Transport Processes and Unit Operations", Allyn and Bacon, Inc., Boston 1978, p.263

(46) Evans, E. V.; Kenney, C. N. Proc. Roy. Soc. London, Ser. A, 1965, 284, 540-550

(47) Bailey, H. R.; Gogarty, W. B. Proc. Roy. Soc. London, Ser. A, 1962, 269, 352-367

(48) Ruzicka, J.; Hansen, E. H. National Bureau of Standards Special Publications, 1978, 519, 501-507

(49) Sternberg, J. C. "Advances in Chromatograghy", Giddings, J. C.; Keller, R. A. ed., 2nd Ed., Marcel Dekker, N.Y. 1966, pp. 205-270

(50) Snyder, L. R. J. Chromatogr., 1976, 125, 287-306

(51) Golay, M. J. E.; Atwood, J. G. J. Chromatogr., 1979, 186, 353-370

(52) Atwood, J. G.; Golay, M. J. E. J. Chromatogr., 1981, 218, 97-122

(53) Rajcsanyi, P. M.; Rajcsanyi, E. "High-Speed Liquid Chromatography", Marcel Dekker, N.Y. 1975

(54) Littlewood, A. B. "Gas Chromatography", 2nd Ed., Academic Press, N.Y. 1970, p.144

(55) Golay, M. J. E. Anal. Chem., 1957, 29, 928-932

(56) Golay, M. J. E. Nature, 1957, 180, 435-436

(57) Golay, M. J. E. "Gas Chromatography 1958", Desty, D. H. ed., Butterworths Publications, Ltd., London, 1958, pp.36-55

(58) Halasz, I. J. Chromatogr., 1979, 173, 229-247

(59) Hofmann, K.; Halasz, I. J. Chromatogr., 1979, 173, 211-228

(60) Giddings, J. C. "Dynamics of Chromatography", Dekker, N.Y. 1965, p.154

(61) Snyder, L. R.; Adler, H. J. Anal. Chem., 1976, 48, 1022-1027

(62) Snyder, L. R.; Levine, J.; Stoy, R.; Conetta, A. Anal. Chem., 1976, 48, 942A-956A

(63) Thiers, R. E.; Reed, A. H.; Delander, K. Clin. Chem., 1971, 17, 42-48

(64) Thiers, R. E.; Cole, R. R.; Kirsch, W. J. Clin. Chem., 1967, 13, 451-467

(65) Evenson, M. A.; Hicks, G. P.; Thiers, R. E. Clin. Chem., 1970, 16, 606-611

(66) Thiers, R. E.; Jeyn, M.; Wildermann, R. F. Clin. Chem., 1970, 16, 832-839

(67) Walker, W. H. C.; Pennock, C. A.; McGowan, G. K. Clin. Chim. Acta, 1970, 27, 421-435

(68) Ertingshausen, G.; Adler, H. J.; Reichler, A. S. J. Chromatogr., 1969, 42, 355-366

(69) Begg, R. D. Anal. Chem., 1971, 43, 854-857

(70) Begg, R. D. Anal. Chem., 1972, 44, 631-632

(71) Walker, W. H. C.; Andrew, K. R. Clin. Chim. Acta, 1974, 57, 181-185

(72) Snyder, L. R.; Adler, H. J. Anal. Chem., 1976, 48, 1017-1022

(73) Concus, P. T. J. Phys. Chem., 1970, 74, 1818-1819

(74) Levich, V. G. "Physiochemical Hydrodynamics", Prentice Hall, Englewood Cliffs, N.J. 1962, p.681, eq.133.26

(75) Patton, C. J.; Rabb, M.; Crouch, S. R. Anal. Chem., 1982, 54, 1113-1118

(76) Deelder, R. S.; Kroil, M. G. F.; Beeren, A. J. B.; van den Berg, J. H. M. J. Chromatogr., 1978, 149, 669-682

(77) Snyder, L. R. Anal. Chim. Acta, 1980, 114, 3-18

(78) Scott, R. P. W.; Kucera, P. J. Chromatogr. Sci., 1971, 9, 641-644

(79) Ruzicka, J.; Hansen, E. H. "Flow Injection Analysis", John Wiley & Sons, Inc., N.Y. 1981

(80) Ramasamy, S. M.; Jabbar, M. S. A.; Mottola, H. A. Anal. Chem., 1980, 52, 2062-2066

(81) Stewart, J. W. B.; Ruzicka, J.; Bergamin Filho, H.; Zagatto, E. A. Anal. Chim. Acta, 1976, 81, 371-386

(82)   Ruzicka, J.; Hansen, E. H.; Zagatto, E. A. Anal. Chim. Acta,
          1977, 88, 1-16

(83)   Ruzicka, J.; Hansen, E. H.; Mosbæk, H.; Krug, F. J. Anal. Chem.,
          1977, 49, 1858-1861

(84)   van den Berg, J. H. M.; Deelder, R. S.; Egberink, H. G. M, Anal.
          Chim. Acta, 1980, 114, 91-104

(85)   Ranger, C. B. Anal. Chem., 1981, 53, 21A-32A

(86)   Betteridge, D. Anal. Chem., 1978, 50, 832A-846A

(87)   Ruzicka, J.; Hansen, E. H.; Mosbæk, H. Anal. Chim. Acta, 1977,
          92, 235-249

(88)   Ramsing, A. U.; Ruzicka, J.; Hansen, E. H. Anal. Chim. Acta,
          1981, 129, 1-17

(89)   Hansen, E. H.; Ruzicka, J. J. Chem. Edu., 1979, 56, 677-680

(90)   Hansen, E. H.; Ruzicka, J.; Ghose, A. K. Anal. Chim. Acta, 1978,
          100, 151-165

(91)   Persson, B.; Rosen, L. Anal. Chim. Acta, 1981, 123, 115-123

(92)   Madsen, B. C. Anal. Chim. Acta, 1981, 124, 437-441

(93)   Betteridge, D.; Fields, B. Anal. Chem., 1978, 50, 654-656

(94)   Stewart, K. K.; Rosenfeld, G. J. Auto. Chem., 1981, 3, 30-32

(95)   Reijn, J. M.; van der Linden; Poppe, H. Anan. Chim. Acta, 1981,
          126, 1-13

(96)   Reis, B. F.; Bergamin Fº, H.; Zagatto, E. A. G.; Krug, F. J.
          Anal. Chim. Acta, 1979, 107, 309-317

(97)   Mindegaard, J. Anal. Chim. Acta, 1979, 104, 185-189

(98)   Åstrom, Q. Anal. Chim. Acta, 1979, 105, 67-75

(99)   Bergamin Fº, H.; Zagatto, E. A. G.; Krug, F. J.; Reis, B. F.
          Anal. Chim. Acta, 1978, 101, 17-23

(100) Ruzicka, J.; Srewart, J. W. B.; Zagatto, E. A. G. Anal. Chim.
          Acta, 1976, 81, 387-396

(101) Reis B. F.; Jacintho, A. O.; Mortatti, J.; Krug, F. J.; Zagatto,
          E. A. G.; Bergmin Fº, H.; Pessenda, L. C. R. Anal. Chim.
          Acta, 1981, 123, 221-228

(102) Ruzicka, J.; Hansen. E. H. Anal. Chim. Acta, 1978, 99, 37-76

(103) Lighthill, M. J. J. Inst. Math. Applics., 1966, 2, 97-108

(104) Gibilaro, L. G. Nature, 1977, 270, 47-48

(105) Reijn, J. M.; van der Linden, W. E.; Poppe, H. Anal. Chim. Acta, 1980, 114, 105-118

(106) Levenspiel, O. "Chemical Reaction Engineering", 2nd Ed., John Wiley & Sons, Inc., N.Y. 1972

(107) Pungor, E.; Feher, ZS; Nagy, G.; Toth, K.; Horvai, G.; Gratzl, M. Anal. Chim. Acta, 1979, 109, 1-24

(108) Vanderslice, J. T.; Stewart, K. K.; Rosenfeld, A. G.; Higgs, D. J. Talanta, 1981, 28, 11-18

(109) Mottola, H. A.; Hanna, A. Anal. Chim. Acta, 1978, 100, 167-180

(110) Karlberg, B.; Johansson, P; Thelander, S. Anal. Chim. Acta, 1979, 104, 21-28

(111) Gine, M. F.; Zagatto, E. A. G.; Bergamin F$^{\text{O}}$, H. Analyst, 1979, 104, 371-375

(112) Stewart, K. K.; Beecher, G. R.; Hare, P. E. Anal. Biochem., 1976, 70, 167-173

(113) Bergamin F$^{\text{O}}$, H.; Medeiros, J. X.; Reis, B. F.; Zagatto, E. A. G. Anal. Chim. Acta, 1978, 101, 9-16

(114) Karlberg, B.; Thelander, S. Analyst, 1978, 103, 1154-1159

(115) Wolff, Ch. M.; Mottola, H. A. Anal. Chem., 1978, 50, 94-98

(116) Ruzicka, J.; Hansen, E. H. Anal. Chim. Acta, 1980, 114, 19-44

(117) Meschi, P. L.; Johnson, D. C. Anal. Chim. Acta, 1981, 124, 303-314

(118) Ramsing, A. U.; Janata, J.; Ruzicka, J.; Levy, M. Anal. Chim. Acta, 1980, 113, 45-52

(119) Betteridge, D.; Ruzicka, J. Talanta, 1976, 23, 409-410

(120) Betteridge, D.; Dagless, E. L.; Fields, B.; Graves, N. F. Analyst, 1978, 103, 897-908

(121) Krug, F. J.; Ruzicka, J.; Hansen, E. H. Analyst, 1979, 104, 47-54

(122) Mayock, K. P.; Tarbell, J. M.; Duda, J. L. Sep. Sci. Tech., 1980, 15, 1285-1296

(123) Gill, W. N.; Ananthakrishnan, V. A. I. Ch. E. Journal, 1967, 13, 801-807

(124) Gaunce, A. P.; D'Iorio, A. Anal. Biochem., 1970, 37, 204-207

(125) Halasz, I., Private Communication with Scott, R. P. W.; Kucera,
        P. J. Chromatogr. Sci., 1971, 9, 641-644

(126) Painton, C. C.; Mottola, H. A. Anal. Chem., 1981, 53, 1713-1715

(127) Pardue, H. L.; Fields, B. Anal. Chim. Acta, 1981, 124, 39-63

(128) Rule, G.; Seitz, W. R. Clin. Chem., 1979, 25, 1635-1638

(129) Hansen, E. H.; Ruzicka, J. U. S. Patent, 4224033, Sep. 23, 1980

(130) Reijn, J. M. "Flow Injection Analysis", Ph.D. Thesis, University
        of Amsterdam, The Netherlands, 1982

(131) van Deemter, J. J.; Broeder, J. J.; Lauwerier, H. A. Appl. Sci.
        Res., 1956, A5, 374-388

(132) Austin, L. R.; Seader, J. D. A. I. Ch. E. Journal, 1973, 19, 85-
        94

(133) Tijssen, R. Anal. Chim. Acta, 1980, 114, 71-89

(134) Stewart, J. W. B.; Ruzicka, J. Anal. Chim. Acta, 1976, 82, 137-
        144

(135) Tijssen, R. "Axial Dispersion in Helically Coiled Open Columns
        for Chromatography", Thesis, Delft, The Netherlands, 1979,
        p.62

(136) Dean, W. R. Phil. Mag. Ser. 7, 1927, 4, 208-223

(137) Dean, W. R. Phil. Mag. Ser. 7, 1928, 5, 673-695

(138) Snyder, L. R. Anal. Chim. Acta, 1980, 114, 3-18

(139) Hiby, J. W. "Proceedings of Symposium on Interaction Between
        Fluids and Particles", Rottenburg, P. A. ed., Institution
        of Chemical Engineers, London, 1962, p.312

(140) White, W. L.; Erickson, M. M.; Stevens, S. C., eds. "Practical
        Automation for the Clinical Laboratory", C. V. Mosby Co.,
        St. Louis, 1968, pp.36-186, 195-198, 309-343

(141) Scott, R. P. W.; Blackburn, D. W. J.; Wilkins, T. "Advances in
        Gas Chromatography, 1967" Zlatkis, A. ed., Preston Technical
        Abstracts, Evanston, Ill. 1967, p.160

(142) Scott, D. S.; Lee, W.; Papa, J. Chem. Eng. Sci., 1974, 29, 2155-
        2167

(143) Reijn, J. M.; van der Linden, W. E.; Poppe, H. Anal. Chim. Acta,
        1981, 123, 229-237

(144) Carnahan, B.; Luther, H. A.; Wilkes, J. O. "Applied Numerical Methods", John Wiley & Sons, Inc., N.Y. 1969, pp.270-272

(145) Douglas, J. Jr. J. A. C. M., 1959, 6, 48-58

(146) Mottola, H. A. Anal. Chem., In Press.

(147) van Deemter, J. J.; Zuiderweg, F. J.; Klinkenberg, A. Chem. Eng. Sci., 1956, 5, 271-280

(148) Tijssen, R. Plenary Lecture I, "Axial and Radial Dispersion Phenomena in Flow Analysis and Related Techniques", Flow Analysis II, International Symposium, Lund, Sweden, June 18-21, 1982

(149) Iob, A.; Mottola, H. A. Clin. Chem., 1981, 27, 195

(150) Ramasamy, S. M.; Mottola, H. A. Anal. Chem., 1982, 54, 283-286

APPENDIXES

APPENDIX A

ADDITIONAL PAPERS OF INTEREST NOT INCLUDED

IN THE REVIEW OF THE DISPERSION STUDIES

Laminar Dispersion in Cylindrical Tubes

Judeikis, H. S. J. Phys. Chem., 1980, 84, 2481-2484

Gill, W. N.; Ananthakrishnan, V.; Nunge, R. J. A. I. Ch. E. Journal,
    1968, 14, 939-946

Reejhsinghani, N. S.; Gill, W. N.; Barduhn, A. J. A. I. Ch. E. Journal,
    1966, 12, 916-921

Anderson, B.; Berglin, T. Proc. Roy. Soc. London. Ser. A, 1981, 377,
    251-268

Smith, R. J. Fluid Mech., 1981, 105, 469-486

van der Linden, W. E. trends in Anal. Chem., 1982, 1, 188-191

Gill, W. N.; Sankarasubramanian, Proc. Roy. Soc. London, Ser. A, 1970,
    316, 341-350

Erdogan, M. E.; Chatwin, P. C. J. Fluid Mech., 1967, 29, 465-484

Gill, W. N.; Ananthakrishnan, V. A. I. Ch. E. Journal, 1966, 12, 906-915

Scholten, A. H. M. T.; Brinkman U. A. Th.; Frei, R. W. Anal. Chem.,
    1982, 54, 1932-1938

Chemical Reaction and Diffusion in

Cylindrical Tubes

Walker, R. E. Phys. Fluid, 1961, 4, 1211-1216

Brown, R. L. J. Res. N. B. S., 1978, 83, 1-8

Daka, N. J.; Laidler, K. J. Can. J. Biochem., 1978, 56, 774-779

Pardue, H. L.; Fields, B. Anal. Chim. Acta, 1981, 124, 65-79

Mathematical Models used in Fluid Dispersion

Bischoff, K. B.; Levenspiel, O. Chem. Eng. Sci., 1962, 17, 245-255

Bischoff, K. B.; Levenspiel, O. Chem. Eng. Sci., 1962, 17, 257-264

Douglas, J. Jr. J. Soc. Indust. Appl. Math., 1955, 3, 42-65

Review or Historical Sketch of Flow

Injection Analysis

Rocks, B.; Riley, C. _Clin. Chem._, 1982, <u>28</u>, 409-421

Mottola, H. A. _Anal. Chem._, 1981, <u>53</u>, 1312A-1316A

APPENDIX B

TRANSFORMATION OF THE DISPERSION EQUATION

The laminar Dispersion equation (Equation 19) is:

$$D\left(\frac{d^2C}{dx^2} + \frac{1}{r}\frac{dC}{dr} + \frac{d^2C}{dr^2} \right) = \frac{dC}{dt} + U_{max}\left(1 - \frac{r^2}{a^2}\right)\frac{dC}{dx}$$

and the transformed parameters are:

$$X = \frac{x(D)}{a^2(U_{max})}; \qquad \tau = \frac{D(t)}{a^2}; \qquad \Omega = \frac{x(D/t)^{\frac{1}{2}}}{a(U_{max})} = X(\tau)^{-\frac{1}{2}};$$

$$y = \frac{r}{a}; \qquad C^* = \frac{C}{C_0}; \qquad N_{pe} = \frac{a(U_{max})}{D} \quad \text{(Peclet Number)}$$

then the transformations are performed as follows:

$$\frac{dC}{dx} = \frac{dC}{d\Omega}\left(\frac{d\Omega}{dx}\right) = \frac{dC}{d\Omega} \cdot \frac{d\{x(D/t)^{\frac{1}{2}} \cdot (aU_{max})^{-1}\}}{dx} = \frac{dC}{d\Omega} \cdot \frac{(D/t)^{\frac{1}{2}}}{a(U_{max})} \tag{151}$$

$$\frac{d^2C}{dx^2} = \frac{d}{dx}\left(\frac{dC}{dx}\right) = \frac{d}{dx}\frac{dC}{d\Omega} \cdot \frac{(D/t)^{\frac{1}{2}}}{a(U_{max})} = \frac{(D/t)^{\frac{1}{2}}}{a(U_{max})}\left\{\frac{d}{dx}\left(\frac{dC}{d\Omega}\right)\frac{d\Omega}{d\Omega}\right\}$$

$$= \frac{(D/t)^{\frac{1}{2}}}{a(U_{max})} \cdot \frac{d^2C}{d\Omega^2} \cdot \frac{d\Omega}{dx} = \frac{D}{a^2(U_{max})^2 t} \cdot \frac{d^2C}{d\Omega^2} = \frac{1}{\tau a^2(N_{pe})^2}\left(\frac{d^2C}{d\Omega^2}\right) \tag{152}$$

$$\frac{dC}{dr} = \frac{dC}{dy} \cdot \frac{dy}{dr} = \frac{dC}{dy} \cdot \frac{d(r/a)}{dr} = \frac{1}{a} \cdot \frac{dC}{dy} \tag{153}$$

$$\frac{1}{r} \cdot \frac{dC}{dr} = \frac{1}{r}\left(\frac{1}{a} \cdot \frac{dC}{dy}\right) = \frac{1}{a^2 y} \cdot \frac{dC}{dy} \tag{154}$$

$$\frac{d^2C}{dr^2} = \frac{d}{dr}\left(\frac{dC}{dr}\right) = \frac{d}{dy}\left(\frac{dC}{dr}\right)\frac{dy}{dr} = \frac{d}{dy}\left(\frac{1}{a} \cdot \frac{dC}{dy}\right)\left\{\frac{d(r/a)}{dr}\right\} = \frac{1}{a^2} \cdot \frac{d^2C}{dy^2} \tag{155}$$

$$\frac{dC}{dt} = \left\{\frac{dC}{d\Omega}\left(\frac{d\Omega}{dt}\right)\right\} + \left\{\frac{dC}{d\tau}\left(\frac{d\tau}{dt}\right)\right\} = \frac{dC}{d\Omega} \cdot \frac{d}{dt}\left\{\frac{x(D/t)^{\frac{1}{2}}}{a(U_{max})}\right\} + \frac{dC}{d\tau} \cdot \frac{d}{dt}\left(\frac{Dt}{a^2}\right)$$

$$= \frac{dC}{d\Omega}\left\{-\frac{1}{2} \cdot \frac{x(D/t)^{\frac{1}{2}}}{a(U_{max})}\right\} + \frac{dC}{d\tau}\left(\frac{D}{a^2}\right)$$

$$= (\frac{D}{a^2})\{(- \frac{xD^{\frac{1}{2}} \cdot t^{\frac{1}{2}}}{a \cdot Umax} \cdot \frac{a^2}{2D \cdot t})(\frac{dC}{d\Omega}) + (\frac{dC}{d\tau})\}$$

$$= (\frac{D}{a^2}) \cdot \{- \frac{1}{2} \frac{\Omega}{\tau}(\frac{dC}{d\Omega}) + (\frac{dC}{d\tau})\} \tag{156}$$

Substituting Equations 152, 154, and 155 into the Equation 19, the left-hand side of the Equation 19 becomes:

$$D \cdot \{\frac{1}{a^2\tau(N_{pe})^2}(\frac{d^2C}{d\Omega^2}) + \frac{1}{a^2y} \cdot \frac{dC}{dy} + \frac{1}{a^2} \cdot \frac{d^2C}{dy^2}\}$$

$$= \frac{D}{a^2} \cdot \{\frac{1}{\tau(N_{pe})^2} \cdot \frac{d^2C}{d\Omega^2} + \frac{1}{y} \cdot \frac{dC}{dy} + \frac{d^2C}{dy^2}\} \tag{157}$$

Substituting Equations 151, and 156 into the Equation 19, the right-hand side of the Equation 19 becomes:

$$(\frac{D}{a^2}) \cdot \{- \frac{1}{2} \frac{\Omega}{\tau}(\frac{dC}{d\Omega}) + \frac{dC}{d\tau}\} + Umax(1 - \frac{r^2}{a^2})(\frac{dC}{d\Omega})\{\frac{(D/t)^{\frac{1}{2}}}{a(Umax)}\}$$

$$= (\frac{D}{a^2})(1 - \frac{r^2}{a^2})\{\frac{a^2(D/t)^{\frac{1}{2}}}{a(D)}\}(\frac{dC}{d\Omega}) + (\frac{D}{a^2})\{- \frac{\Omega}{2\tau}(\frac{dC}{d\Omega}) + \frac{dC}{d\tau}\}$$

$$= (\frac{D}{a^2})(1 - y^2)\{a/(Dt)^{\frac{1}{2}}\}(\frac{dC}{d\Omega}) + (\frac{D}{a^2})\{- \frac{\Omega}{2\tau}(\frac{dC}{d\Omega}) + \frac{dC}{d\tau}\}$$

$$= (\frac{D}{a^2})(1 - y^2)(\tau)^{-\frac{1}{2}} \cdot (\frac{dC}{d\Omega}) + (\frac{D}{a^2})\{- \frac{\Omega}{2\tau}(\frac{dC}{d\Omega}) + \frac{dC}{d\tau}\}$$

$$= (\frac{D}{a^2})\{\frac{dC}{d\tau} + (\frac{1 - y^2}{\tau^{\frac{1}{2}}} - \frac{\Omega}{2\tau})(\frac{dC}{d\Omega})\} \tag{158}$$

The (D/a^2) term in both Equation 157 and Equation 158 can be eliminated by dividing them into each other. Thus, the laminar dispersion equation is now transformed into the following:

$$\frac{1}{\tau(N_{pe})^2} \frac{d^2C}{d\Omega^2} + \frac{1}{y} \frac{dC}{dy} + \frac{d^2C}{dy^2} = \frac{dC}{d\tau} + \{\frac{(1-y^2)}{\tau^{\frac{1}{2}}} - \frac{\Omega}{2\tau}\}(\frac{dC}{d\Omega}) \tag{159}$$

Correspondingly,

$$\frac{1}{\tau(N_{pe})^2} \frac{d^2C^*}{d\Omega^2} + \frac{1}{y} \frac{dC^*}{dy} + \frac{d^2C^*}{dy^2} = \frac{dC^*}{d\tau} + \{\frac{(1-y^2)}{\tau^{\frac{1}{2}}} - \frac{\Omega}{2\tau}\}(\frac{dC^*}{d\Omega}) \tag{160}$$

The initial and boundary conditions associated with the equation above
are:

$$\begin{cases} C^*(0, \ \Omega, \ y) = 0 \ \text{for} \ \Omega > 0; \\\\ C^*(\tau, \ 0, \ y) = 1 \ \text{for} \ \tau > 0 \ ; \\\\ C^*(\tau, \ \infty, \ y) = 0; \end{cases} \tag{161}$$

and

$$\frac{dC^*}{dy}(\tau, \ \Omega, \ 0) = \frac{dC^*}{dy}(\tau, \ \Omega, \ 1) = 0 \tag{162}$$

APPENDIX C

A LISTING OF THE COMPUTER PROGRAM FOR

NUMERICALLY SOLVING THE LAMINAR

DISPERSION EQUATION

```
C * * * * * * * * * * * * * * * * * * * * * * * * * * * * *
C
C * PURPOSE:   THIS PROGRAM IS TO SOLVE THE LAMINAR DISPERSION        *
C *            EQUATION NUMERICALLY BY THE ALTERNATING FINITE DIFFER-
C *            ENCE METHOD. SIMULATED CONCENTRATION VERSUS TIME DATA   *
C *            ARRAY ARE GENERATED FOR AN EXPERIMENTAL CONDITION
C *            COMMCNLY USED IN FLOW INJECTION ANALYSIS.               *
C
C * DEFINITION OF THE VARIABLES:                                      *
C    TAU = REDUCED TIME                    PE = PECLET NUMBER
C *  DTAU = TIME INTERVAL                   AL = ALPHA COEFFICIENT     *
C    DX = LONGITUDINAL DISTANCE INTERVAL   BE = BETA COEFFICIENT
C *  ML = PLUG FRONT TRAVEL LENGTH         CA = GAMMA COEFFICIENT      *
C    MT = PLUG TAIL TRAVEL LENGTH          D = CONSTANT TERM
C *  DY = RADIAL DISTANCE INTERVAL                                     *
C    I = LONGITUDINAL INCREMENT
C *  J = RADIAL INCREMENT                                              *
C    N = NO. OF RADIAL INTERVALS
C *  T = NO. OF LONGITUDINAL INTERVALS                                 *
C    CONC = TOTAL CONCENTRATION IN THE FLOW CELL
C *  T = POINT CONCENTRATION AT A FULL TIME-STEP FOR A SAMPLE PLUG     *
C    TPIMEI = LONGITUDINAL POINT CONCENTRATION
C *  TPIMEJ = RADIAL POINT CONCENTRATION                              *
C    TSTAR = POINT CONCENTRATION AT A HALF TIME-STEP
C *  TL = POINT CONCENTRATION AT A FULL TIME-STEP FOR SAMPLE PLUG      *
C       LEADING SECTION
C *  TT = POINT CONCENTRATIONS AT A FULL TIME-STEP FOR SAMPLE PLUG     *
C       TRAILING SECTION
C *  RC = REDUCED RATE COEFFICIENT                                     *
C    TMAX = THE TOTAL TIME OF INTEREST
C *  MONIT = LOCATION OF THE FLOW CELL WHERE THE CONCENTRATION OF      *
C       THE SAMPLE IS MONITORED
C *  A,B,E,F = COEFFICIENTS OF THE DIFFERENCE EQUATIONS                *
C    OMEGA,GAMMA = INTERMEDIATE SOLUTIONS FOR THE TRIDIAGONAL
C *                MATRIX                                              *
C
C * REFERENCES:                                                       *
C    ANANTHAKRISHNAN, GILL, & BARDUHN. A.I.CH.E.JOURNAL,11,1063,1965
C *  CARNAHAN, LUTHER, & WILKES, "APPL. NUMERICAL METHODS",1969        *
C
C * * * * * * * * * * * * * * * * * * * * * * * * * * * * *


      DIMENSION A(196),F(196),ALX(196),CAX(196),ALY(11),BEY(11),CAY(11),
     1D(196),T(196,11),TPRIMI(196),TPRIMJ(11),TSTAR(196,11),TL(196,11),T
     2T(196,11),OMEGA(196),GAMMA(196)
      DATA IN/5/,LP/6/

      READ,DTAU,TMAX,ML,MT,DX,PE,LPLUG
      N = 10
      DY=0.1
      TAU=0.00
      MONIT=89
      PI=3.14159
      NN=N+1
      LPLUG=MT-ML
      E=DTAU/(DY*DY)
```

```
      WRITE(LP,200)DTAU,TMAX,ML,MT,N,PE
  200 FORMAT(1X,'LAMINAR DISPERSION OF SOLUTE IN A TUBULAR REACTOR'/1X,'
     1IMPLICIT ALTERNATING-DIRECTION METHOD, WITH PARAMETERS:'/3X,'DTAU
     2= ',F8.3/3X,'TMAX = ',F8.2/3X,'ML   = ',I5/3X,'MT   = ',I5/3X,'N
     3  = ',I5/3X,'PE   = ',F12.4///)
      WRITE(LP,202)
  202 FORMAT(1X,'    TAU','    CONC'/)

C ** INITIAL AND BOUNDARY CONDITIONS FOR THE LEADING EDGE OF THE
C    INJECTED SAMPLE PLUG

      M=ML+1
      DO 2 J=1,NN
        TL(1,J)=1.0
        DO 2 I=2,M
          TL(I,J)=0.0
    2 CONTINUE

C ** INITIAL AND BOUNDARY CONDITIONS FOR THE TRAILING EDGE OF THE
C    INJECTED SAMPLE PLUG

      MM=MT+1
      MPL=LPLUG+1
      MPLL=MPL+1
      DO 3 J=1,NN
        TT(1,J)=0.0
        DO 3 I=2,MPL
          TT(I,J)=1.0
    3 CONTINUE
      DO 4 J=1,NN
        DO 4 I=MPLL,MM
          TT(I,J)=0.0
    4 CONTINUE

C ** COEFFICIENT ARRAYS FOR Y-IMPLICIT EQUATIONS IN RADIAL DIMENSION

      DO 9 J=1,NN
        IF(J .EQ. 1) GO TO 5
          GO TO 6
    5   ALY(J)=0.0
        BEY(J)=1.0+4.0*E
        CAY(J)=-4.0*E
        GO TO 9
    6   IF(J .NE. NN) GO TO 7
          GO TO 8
    7   F(J)=FF(J,DY,DTAU)
        ALY(J)=-E+F(J)
        BEY(J)=2.0*E+1.0
        CAY(J)=-E-F(J)
        GO TO 9
    8   ALY(J)=-2.0*E
        BEY(J)=1.0+2.0*E
        CAY(J)=0.0
    9 CONTINUE
```

```
C ** TIME-STEP INCREMENTS

   10 TAU=TAU+DTAU
              B=(DTAU/(DX*DX))*(1.0/(TAU*PE*PE))
              BEX=1.0+2.0*B

C ** COEFFICIENT ARRAYS AND SOLUTIONS FOR X-IMPLICIT EQUATIONS IN LONGI-
C    TUDINAL DIMENSION --- FOR THE LEADING PORTION OF THE SAMPLE PLUG

      DO 16 J=1,NN
      DO 15 I=2,ML
   50    A(I)=AF(I,J,DX,DY,TAU,DTAU)
         ALX(I)=-A(I)-B
         CAX(I)=A(I)-B
         IF(J .EQ. 1) GO TO 11
            GO TO 12
   11    D(I)=(1.0-4.0*E)*TL(I,J)+4.0*E*TL(I,J+1)
         GO TO 15
   12    IF(J .NE. NN) GO TO 13
            GO TO 14
   13    F(I)=FF(J,DY,DTAU)
         D(I)=(E-F(I))*TL(I,J-1)+(1.0-2.0*E)*TL(I,J)+(F(I)+E)*TL(I,J+
     1))
         GO TO 15
   14    D(I)=(1.0-2.0*E)*TL(I,J)+2.0*E*TL(I,N)
   15    CONTINUE
         CALL TRIDAG(2,ML,1,ALX,BEX,CAX,D,TPRIMI,OMEGA,GAMMA)
         TSTAR(1,J)=0.0
         TSTAR(M,J)=0.0
         DO 16 I=2,ML
            TSTAR(I,J)=TPRIMI(I)
   16 CONTINUE

C ** SOLUTIONS FOR Y-IMPLICIT EQUATIONS --- FOR THE LEADING PORTION OF
C    THE SAMPLE PLUG

      TAU=TAU+DTAU
   55         B=(DTAU/(DX*DX))*(1.0/(TAU*PE*PE))
      DO 18 I=2,ML
   60    DO 17 J=1,NN
            A(J)=AF(I,J,DX,DY,TAU,DTAU)
            D(J)=(A(J)+B)*TSTAR(I-1,J)+(1.0-2.0*B)*TSTAR(I,J)+(B-A(J))*T
     1STAR(I+1,J)
            TL(1,J)=TSTAR(1,J)
            TL(M,J)=TSTAR(M,J)
   17    CONTINUE
         CALL TRIDAG(1,NN,NN,ALY,BEY,CAY,D,TPRIMJ,OMEGA,GAMMA)
         DO 18 J=1,NN
            TL(I,J)=TPRIMJ(J)
   18 CONTINUE

C ** COEFFICIENT ARRAYS AND SOLUTIONS FOR X-IMPLICIT EQUATIONS --- FOR
C    THE TRAILING PORTION OF THE SAMPLE PLUG


      TAU=TAU-DTAU
              B=(DTAU/(DX*DX))*(1.0/(TAU*PE*PE))
      DO 24 J=1,NN
      DO 23 I=2,MT
   70    A(I)=AF(I,J,DX,DY,TAU,DTAU)
         ALX(I)=-A(I)-B
         CAX(I)=A(I)-B
         IF(J .EQ. 1) GO TO 19
            GO TO 20
   19    D(I)=(1.0-4.0*E)*TT(I,J)+4.0*E*TT(I,J+1)
         GO TO 23
   20    IF(J .NE. NN) GO TO 21
            GO TO 22
   21    F(I)=FF(J,DY,DTAU)
         D(I)=(E-F(I))*TT(I,J-1)+(1.0-2.0*E)*TT(I,J)+(F(I)+E)*TT(I,J+
     1))
         GO TO 23
   22    D(I)=(1.0-2.0*E)*TT(I,J)+2.0*E*TT(I,N)
   23    CONTINUE
         CALL TRIDAG(2,MT,1,ALX,BEX,CAX,D,TPRIMI,OMEGA,GAMMA)
         TSTAR(1,J)=0.0
         TSTAR(MM,J)=0.0
         DO 24 I=2,MT
            TSTAR(I,J)=TPRIMI(I)
   24 CONTINUE

C ** SOLUTIONS FOR Y-IMPLICIT EQUATIONS --- FOR THE TRAILING PORTION OF
C    THE SAMPLE PLUG

      TAU=TAU+DTAU
              B=(DTAU/(DX*DX))*(1.0/(TAU*PE*PE))
      DO 26 I=2,MT
   80    DO 25 J=1,NN
            A(J)=AF(I,J,DX,DY,TAU,DTAU)
            D(J)=(A(J)+B)*TSTAR(I-1,J)+(1.0-2.0*B)*TSTAR(I,J)+(B-A(J))*T
     1STAR(I+1,J)
            TT(1,J)=TSTAR(1,J)
            TT(MM,J)=TSTAR(MM,J)
   25    CONTINUE
         CALL TRIDAG(1,NN,NN,ALY,BEY,CAY,D,TPRIMJ,OMEGA,GAMMA)
         DO 26 J=1,NN
            TT(I,J)=TPRIMJ(J)
   26 CONTINUE

C ** THE POINT CONCENTRATION DISTRIBUTION FOR THE SAMPLE PLUG

      DO 28 J=1,NN
      DO 27 I=1,LPLUG
         T(I,J)=TT(I,J)
   27 CONTINUE
      DO 28 I=MPL,MM
         T(I,J)=TL(I-LPLUG,J)-TT(I,J)
   28 CONTINUE
```

185

```
C ** INTEGRATE THE TOTAL CONCENTRATION WITHIN THE DIMENSION OF THE FLOW
C    CELL

     CONC=T(MONIT,1)
     DO 29 J=2,NN
        SUBCON=2*PI*J*DY*T(MONIT,J)
        CONC=CONC+SUBCON
  29 CONTINUE

C ** PRINT OUT THE CONCENTRATION VERSUS TIME DATA ARRAY

     WRITE(LP,201)TAU,CONC
 201 FORMAT(1X,F10.2,G15.7)

C ** TIME STEP INCREMENT CHECK

     IF(TAU .LE. TMAX) GO TO 10
     STOP
     END


C  THIS FUNCTION IS FOR CALCULATING THE COEFFICIENT, A, OF THE
C  DIFFERENCE EQUATIONS

     FUNCTION AF(I,J,DX,DY,TAU,DTAU)
        JJ=J-1
        II=I-1
        AA=1.0-JJ*JJ*DY*DY
        AB=SQRT(TAU)
        AC=0.5*II*DX/TAU
        AD=DTAU/(2.0*DX)
        AF=AD*((AA/AB)-AC)
        RETURN
     END


C  THIS FUNCTION IS FOR CALCULATING THE COEFFICIENT, F, OF THE
C  DIFFERENCE EQUATIONS

     FUNCTION FF(J,DY,DTAU)
        JJ=J-1
        FF=DTAU/(2.0*JJ*DY*DY)
        RETURN
     END


C  GAUSSIAN ELIMINATION METHOD FOR SOLVING SIMULTANEOUS EQUATIONS WITH
C  TRIDIAGONAL MATRIX COEFFICIENTS

     SUBROUTINE TRIDAG(IF,L,LL,AL,BE,CA,D,V,OMEGA,GAMMA)
     DIMENSION AL(L),BE(L),CA(L),D(L),V(L),OMEGA(L),GAMMA(L)
     IF(LL .EQ. 1) GO TO 31
        GO TO 33
```

```
  31 OMEGA(IF)=BE(LL)
     GAMMA(IF)=(D(IF)-AL(IF))/OMEGA(IF)
     IFP1=IF+1
     DO 32 I=IFP1,L
        OMEGA(I)=BE(LL)-AL(I)*CA(I-1)/OMEGA(I-1)
        GAMMA(I)=(D(I)-(AL(I)*GAMMA(I-1)))/OMEGA(I)
  32 CONTINUE
     GO TO 35
  33 OMEGA(IF)=BE(IF)
     GAMMA(IF)=D(IF)/OMEGA(IF)
     IFP1=IF+1
     DO 34 I=IFP1,L
        OMEGA(I)=BE(I)-AL(I)*CA(I-1)/OMEGA(I-1)
        GAMMA(I)=(D(I)-(AL(I)*GAMMA(I-1)))/OMEGA(I)
  34 CONTINUE
  35 V(L)=GAMMA(L)
     LAST=L-1
        DO 36 KK=IF,LAST
        K=LAST+IF-KK
        V(K)=GAMMA(K)-(CA(K)*V(K+1)/OMEGA(K))
  36    CONTINUE
        RETURN
     END


SENTRY
```

APPENDIX D

LISTING OF THE COMPUTER PROGRAM FOR SIMULATING

A CONCENTRATION-TIME CURVE BY

TAYLOR'S MODEL

```
 1: flt 9;enp "Radius, A",A
 2: if flg13;jmp -1
 3: enp "Umax, U",U
 4: if flg13;jmp -1
 5: enp "Mass, M",M
 6: if flg13;jmp -1
 7: enp "Travel Length, L",L
 8: if flg13;jmp -1
 9: enp "Diffusion Coefficient, D",D
10: if flg13;jmp -1
11: enp "Xmin, X",X
12: if flg13;jmp -1
13: enp "Xmax, Z",Z
14: if flg13;jmp -1
15: enp "Ymin, Y",Y
16: if flg13;jmp -1
17: enp "Ymax, B",B
18: if flg13;jmp -1
19: enp "Xdivision, E",E
20: if flg13;jmp -1
21: enp "Ydivision, F",F
22: if flg13;jmp -1
23: scl X-E,Z,Y-F,B
24: plt Z-3.9E,B-F,1;lbl "CONCENTRATION-TIME CURVE"
25: csiz 2,1.5,7/10,0
26: csiz 1.5,1.5,7/10,0
27: cplt -28,-1;lbl "[no chemical reaction]"
28: cplt -22,-2;lbl "Equation:"
29: cplt -9,-1.5;lbl "Date:"
30: cplt -3,-1.5;lbl "A=    cm  U=    cm/sec"
31: cplt -22,-1;lbl "M=    g  L=    cm"
32: cplt -18,-1;lbl "D=      cm.cm/sec"
33: axe X,Y,E,F
34: fxd 1
35: csiz 1.5,1.5,7/10,0;0→P
36: Y+2F→Y;P+1→P
37: plt X,Y,1;cplt -5,-.3;lbl Y
38: if Y<B-2F;gto 36
39: cplt -5,3;csiz 2,1.5,7/10,270
40: lbl "CONCENTRATION [ARBITRARY UNIT]"
41: csiz 1.5,1.5,7/10,0;0→Q
42: X+2E→X;Q+1→Q
43: plt X,Y-2PF,1;cplt -2.5,-1;lbl X
44: if X<Z-2E;gto 42
45: cplt -35,-2;csiz 2,1.5,7/10,0;lbl "TIME [sec]"
46: for T=X-2QE to Z by .5
47: UA*UA/192D→K
48: L-.5(UT)→H
49: .5M/A^2π^1.5√(KT)exp(H^2/4KT)→C
50: plt T,C
51: next T
52: pen;dsp "Change parameters & press CONTINUE";stp
53: gto 46
54: end
```

APPENDIX E

A BATCH STUDY OF ESTIMATING THE RATE COEFFICIENT

FOR THE OXIDATION OF L-ASCORBIC

ACID BY DICHROMATE

The study was conducted under the following condition: The concentration of dichromate solution was 1.00 mM, and the concentration of L-ascorbic acid solution was 100.0 mM (in excess to assure pseudo-first order kinetics). The pH of the system was 4.76.

1.50 mL of L-ascorbic acid was injected into a standard spectrophotometric cell, containing 1.50 mL of dichromate solution, placed in the spectrophotometer, then the mixed solution was immediately monotored spectrophotometrically. The injection was done by means of a syringe, equiped with a long teflon needle which was secured on the inside wall (but not in the light path) of the detecting cell. The experiment was repeated four times, each run was done with the injection teflon needle inserted into a different location inside the cell.

The recorded data were treated by the numerical testing method. A typical result is plotted in Figure 50. The rate coefficient obtained from four runs is 0.0186 ± 0.0009 sec^{-1}.
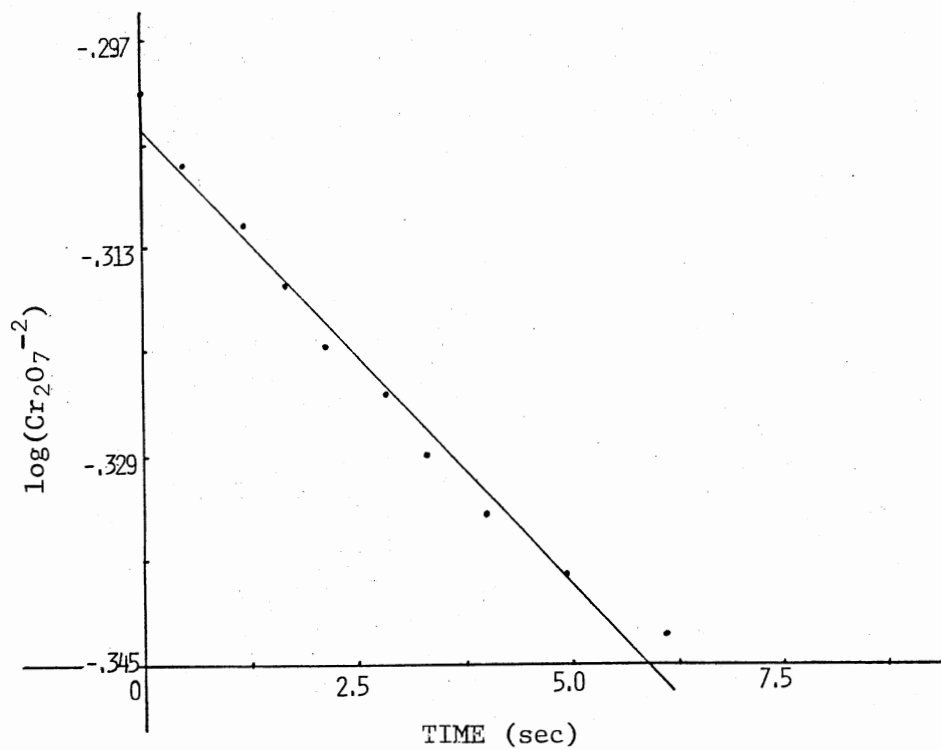
Figure 50. Typical First-Order Plot for the Determination of Rate Coefficient

VITA 2

CHIH-DUEN CHAO PAINTON

Candidate for the Degree of

Doctor of Philosophy

Thesis: CHEMICAL CONTRIBUTIONS TO DISPERSION - THEIR ANALYTICAL IMPACT
IN FLOW INJECTION SAMPLE PROCESSING SYSTEMS

Major Field: Chemistry

Biographical:

Personal Data: Born in Taiwan, the Republic of China, February 24,
1950, the daughter of Mr. and Mrs. Gon Chao; married to Scott
Wayne Painton on October 20, 1977; one child: Lee Wayne
Painton.

Education: Graduated from Hsin Chu Girls' High School, Taiwan, the
Republic of China, in June, 1967; received Bachelor of Science
degree in Chemistry from Providence College, Taiwan, the
Republic of China, in June, 1971; completed the requirements
for the degree of Doctor of Philosophy in Chemistry at
Oklahoma State University, Stillwater, Oklahoma, in December,
1982.

Professional Experience: Science Teacher at Gwan Fu High School,
Taiwan, the Republic of China, August, 1971 to February 1972;
Science Teacher at Grun Shee Junior High School, Taiwan, the
Republic of China, March, 1972 to February, 1973; Graduate
Teaching Assistant at Oklahoma State University, Stillwater,
August, 1976 to December, 1980; Graduate Research Associate at
Oklahoma State University, Stillwater, January 1981 to date.
Member of American Chemical Society, Sigma Xi, Phi Lambda
Upsilon Honorary Chemical Society, and the Honor Society of
Phi Kappa Phi.